Reaction diffusion modelling of bacteria colonies: microbial quiescence and chemotaxis

by

Phindile Dumani

Submitted in partial fulfilment of the requirements for the degree

Philosphiae Doctor

In the Department of Mathematics and Applied Mathematics
in the Faculty of Natural & Agricultural Sciences

University of Pretoria

Pretoria

11 November 2022

Declaration

I, the undersigned, declare that the thesis, which I hereby submit for the degree *Philosphiae Doctor* at the University of Pretoria, is my own independent work and has not previously been submitted by me for a degree at this or any other tertiary institution.

.....

(Phindile Dumani)

Date: 11 November 2022

Acknowledgements

I am truly grateful to my family for the support and encouragement, especially, my younger brother, Siphumelele Radebe, who made sure I did not lose myself, my smile and laughter.

I would like to thank my supervisor, Prof. Michael Chapwanya, for his support and guidance. I would also like to extend my appreciation to the Department of Mathematics and Applied Mathematics and The New Generation of Academics Programme (nGAP) for awarding me opportunities to grow in research and in my teaching career.

Abstract

The physiological structure of microbial communities in natural environments is typically a response to changes in internal and external conditions. External conditions may include the availability or depletion of growth-limiting nutrients, and presence of inhibiting or toxic substances while internal conditions may include cell to cell interactions. We present and investigate spatiotemporal bacterioplankton-nutrient-chemoattractant-chemorepellent interaction models that take into account the quiescent stage and chemotaxis. We establish conditions under which microbial population oscillations (boom-and-bust) may occur. In the study, we observe that population oscillations occur when the switching of states is dependent on the active microbial density in the environment or cell-to-cell interaction. Furthermore, in the case where dormant cells are neglected or disregarded, oscillations are not observed in the bacterioplankton population dynamics.

It is well known from experiments that colonies of *Escherichia coli* and *Salmonella typhimurium* exhibit various patterns, therefore, we establish the existence of traveling wavefronts for the proposed reaction-diffusion model. Using the theory of monotone wave fronts for cooperative and partially degenerate reaction-diffusion systems, we show that the minimal wave speed coincides with the spreading speed. However, that is for the constant switch rates case. Whereas, for the switch functions dependent on the chemoattractant concentration we numerically observe that the model admits non-monotonic traveling wave profiles. Moreover, we demonstrate that neglecting dormant cells overestimates the spreading speed of the colony. Numerical results also indicate the importance of the quiescent stage in the speed of spread.

Microbial populations depend on their environment but can also modify it. Instead of breaking down complex nutrients for their growth, microbes can exhibit negative local or global behaviour by engineering the environment in ways that are detrimental to their proliferation. A reaction diffusion model system consisting of active and inactive microbial population in a harsh environment accounting for the directed movement and switch of cells to dormancy at high concentration is studied. Results show an essential mechanism generating oscillating patterns in microbial populations under environmental stress. Bifurcation analysis of the model and the interplay between Turing and Hopf instability is discussed. Theoretical and numerical investigation of the proposed model is presented to provide insight into the conditions that may lead to the extinction of the microbial population – ecological suicide. A qualitative study of the proposed numerical schemes is presented. Numerical simulations are provided to support our theoretical observations.

Contents

List of Figures

List of Tables

Chapter 1

Introduction

Microbial populations are generally found to exist in the form of biofilms. A biofilm is a formation of bacterial communities embedded within a slimy extracellular matrix consisting of proteins, extracellular DNA, and polysaccharides [115]. Biofilms can be found anywhere and everywhere in natural and industrial environments. The formation, development and growth of biofilms are multistage processes. These dynamical processes are largely influenced by the environmental conditions that include nutritious substrates supplied by the surrounding environment and autotrophic microbes, diffusion limitations of substrates, bulk fluid shear stress as well as types and characteristics of bacteria contained in the biofilm. They are known to consist of multispecies such as algae, fungi, extracellular polymeric substances, other microbes, and solvent [115].

Biofilms can cause tremendous harm resulting in product contamination, medical infections and financial loss, but are also beneficial and useful in processes such as bioremediation, biodegradation and biofiltration of wastewater, moreover, forming bio-barriers to keep and prevent groundwater and soil from getting contaminated. However, the formation of biofilms is a very complex dynamical process that is influenced and controlled by different biological, physical as well as chemical properties and mechanisms. Biofilm experiments with the aid of mathematical modelling are of great importance to get deeper insight, better understanding and a broader perspective of the dynamics of complex microorganisms behaviour. Mathematical modelling not only helps in verifying experiments but is a tool used for future predictions.

1.1 Early work

Biofilm phenotype of bacteria has been observed by scientists for several hundreds of years. Historically, examination of biofilm growth at the level of single cells formally started when the microscope became a commonly used biological tool by microbiologists and cardiologists [142]. The experiments or microscopic observations of biofilms date back

from 1683 to 1708 in the letters [109, 110] published by *Anthoni van Leeuwenhoek* referred to as "the Father of Microbiology". Using a microscope that he designed and made, the scientist observed and described matter from his mouth as aggregated microorganisms in the "scurf of the teeth" as well as "particles scraped off his tongue" [78, 79]. The particles scraped off the tongue were later described by countless dentists in [45] as the dental plague development and normal microbial communities of the tongue mucosa. Among others, dentists were the first to recognise the effects and impacts of aggregating microbes in connection with all dental problems [88] and infections [89].

Louis Pasteur, a pioneer of microbiology, in the year 1864 observed and gave a diagram, shown in Fig. 1.1, of bacteria aggregates as a result of wine getting acetic [144] leading him to discover pasteurization [78]. For the succeeding century, medical microbiologists and other microbiological researchers had no interest in microorganism biofilm growth, in addition, the concept of biofilm-secreting microorganisms was unknown to most of them [78, 79]. From 1933 to 1935, the term "film" referring to bacteria aggregation, adhesion and proliferation was being used in the field of marine microbiology to differentiate adhering (immobile) microbes from free-swimming "planktonic" microorganisms [72, 196]. Then, the focus was on the planktonic microorganisms together with their pathogenic properties. However, in the early 1920s there was a report to the US Navy Department on bacteria found in the form of slime on the bottom of ships when biofouling occurs on surfaces such as ship and submarine hulls [6]. Studying the bacterial flora of a lake or pond in detail using the usual methods requires an investment of time, labour as well as costly equipment that in most cases cannot be readily obtained. Thus, authors in [72] proposed a procedure that minimizes the equipment and labour used by employing microscopic slides placed in an aquatic environment for a definite period of time. The method tracked different numbers and types of bacteria that develop in various freshwater habitats or aquatic environments with the expectation that such an experiment will provide insight into the nature and dynamics of the water bacteria and their role in the lake, stream or ecosystem.

Thereafter, the study of biofilm also broadened and developed in the field of medicine. In the year 1970 to 1972, a link between bacteria aggregation and the aetiology of chronically persistent infection was observed in medicine from cystic fibrosis patients with chronic *Pseudomonas aeruginosa* (*P. aeruginosa*) lung infection through a microscopic examination, [80, 77, 81]. Between 1974 to 1978, they linked and observed bacteria aggregation in autopsies of cystic fibrosis patients who died as a result of *P. aeruginosa* lung infection. A biofilm of aggregated bacteria surrounded by slime in the sputum of those patients infected with mucoid phenotypes was observed. Since then, biofilm has been studied in basic, technical and environmental microbiology [38, 100, 39], medical microbiology as well as biochemistry [135].

Extensive research on biofilms has been conducted for the past four decades with

(a) The instrument constructed for the study.

(b) *Dépôt* from red wine with aggregates.

Figure 1.1: Original drawings by *Louis Pasteur* [78].

models that have been successfully used to better understand and predict the growth and other dynamics of biofilms in different environments. Generally, the formation of biofilm mathematical models range from simple to complex, one spatial to multi-dimensional models, single to multi-species, and from temporal to spatial-temporal models, etc.

The authors in [154, 153] first did an experiment using laboratory-scale biofilm reactors to evaluate the steady-state biofilm kinetics as well as the idea that there exists a threshold substrate concentration below which no steady-state activity occurs. From the experiment, it was observed that as the rate-limiting substrate concentration approaches a critical value, the substrate removal and the thickness of a biofilm immediately get reduced. Thereafter, they proposed and considered a steady-state biofilm model that couples substrate utilization to microbial growth. The study investigated the critical bulk substrate concentration needed for the development and sustainability of a biofilm in various conditions and the substrate flux into a biofilm over the concentration range between two extreme cases. Furthermore, [183, 184] made experimental observations to describe and analyse the competition for space and rate-limiting substrate between several microbial species. In the study, they too discuss the case of steady-state and both the autotrophic and heterotrophic organisms dependent on a common nutrient (oxygen). Using a continuum approach, they developed a mathematical model of biofilms that describes the dynamics and spatial distribution of the various species as well as predict the changes in the biofilm thickness. Differences in substrate concentrations in the bulk fluid and restriction of external mass transfer with biomass detachments as a result of shear

stress and sloughing are included in the model. The studies mentioned above are focused on the dynamics of the steady-state biofilm growth models that take into account the thickness of biofilms, the spatial distribution of various species as well as the substrate concentration.

Subsequently, mathematical models of biofilm growth and pattern formation have been developed and studied using diffusion-limited aggregation (DLA) models. The growth pattern was first studied in [190] using the DLA model through computer simulations where they considered a model applicable to a metal-particle aggregation process with correlations. Their simulations produced aggregates that have a power-law correlation. In addition, they compared the dynamics of the model to other models producing low-density objects: random animals, the Eden growth model, percolating aggregates, and self-avoiding motions. Later on, authors in [60] presented the first biological DLA study on a DLA colony of *Bacillus subtilis* on agar plates. They observed that there is a high probability for bacterial Bacillus subtilis colonies to grow in line with the DLA process on agar plates. In [168, 118, 59] more experimental and modelling research was done showing that the bacterial colonies of *Bacillus subtilis* grow two-dimensionally and self-similarly through diffusion-limited aggregation processes in a nutrient concentration environment. Further, they observed that the bacterium grew a round colony similar to the Eden model dynamics, a bacterial colony that has a straight and dense branch formation as well as a dense colony diffusing with concentric rings. See for example, Fig. 1.2.

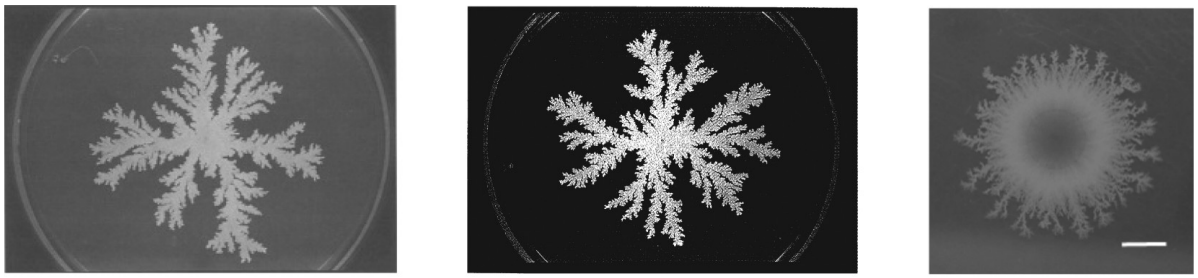

(a) *B. subtilis* **(b)** *B. subtilis* **(c)** *S. cerevisiae*

Figure 1.2: Experimental examples of DLA microbial colonies growing in low-nutrient environments [170]. Given are colonies of (a) *B. subtilis* [118], (b) *B. subtilis* [60], and (c) *S. cerevisiae* [169].

As mentioned earlier, bacterial colony growth yield to and is controlled by various physical, chemical and biological laws or factors in the environment. All these factors and laws play a crucial role in the proliferation and can affect the morphology of the bacterial colonies. However, colony morphology also varies with different microbial species. Generally, the mechanisms and dynamics of bacterial colony growth are highly complex. The characteristics of colony patterns and growth patterns are not easy to explain solely by experiments, but can be explained using mathematical models that are based on

already-known biology. Whether or not a pattern will form depends on the local interactions between bacterial colony and the chemical kinetics as well as the competition involving diffusive dispersal and chemotactic aggregation, [131].

A capillary assay method was developed to study the behavior and possible patterns formed by bacteria in response to a chemoattractant in [3]. The assay method has since been used to study and better understand the response of bacterial species to chemoattractants, nutrients and repellents and verify mathematical models [167]. Later in [21, 22] the authors carried out a series of experimental studies on patterns formed by S. *typhimuriun* and E. *Coli*. They used three experimental methods with different mediums resulting in three different pattern mechanisms formation. In the experiment, bacteria are placed in two mediums: liquid and semi-solid medium procedures. The results showed that a bacterial colony have the ability to form intriguing regular patterns when they consume or are exposed to succinate and fumarate, also secreting aspartate and a potent chemoattractant [131]. See for example, Figs. 1.3 and 1.5. The experiments and mathematical models in [21, 22, 175, 131] along with dynamics and various behaviour exhibited by microbial populations in different environmental conditions have inspired this work.

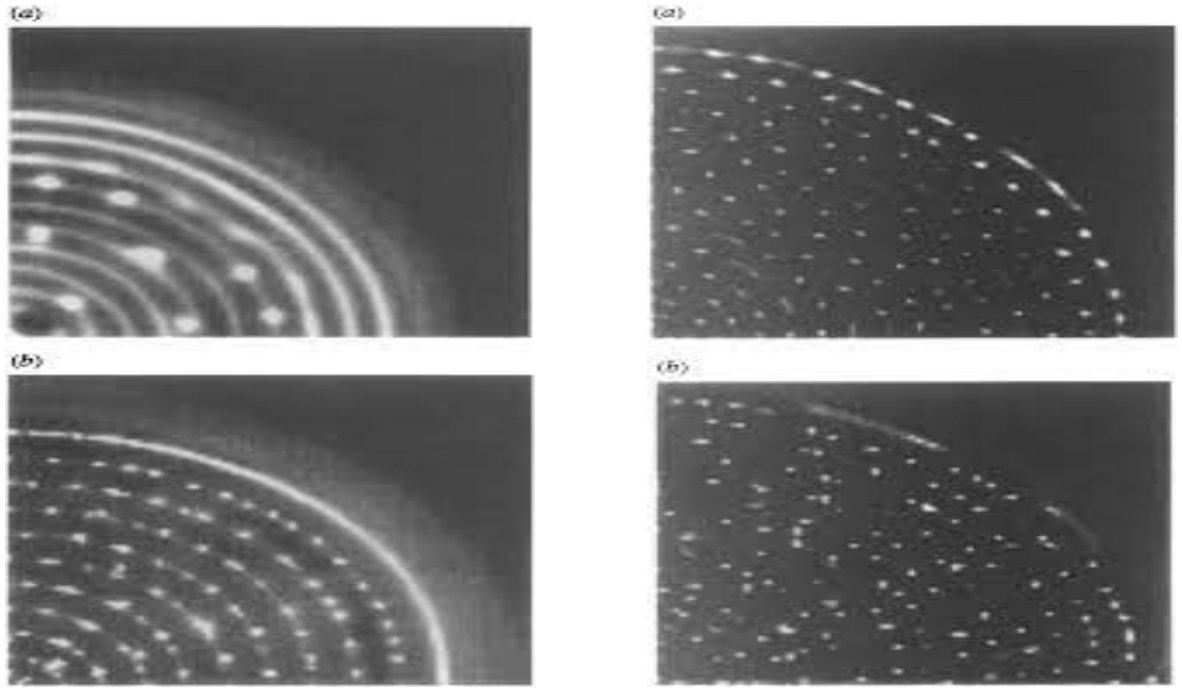

(1) *S. typhimurium* patterns (2) *E. coli* patterns

Figure 1.3: Semi-solid medium models. (1a) concentric rings (transition to spotted rings pattern) and (1b) concentric spotted rings. With (2a) showing interdigitated spots, and (2b) radial spots [175].

1.2 Mathematical modelling

Existing mathematical models studying the growth of bacteria colonies based on the physical mechanisms for diffusing and spreading are mostly computationally intensive. However, mathematical simplifications can be implemented such that models are easily applicable and most importantly, address crucial and practical matters in question. Early models were one-dimensional, for example, [153, 154, 183, 184], but the biofilm dynamics and mechanisms lead to the revelation that biofilm growth is more complex, heterogeneous and of three-dimension with tower and mushroom-like anatomy [189]. In contrast to biofilms of the well-studied cells: *P. aeruginosa*, *E. coli*, and *V. cholerae*, the *Caulobacter crescentus* (CB15) cells form biphasic biofilms, consisting predominantly of a cell monolayer biofilm and a densely packed biofilm with mushroom-shaped structures [51]. See Fig. 1.4. More recent models are three-dimensional. In [48] they proposed and studied a continuum model that describes the development of spatially heterogeneous biofilm structures and the interaction of nutrient availability and biomass production. Moreover, authors in [99, 97] presented a substrate-limiting model of a growing biofilm layer. In their case, the biofilm is modeled as a viscous, incompressible fluid of constant density governed by Darcy's Law. Since biofilms are not necessarily flat and homogeneous but instead often exhibit complex structural heterogeneity, a more advanced model was presented in [35, 36] considering an extra-cellular polymeric substance (EPS) matrix to study the development of heterogeneous biofilm morphology. They assumed that the bacteria are enmeshed in the network and produce the polymer and that the biofilm is a biological gel containing EPS and water. A model of a biofilm growing inside a long channel with biomass assumed to have a viscous polymer solution rheology was presented in [188]. The work considered a case where the biofilm growth is enough to influence the flow (i.e, clogging). Similar models have been investigated as in [1, 98], providing fundamental insight on the role and importance of biofilm growth in fluid transport through porous media. Different mathematical models with various assumptions on the dynamics of biofilms or microbes in any environment have been studied.

1.3 Bacteria quiescence

In many populations, not all individuals are actively growing and proliferating but some are in a quiescent state [67]. Under certain circumstances or conditions, a normally growing microorganism can transition to a quiescent stage and later transition back to an active state. Dormance or quiescence refers to a reversible state of low metabolic activity in which living microorganisms can persist for extended periods without proliferation to survive nutritionally unfavourable conditions or environmental toxins [91]. Quiescent phase has been identified under different names in the literature, e.g., dormacy, resting

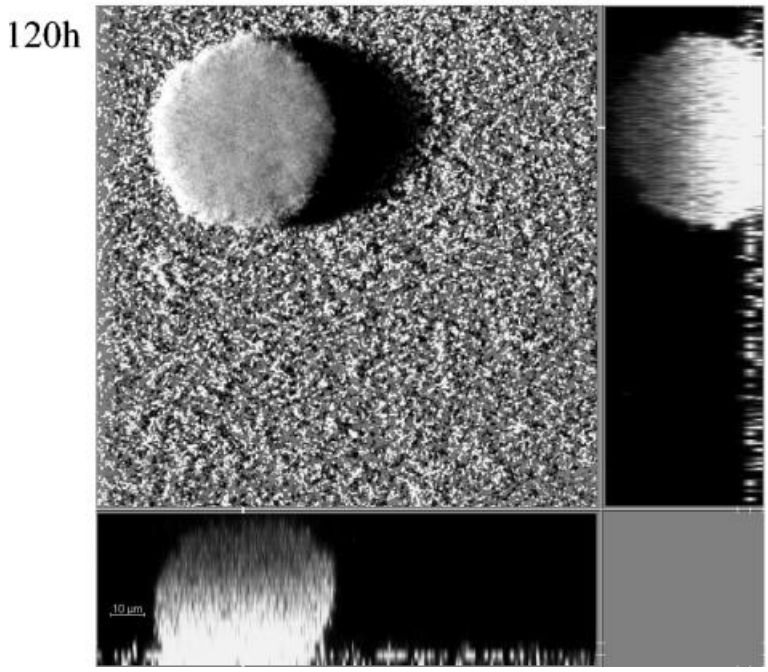

Figure 1.4: Images displaying shadow projections of the ushroom-shaped structures of biofilm from different angles [51].

phase, hibernation, and ecological refugee, to name a few [181]. Dormance occurs in various biological phenomena involving different species or living organisms, for example, a seed-producing plant reproduces seeds that can germinate immediately and develop into active plants while other seeds remain in the soil for long periods of time until they grow into plants. Quiescent cells of pathogens may produce latent infections when resuscitated, additionally, dormant bacteria are not responsive to many antimicrobial agents since these agents are known to be effective only against growing cells [117]. Moreover, *Mycobacterium tuberculosis* can be dormant due to oxygen limitation in the host for a very long time without producing a virus, then resuscitate and start the production of lesions and progressive tuberculosis [85, 185]. This work includes and focuses on microbial quiescence as a result of nutrients, stimulants and chemoattractants limitations or in response to repellents in their surroundings.

Since the probability that a single microorganism switches states from being dormant and to becoming active and vise-versa depends on its age, size and other quantities, studying the development and growth of populations with quiescence includes the dynamics of an entire ecosystem comprising of a general microbial population and naturally falls in the domain of population dynamics. Neglecting responses of microbes in different conditions or environments with unfavourable conditions (that include either regular or long-lived shortage of nutrient) fails to capture the biogeochemical system. Therefore, one of the main objectives of this work is to study and model the behaviour of the bacterial population as a whole using known dynamics or behaviour of cells as well as their

local and global interactions.

Cell proliferation is affected by chemical and physical factors in the environment such as growth-limiting nutrient supply, temperature, light intensity, pH and pressure levels. In [87] a chemostat *Monod* model for microbial growth taking into account active and quiescent cells was proposed and analysed. In the study, transient oscillatory growth behaviours in bacterial and chemostat cultures under nutrient limitations were observed. The model proposed takes the form

$$\begin{aligned} \frac{dn}{dt} &= k_3(n^0 - n) - k_4\frac{f(n)u}{Y}, \\ \frac{du}{dt} &= k_4 f(n)u - k_3 u - k_1 u + k_2 w, \\ \frac{dw}{dt} &= -k_3 w + k_1 u - k_2 w, \end{aligned} \tag{1.1}$$

where $w(t)$, $u(t)$ and $n(t)$ denote bacterial cell density of quiescent and active cells and the concentration of the growth-limiting nutrient in the chemostat, respectively, n^0 is the concentration of the limiting nutrient in the medium constant supplied into the chemostat, k_3 is the dilution rate, k_4 is the growth rate, k_1 is the rate of change from active cells to quiescent ones, k_2 is the rate of change from quiescent cells to active ones, Y is the yield constant and $f(n)$ denotes the growth rate. Numerous mathematical models taking into consideration cells that change their metabolism to adjust to environmental changes have been proposed and analysed, see for example, [134]. In the work they investigated cell consumption kinetics depending on pH levels, moreover, authors in [108] proposed a kinetic model of flocculation considering the possibility that dispersed bacteria and bacteria aggregated in a floc have different physiological states. From the model, it was observed that the floc phase and dispersed phase bacteria exhibit different growth rates. Additionally, in [67] they considered a model that assumes a single cell fully characterised by its age, and state (either active or dormant). The model is continuous in time and consists of partial differential equations with an analysis that focuses on extinction or exponential growth. The work [68] and [69] extended the study by considering a nonlinear structured cell population model of tumor growth. The models differentiate between two types of cells with the tumor (the proliferating and quiescent), and assume that the probability of switching states is controlled by the total tumor size. The mathematical models predict that tumor growth occurs in its early stages similarly to tumors forming a necrotic center and then grow exponentially.

Furthermore, to name a few, the work [117, 70, 17] have contributed to a better understanding of the ability of certain living organisms to reversibly enter a quiescent state that has crucial implications for their survival, especially in environments involving stress such as extreme temperatures, toxins, water and nutrient limitations. An interesting feature of the above-mentioned models, due to the inclusion of a quiescent state, is

that oscillatory growth behaviour or bacterioplankton blooms are observed. In bacterial and algae chemostat cultures, it has been established that if slow-growing microbes are inoculated in the system, the population washes out or remains in the same state as long as the limiting nutrient level remains below a threshold level. If the fast growing cells are inoculated in the chemostat, the microbial population could still survive the slow growth mode even when the nutrient input concentration remains low or below critical level [117, 87]. Competition between two species that can switch from slow to fast-growing modes and uptake nutrient and vise-versa has been considered to result in oscillatory growth dynamics. In [56] a model involving two species, oceanic biomass and nutrient, with similarities to models proposed to explain the sawtooth oscillation behaviour in glycolysis is discussed. The authors extended the analysis by proposing a more complex model that includes competition between planktonic species. Subsequently, an extension of a model on a system of competing species of microbial populations was proposed in [57] were they showed that in conditions of starvation, self-sustained oscillations are extreme resulting in *boom-and-bust* dynamics where there are concentrated population spikes at regular intervals that are separated by significantly low population densities.

Population oscillations are a phenomenon that sometimes arises in population dynamics. For example, the study conducted in [133] on the recurrence of fox rabies outbreaks as well as models on humoral immune response taking into account the time lags in antibody production and in immune memory formation in [42], to name a few. In seeking to study, understand and explain the biological phenomenon of unrealistically low population levels in models of self-sustained oscillatory population growth, authors in [58] introduced a model capable of explaining the occurrence of self-sustained oscillations of boom-and-bust character similar to plankton blooms under conditions of low growth-limiting nutrient supply (starvation) with increasingly long intervals between the outbreaks as nutrient is depleted. The model describing the above dynamics is given as

$$\begin{aligned}
\frac{dw}{dt} &= k_1 q(a) u - k_2 p(b) w, \\
\frac{du}{dt} &= k_4 Y f(n) u - k_3 u - k_1 q(a) u + k_2 p(b) w, \\
\frac{dn}{dt} &= n^0 - k_4 f(n) u,
\end{aligned} \tag{1.2}$$

the $q(a)$ and $p(b)$ are resuscitation and hibernation functions, respectively, thought of as cell-specific probabilities of switching states. That is, $a, b \in \{u, n\}$, which means the assumption of a nutrient-dependent switch implies that p and q are increasing and decreasing functions of n, respectively; and if p and q are functions of u then the switch is due to paracrine signaling. The above model forms the basis of our study that focuses on microbial population dynamics.

1.4 Keller-Segel models

From microbial species to large mammals, the survival of many various living organisms is dependent on their essential, basic property and ability to respond and navigate within complex environmental changes by detecting, integrating as well as processing different internal and/or external indicators [74, 13]. Generally, microbial populations do not randomly move, but respond to environmental changes or disturbances through sensing. The motion is essential for different behavioural aspects, taking into account the location and availability of nutrient sources and avoidance of predators and/or toxins. The bias or directed movement of cells and organisms in response to external stimulants/signals or various environmental factors such as light, chemicals gradients and temperature – chemotaxis, has attracted interest since it plays a crucial role in biology, [74, 13]. Chemotaxis regulates different biological phenomena [3], that include chemotactic mechanisms such as sperm motivation during fertilisation; where the chemoattractant gradient provides cues that guide sperm to the egg [93, 73], would healing; where fibroblasts (cells responsible for tissue homeostasis under normal physiological conditions) migrate into the wound site to begin the proliferative phase and deposit new extracellular matrix that will then initiate and facilitate healing and closure [43, 113], in cancer growth; where tumor cells can move randomly and directionally allowing cell invasion, migration, and dispersal or stimulation and development of new blood vessel growth in the surrounding microenvironment [156, 105, 37], and in patterning of the nervous system; where mechanisms guiding axon projection and neuronal migration appear to be conserved with those for chemotactic leukocytes [143].

Extensive theoretical and experimental research has been done for biological species undergoing chemotaxis, particularly in *Escherichia Coli* [18], *Salmonella typhimurium* [191], slime mold amoebae *Dictyostelium discoideum* and human endothelial, *Rhodobacter sphaeroides*, *Bacillus subtilus* and many more. Theoretical and mathematical modelling of chemotaxis was first studied in the late nineteenth century in [49, 50, 146] and the interest in bacterial population has since increased [145], especially in the last 50 years driven by the increasing experimental and theoretical insight both on the global, local population and individual scale together with the recent and detailed mathematical models at different scales. We start with the continuum model of bacterial chemotaxis considered in [95, 94], the models were developed to study and better understand the movement and behavior of chemotactic bacteria in the context of slime molds. The general form of a

Keller-Segel model for chemotaxis takes the form

$$\begin{aligned}
\frac{\partial u}{\partial t} &= D_u \nabla^2 - \nabla \cdot (\chi(u,v)\nabla v) + f(u,v), \\
\frac{\partial v}{\partial t} &= D_v \nabla^2 + g(u,v) - h(u,v)v, \\
\frac{\partial u}{\partial \tau} &= 0, \quad \frac{\partial v}{\partial \tau} = 0, \quad x \in \partial\Omega,
\end{aligned} \tag{1.3}$$

where $x \in \Omega \subset \mathbb{R}^m$, $\partial\Omega$ is the surface boundary enclosing Ω, ∇^2 is the *Laplacian operator* with respect to x and $\partial/\partial\tau$ denoting the derivative along the outward normal. The function $v(x,t)$ represents the concentration of the chemoattractant at spatial position x and time t. The function $f(u,v)$ describes the growth and death of cells while $g(u,v)$ and $h(u,v)$ are kinetic functions denoting the production and consumption of the chemoattractant, respectively. The chemotaxis response function is represented by $\chi(u,v)$, D_u is the bacterial diffusion coefficient and D_v is the diffusion coefficient. The model mainly describes the aggregation of microbial species evoked by the stimuli/chemical with the aggregation balanced by cell diffusion [13]. Among all the properties of chemotaxis behavior and dynamics, the ability of cells to aggregate remains the most important mechanism for self-organisation of biological systems being studied.

Various forms of the *Keller-Segel* model have been used and studied in modelling broad biological and ecological systems. Such models have fascinated researchers and modellers, especially applied mathematicians because of the qualitative behaviour they show such as the concentration of aggregation of microbes referred to as blow-up, pattern formation, stabilization, traveling waves, and many more. In bacterial chemotaxis, determining how these complex patterns or arrangements and aggregations form from local cell interactions is still a difficult task [175]. Since the pioneering work of *Keller* and *Segel* in [95, 94], a vast amount of theoretical and mathematical modelling research has been expended on bacterial chemotaxis, the patterns and behaviour thereof. Some of the areas that have expanded and benefited from the work in [95, 94] include the following:

- response to cell starvation: models that capture main features of the lifecycle of slime mold *Dictyostelium discoideum* have been developed studying morphogenesis during the aggregation process conducted by the relay as well as migration of cells in response to the stimuli cyclic AMP gradients, [76, 95].

- In understanding microbial population pattern formation: various bacteria including *E. Coli* and *S. typhimurium* can form different spatial patterns under favourable environmental conditions [21, 22, 191].

- Studies have been presented to better understand embryonic pattern forming processes using chemotaxis, such as an early development and dynamics of an embry-

onic structure coordinating tissue motions [140] and in cell migration/colonisation during embryonic growth [102].

- Cell-chemotaxis models have been developed to study pigmentation or mechanisms for generating some of the common, simple and complex patterns found on fish [141], skin of snakes [132] and other species [4].

- The inflammatory response consists of physical, chemical, and cellular processes resulting to a rapid accumulation of phagocytic white blood cells at the site of tissue invasion causing bacterial infections. In [5, 106] they model the inflammatory response of leukocytes to bacterial invasion. Studies of leukocytes migration in a Boyden chamber [160, 24] have been conducted. Cell migration phenomena underlie many biological processes, as a result, the Boyden chamber is a method used for assessing cell migration and measuring cell motility coefficients at the population level [34].

- On the pathological side, tumor cells migrating into the circulatory system and causing metastasis is still a critical challenge for cancer treatment [34] and other diseases in medicine. Consequently, in [116] they study the role of microglia and the phenomena associated with formation of senile plaques that form in the central nervous system (CNS) in the devastating neurodegenerative Alzheimer's disease. Moreover, in [25] the behavior of tumor cells and their interaction with normal cells, noninvasive tumor cells and other cells including the movement of invasive cancer cells is studied. Also in tumour-induced angiogenesis, the invasive cancerous cells of a solid tumour secret chemicals, known as tumour angiogenic factors into the surrounding tissue [27]. These angiogenic factors spread through the tissue resulting to chemical gradients in the tissue surrounding the tumour.

- One of the most studied biological phenomenon in spatial ecological processes is prey-taxis, where the active movement of predators controlled by prey density is investigated [92, 107].

In bacterial chemotaxis, it is challenging to determine how complex arrangements or patterns form from local interactions between cells. In such cases where biology fails to provide a sufficient explanation, mathematical modelling thus plays a crucial role. Since the pioneering study conducted in [94, 96], extensive research has been done on microbial population interactions and patterns. To name a few, spatial patterns similar to the *E. coli* experimentally observed patterns were obtained in [15, 171]. Using a nonlocal "communicating walkers" model, they demonstrated how signaling or communication allows the bacterial colony to develop complex patterns in response to unfavourable conditions.

In [20] they observed that bacteria congregate into regular patterns. Even though chemotaxis and an attractant produced by the same bacteria can result in pattern-forming instability, chemotactic bacteria are not capable of forming patterns from just a point. It was clear that these patterns (that include various stripes and spots and swarm rings) can be formed through the help of proliferation and depletion of limiting nutrients in the medium. In [19] the authors investigated the formation of *E. coli* patterns in a semi-solid medium and observed that via chemoattractant signaling, the bacteria organize themselves into swarm rings and aggregate, and these rings move when the chemoattractant is depleted. See for example, Fig. 1.5.

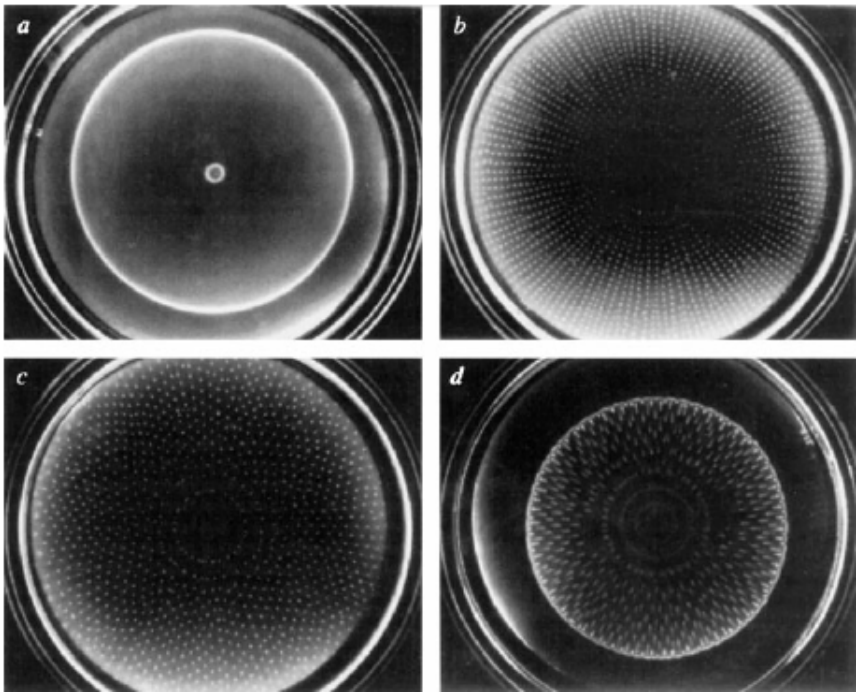

Figure 1.5: More dramatic patterns exhibited by *E. coli* in a semi-solid medium with the light regions representing high bacteria density [131]. In (a) bacterial density in the swarm ring increases until the ring becomes unstable, in (b) aggregates remain bright and full of aggressively active bacteria for a short period of time, while in (c) and (d) aggregates dissolve as the bacteria move towards the swarm ring with dormant bacteria left behind as a radial streak [131].

Different models have considered various assumptions that are more or less reasonable revealing intriguing patterns and other bacteria dynamics. In [175], presented is a mathematical model that captures all three pattern-formating processes (production, uptake and degradation of nutrient) experimentally observed in colonies of *E. coli* and *S. typhimurium* based on minimum assumptions. Combining these important biological processes of microbial populations, they proposed a mathematical model that is a system

of three equations given by

$$\begin{aligned}\frac{\partial u}{\partial t} &= D_u\nabla^2 - \nabla\cdot(\chi(u,v)\nabla v) + f(u,n),\\ \frac{\partial v}{\partial t} &= D_v\nabla^2 + g(u,n) - h(u,v),\\ \frac{\partial n}{\partial t} &= D_n\nabla^2 - \ell(u,n),\end{aligned} \tag{1.4}$$

where $n(x,t)$ represents the concentration of the main nutrient and $\ell(u,n)$ denotes the nutrient consumption or uptake function.

The important part of modelling is quantifying each term in the equations. We first discuss diffusion, random migration as well as chemotaxis terms. The chemoattractant and the stimulant undergo classical *Fickian* diffusion. Studies have shown that bacteria do not solely diffuse, but their motion involves a sequence of runs and tumbles. That is, a bacterium moves in a certain direction consisting of a combination of motions; randomly diffusing and then rotating itself to get ready to repeat the process. Organisms move from a lower concentration to a higher concentration of the chemoattractant; positive chemotaxis. Similarly, the movement from higher concentration to lower concentration of the chemorepellent is known as negative chemotaxis [13]. Chemoattractants and repellents are organic or inorganic substances that induce microbial motility [13]. Microorganisms employ chemotaxis to position themselves in a favourable portion of the environment or natural habitat by monitoring the concentration gradients of either chemoattractants or repellents in their surrounding. The chemotaxis term is known as the chemotactic flux. The average velocity with which the microbial population responds to the chemoattractant or repellent gradient is proportional to the gradient, chemotactic flux. Consequently, the chemotactic flux is proportional to the product of the density of the microbes and the chemoattractant/repellent gradient.

Experimental observations of microbes conducted in [19, 16] suggest that the flux of bacteria consists of two terms, $J = J_r + J_c$, where the first term refers to random-diffusion motion in the absence of chemotaxis while the second term denotes the directed movement in response to a gradient of chemoattractant or repellent [103]. A mathematical expression or general form of the chemotaxis term is the divergence of the chemotactic flux given by

$$\nabla J = \nabla\cdot(\chi(u,v)\nabla v)\,,$$

where J is the chemotactic flux and $\chi(u,v)$ is the chemotaxis response/sensitivity function. An extensive research has been done mainly to find the most biologically accurate functional form of the chemotaxis function either from a microscopic point of view or by curve-fitting population experimental data. Reviews and analysis of the types of functions

that have been investigated can be found in [55] and [13], to name a few. On reaction terms, exact functional forms of uptake, production and degradation of the chemoattractant or repellent are not critical [175]. Based on the assumptions of the study, they can vary from constant, linear functions to any type of *Holling* functional response and many more.

For example, the relationship between the microbial population growth rate, μ_2, and the nutrient concentration, n, is a valuable tool in biotechnology [137]. The classical models which have been employed to microbial population growth include the *Verhust* [177] and *Gompertz* [64] functions. The *Verhust* function is based on the population growth by adjusting the exponential growth model (logistic growth), whereas, the *Gompertz* function is contingent on the exponential relationship between the population density and the specific growth rate [137]. The *Gompertz* functional is given by

$$u(t) = Ce^{e^{-B(t-M)}},$$

where C represents the maximum population density, M denotes the time at which the absolute growth rate is maximal and B is the relative growth rate at M.

In [62] the *Gompertz* function was modified to a function that describes the cell density against time in bacterial growth profiles in connection to exponential growth rates as well as the lag phase period. The modification was gives as

$$\log u(t) = A + De^{-e^{-B(t-M)}}, \tag{1.5}$$

where A denoting the value of the lower asymptote is given by $\log u(-\infty)$ and D represents the difference between the upper and lower asymptote, $\log u(\infty) - \log u(-\infty)$. The concept of microbial growth kinetics was overtaken by an empirical model proposed by *Monod* in [129] which introduced the idea of a growth-limiting substrate. The *Monod* is as follows:

$$k_4 = \mu_{\max}\frac{n}{K_n + n}, \tag{1.6}$$

where k_4 is the specific growth rate, $\mu_{\max}$ is the maximum specific growth rate, n denotes the substrate concentration and K_n represents the substrate saturation constant or the substrate concentration at half maximum specific growth rate.

In the *Monod*'s functional, there is a relationship between the growth rate and the concentration of the growth-limiting substrate through $\mu_{\max}$ and K_n. Moreover, *Monod* connected the yield coefficient $(Y_{x/n})$ to both the growth rate of biomass and substrate utilization (γ)

$$Y_{x/n} = \frac{dx}{dn}, \quad \text{and} \quad k_4 = \frac{Y_{x/n}}{X}\cdot\frac{dn}{dt} \cong Y_{x/n}\gamma,$$

respectively.

In the experimental study on *E. coli* and *S. typhimurium* in [21, 22] mathematically described using (1.4), it was observed that microbes grow at a constant rate that is affected by the availability of nutrient in the environment. In [175], modelling and analysing the experimental study the authors assumed a proliferation term that involves both the growth and death of cells given in the form

$$f(u,n) = k_5 u\left(k_6\frac{n^2}{\mu_n + n^2} - u\right). \tag{1.7}$$

This term looks like a *Logistic* growth with a carrying capacity that depends on the availability of nutrient, n, [131]. We see from equation (1.7) that the population of bacteria increases when the density of cells is below the carrying capacity. It is expected that the nutrient gets depleted in the medium at a rate proportional to that which cells are proliferating [131], suggesting the form

$$\ell(u,n) = k_7\frac{n^2}{\mu_n + n^2}. \tag{1.8}$$

There is minimal studies available in the literature on the chemoattractant production term. In [74] and [13] they reviewed and discussed some models that consider fundamental forms. The authors in [175] assumed that the amount of chemoattractant produced increases as the nutrient concentration increases and possibly saturates with time suggesting the following form

$$g(u,n) = k_8 n\frac{u^2}{\mu_u + u^2}. \tag{1.9}$$

As for the chemoattractant consumption term, the form could have a sigmoidal characteristic. Other non-saturating alternatives such as $h(u,v) = k_9 uv$ are also plausible.

Kinetics equations describing the activity of microbial population on a specific nutrient, chemoattractant or repellent are very important in understanding various phenomena in biological and biotechnological processes. For the design and development of biological transformation processes, experimental data is needed. Different mathematical models with a variety of kinetic terms have been proposed to describe the behaviour of metabolism of compounds in pure cultures of microbes or microbial populations in their natural habitat [137].

Therefore, it is of great importance that mathematical models capture the dynamics of realistic biological and experimental processes. We can make use of simplistic models in line with realistic observations such as the Keller-Segel model proposed in [94] to obtain the fundamental behaviour of the microbial population. However, we have to compromise on the simplicity of a model to gain true and realistic insight of a phenomenon. For

example, we can extend the Keller-Segel model by taking into account quiescent microbes, delay of transitioning from one state to the other, and a stimulant in the system to obtain a system of four equations. With the help of computer simulations and numerical schemes to assist in approximating solutions of complex mathematical models, modelling can be improved to be more realistic so that informative knowledge can be drawn.

1.5 Traveling-waves

Reaction-diffusion equations systems are commonly used to describe biological invasion processes. Over the years, a considerable amount of attention and many other significant results on the existence of traveling wave solutions for various partial differential systems of equations have been observed.

In the recent pioneering studies found in [178, 186, 112, 114, 187, 54], spreading speeds and traveling wave solutions for cooperative reaction-diffusion systems were established. However, as a result of different biological or physical constraints, various reaction-diffusion systems are not necessarily cooperative. Studies on non-cooperative reaction-diffusion systems are minimal but have been slowly growing over the years since the work of [166] where they showed that the asymptotic spreading speed of a model with nonmonotone growth functions can still be obtained through constructing lower and upper monotone functions of the system. See for example, [180], [86] and references therein.

Investigations on the existence of traveling wave solutions and spatial dynamics for n-dimensional reaction-diffusion systems of different types of models studying different phenomena that include physical dynamics, chemical kinetics, as well as spatial ecology, have been carried out. The general form of these n-dimensional ($n \geq 2$) models is as follows

$$\boldsymbol{u}_t = D\boldsymbol{u}_{xx} + \boldsymbol{f}(\boldsymbol{u}), \quad x \in \mathbb{R},\ t > 0, \tag{1.10}$$

with initial conditions $\boldsymbol{u}(x,0) = \boldsymbol{u}^0(x)$ for $x \in \mathbb{R}$, where $\boldsymbol{u} = (u_i)$, $D = \text{diag}(d_1, d_2, \ldots, d_n)$, $d_i \geq 0$ or $d_i > 0$ for $i = 1, 2, \ldots, n$ and $\boldsymbol{f}(\boldsymbol{u}) = (f_1(\boldsymbol{u}), f_2(\boldsymbol{u}), \ldots, f_n(\boldsymbol{u}))$. System (1.10) is said to be non-degenerate provided that each diffusion coefficient, d_i, is positive and partially degenerate if some of the diffusion coefficients are zero. Another important factor in these studies is the nonlinearities for $\boldsymbol{f}$ which could either be monostable or bistable depending on the number and the stability of steady-states of the ordinary differential equation,

$$\boldsymbol{u}_t = \boldsymbol{f}(\boldsymbol{u}). \tag{1.11}$$

Furthermore, system (1.10) is defined as cooperative if

$$\partial_{u_j} f_i(\boldsymbol{u}) \geq 0, \quad \forall 1 \leq i \neq j \leq n, \tag{1.12}$$

while the converse refers to a competitive system. A traveling wave of system (1.10) is a solution of the form $\boldsymbol{u} = \boldsymbol{u}(\xi)$, with $\xi = x + vt$, such that if we substitute this solution into the system, we have the wave equation

$$D\boldsymbol{u}''(\xi) - v\boldsymbol{u}'(\xi) + \boldsymbol{f}(\boldsymbol{u}(\xi)) = 0, \ \xi \in \mathbb{R}. \tag{1.13}$$

In [178] they presented the existence of the minimal wave speed and stability of traveling waves for the non-degenerate case while authors in [186] considered and used a general cooperative system of reaction-diffusion equations to obtain the estimate of the spreading wave speed. In addition, in [114] it was shown that for the non-degenerate case, the spreading speed coincides with the minimal wave speed. In population dynamics, partially degenerate reaction-diffusion models of the form (1.10) apply. A reaction-diffusion system describing the spatial spread of bacterial diseases is studied in [26] where the system consists of two nonlinear parabolic equations which take into account the evolution of the bacteria population and human infective population. Later in [195] the existence of traveling wave solutions through the method of constructing upper and lower solutions was established. Similarly in [165], the existence of the spreading speed is studied for a population model reduced to an integral equation, non-local and time-delayed reaction-diffusion model, and a time-delayed and diffusive epidemic model. One of the most refined models was proposed in [35, 36] where they considered some physical processes that occur in the genesis of biofilm structure, specifically, a biofilm as gel composed of extracellular polymeric substance embedded in a fluid solvent. In [189] the authors considered the same model and used dimensional analysis to show the existence of a travelling wavefront solution at large times.

We will focus on investigating and establishing the existence of monotone and non-monotone traveling wave solutions for partially-degenerate reaction-diffusion systems in microbial populations with quiescence dynamics.

1.6 Aims and objectives of the thesis

Motivated by the existing literature [58, 117, 131, 87], we propose reaction-diffusion differential systems that take into account active and quiescent microbial population in response to an environment that could be unfavourable for their growth either due to insufficient or depletion of the growth-liming nutrient or toxins excreted by same microorganisms. In this work, we study the sustained oscillatory bacterial behaviour

or boom-and-bust dynamics that have been observed for bacterioplankton in literature. That is, we aim to investigate whether the change or transition of bacterial cells between states is due to bacteria responding to environmental changes or paracrine signaling. Furthermore, we propose partially degenerate reaction-diffusion systems that assume the random-bias movement of active microbes, and dispersal of chemoattractant or repellent and non-diffusing dormant cells. Thereafter, bifurcation analysis will be presented to study experimentally observed or possible patterns that could be exhibited by microbial populations in response to environmental changes that can be detrimental to proliferation.

We will study the existence of traveling wave fronts describing the movement and dispersal of microbes as well as the effect that the nonlinear conversion rates and the growth-limiting nutrient have on the wave speed. With the aid of numerical simulations, we will present numerical nonstandard finite and finite volume difference methods to support and verify our theoretical results.

In this work, we propose mathematical models constructed through combining some of the key realistic biological and ecological processes with the aim to describe and capture realistic observations.

The thesis is organised as follows: in Chapter 2, we study the dynamics of the phytoplankton populations with quiescence and their interaction with the growth-limiting nutrient. In this section, we first investigate a uniform steady-state model to determine whether the observed self-sustained oscillatory behaviour is a result of cell-to-cell signaling or a change in the nutrient concentration. We then consider a diffusive model since the active population bias-randomly move for the nutrient uptake to occur. The dispersal of the growth-limiting nutrient is also taken into account. We establish the existence of traveling wavefronts when the cells switch states at a constant rate and numerically show for general switch rates.

In Chapter 3, using the theory of monotone wavefronts for cooperative and partially degenerate reaction-diffusion systems we study the existence of traveling waves for a reduced (without quiescence). For a full model, we assume a bacteria-chemoattractant interaction system when the behaviour of the active and inactive cells is influenced by the change in chemoattractant concentration. We study the nonlinear conversion rates in-depth and the effects they have on the type of system (cooperative or noncooperative) and traveling wave solutions (monotone or nonmonotone) we will observe. In this case, we assume that the growth of bacteria does not depend on the nutrient/chemoattractant but follows a *Logistic* growth.

A model comprising a general microbial population capable of modifying its environment to pH levels that are not hospitable for their survival is investigated in Chapter 4. The microbial population is assumed to excrete toxins. A reduced model assuming bacteria that either die or transition to a state of dormancy without switching back is studied. The investigation is based on how microbes can derive themselves to extinction leading

to the occurrence of self-sustained oscillations in the microbial population mediated by the change in concentration levels of the toxin. Furthermore, spatial-temporal models of the reduced and full models are studied. Linear stability analysis and the supporting numerical simulations of the models are presented to study possible behavioural changes in unfavourable environmental conditions.

In Chapter 5, we propose a numerical scheme of the mathematical model in Chapter 4 constructed using the nonstandard finite difference and finite volume methods. Using standard techniques, we verify that the proposed scheme is dynamically consistent with the continuous model. We make use of numerical schemes and simulations as tools to verify and support our theoretical results.

Chapter 2

Existence of self-sustained oscillations in response to environmental stress

2.1 Introduction

Microbial populations play a crucial role in ecological, environmental, as well as industrial processes. Regardless of their preponderance contribution in biology to sustain life on the planet, there is minimal knowledge about microbial biology. For instance, one small insect can contain thousands of microbial organisms of many different species. Despite these limitations, robust experimental work making use of axenic culture methods (among others) have been done over the last several decades. Such studies have provided basic knowledge and understanding of the dynamics and development of microbiology. However, the dynamics or interactions observed using such methods are unrealistic. In reality, there is a wide variety of microbial species and complex interactions that pure culture methods do not capture, see for example [41] for a review.

Numerous microorganisms have the ability to resist stressors such as antibiotics, temperature and desiccation by entering a state of low metabolic activity i.e., dormancy, see for example [90] and the literature therein. However, it has also been found that bacteria may be dormant under natural environmental conditions. Microbial populations in a state of dormancy are neither dead nor active which allows them to persist under various environmental challenges [163, 75], which is a strategy of great importance in medical studies. A distinct characteristic of microbes in a dormant state is the ability to transition between an active state and a relatively inactive but live state and thereafter be reactivated again. Although individual cells acquit independently, bacterial populations exhibit collective behaviour, as a result, local interaction of bacteria brings about global behaviour. Consequently, to have and acquire better knowledge and forecast of the bac-

terial behaviour in their habitat, it is of great importance to understand the analogous mechanisms that affect or cause these behavioural changes.

Active cells are responsible for proliferation and forming colonies on any medium independent of a preceding resuscitation or transition phase. Seasonal changes and environmental conditions, depending on the medium, have different rates of substrate supply which may or may not result in resource limitation. Consequently, uneven distributions of the resources could potentially affect both the rates of dormancy and reawakening even in cases where there are enough resources.

Most of the existing mathematical modeling literature considers the macroscopic generalisation of bacteria growth and decay in the form of biofilms, [35, 36, 189]. Particularly, they do not take into consideration the changes in physiological states and, thus, assume biomass only involves active microbes. In most cases, models are developed from the idea of a nutrient diffusing into a growing biofilm and being consumed. The foundation of numerous biofilm models is diffusion-limited biofilm growth where limiting nutrient diffuses into the biofilm from an external source. Further, determining nutrient transport rate and its relationship to the biofilm growth and productivity [98].

Environmental heterogeneity has been observed to contribute to patchiness in oceanic plankton populations. Biological interactions involving phytoplankton populations can result to similar patterns and dynamics. The formation of spontaneous patterns even in homogeneous environments is a phenomenon that is a trait of reaction-diffusion equations employed to model similar systems, see for example [111], and more recent work in [30, 31]. Bacterioplankton are bacteria and archaea, which play an important role in remineralising organic material in lakes and oceans. Many phytoplankton are also bacterioplankton. Plankton population movement is subject to other factors such as currents and turbulent lateral diffusion, [157]. The environment as well as conditions in nature vary from those of laboratories [91]. Mathematical models formulated with the aim to explain phytoplankton blooms are available in the literature. See for example, the work [30, 31]. In this work, we model the dynamics of the phytoplankton populations and nutrient interaction using reaction-diffusion equations. The novelty of this work is threefold. First, motivated by the above discussion, we propose a reaction-diffusion system incorporating dormant and active population. Using the reduced spatially independent model, we address whether the observed microbial population oscillations are a response to the change in rate-limiting nutrient concentration levels or a result of paracrine signalling. Furthermore, we will establish the conditions under which the travelling wave solutions exist.

The remainder of this chapter is organized as follows. We begin in Section 2.2 by proposing a nutrient-bacterioplankton reaction-diffusion model. The modeling assumptions are included in this section. A uniform steady state model is investigated in Section 2.3 with the aim to establish if the observed population oscillations are a response to the rate-limiting nutrient concentration levels or a result of paracrine signalling. The

existence of traveling waves is established in Section 2.4 and we conclude in Section 2.5.

2.2 Model formulation

We begin by describing in detail the model kinetics. Autotrophs are organisms that are capable of producing their own food by using various inorganic components like water, sunlight, air, and other chemical substances. They convert an abiotic source of energy into energy stored in organic compounds, which can be used by other organisms (e.g. heterotrophs) [158]. Phytoplankton are the autotrophic components of the plankton community and a key part of ocean and freshwater ecosystems. In this work, $w(t)$ and $u(t)$ denote the density of active and inactive autotroph microorganisms, respectively, and $v(t)$ is the concentration of the nutrient, or the energy. There is a wealth of literature on the construction of mathematical models for the interaction of nutrients and growing microorganisms, see for example [189, 83] and the literature therein. In this work, the growth rate of active microorganisms is given by

$$\frac{1}{u}\frac{du}{dt} = k_4 f(v),$$

where k_4 is the utilisation constant. Furthermore, $f(v)$ is the response function which may take different forms [194, 58]. For simplicity we ignore Monod kinetics [58] and assume the following general hypothesis;

$\mathcal{G}$: $f : \mathbb{R}_+ \to [0, +\infty)$ is C^1 and $f'(v) \geq 0$ for all v.

The simplest form will be a linear function, $f(v) = v$, with the possibility of nonlinear behavior as expressed by the Monod law, $f(v) = \dfrac{v}{\mu_v + v}$, [194]. For mathematical convenience, in this chapter, we further assume $f(v) = vh(v)$ which satisfies hypothesis $\mathcal{G}$. The efficiency of conversion of $v(t)$ into $u(t)$ is measured by the yield constant Y, such that

$$\frac{du}{dt} = -Y\frac{dv}{dt}.$$

We hypothesise that the microorganisms may enter a quiescent phase in which they need resuscitation for proliferation as opposed to active ones, [194, 58]. Consequently, only the active microbes contribute towards the biomass growth [163]. The transformation of $w(t)$ to $u(t)$ (awakening), takes place at rate k_2, and the hibernation, i.e., from $u(t)$ to $w(t)$ takes place at the rate k_1. We also introduce the hibernation and reawakening functions, $q(a)$ and $p(b)$, respectively, each of them $\in (0, 1)$. The variables a and b describe the dependence of switching, and these variables can either be $u(t)$ or $v(t)$. For example, if both processes are nutrient-dependent, then p and q will be functions of $v(t)$. In particular, assuming a switch dependent on the nutrient suggests that q and p are increasing and decreasing functions of v, respectively; with q and p as functions of u if the

switch is due to paracrine signalling. This, of course, as argued in [58], may need further investigation when the reactivation of dormant cells is controlled by microbial density. These biological processes lead to the following equations governing the dynamics of the active and dormant microorganisms

$$\begin{aligned} \frac{dw}{dt} &= k_1 q(a) u - k_2 p(b) w, \\ \frac{du}{dt} &= k_4 Y f(v) u - k_3 u - k_1 q(a) u + k_2 p(b) w, \end{aligned} \tag{2.1}$$

where we assume density-dependent natural mortality with rate k_3. The switch functions are assumed to be monotonic, and they saturate. In addition, we have

$$\mathcal{F}_1 \ : \ p : \mathbb{R}_+ \to (0,1] \text{ is } C^1,\ p'(b) \geq 0 \text{ for all } b \text{ and } \lim_{b\to\infty} p(b) = 1,$$

$$\mathcal{F}_2 \ : \ q : \mathbb{R}_+ \to (0,1] \text{ is } C^1,\ q'(a) \leq 0 \text{ for all } a \text{ and } \lim_{a\to\infty} q(a) = 0.$$

The choice of a and b will be discussed further in Section 2.3.1.

The active microorganisms are assumed to produce a nutrient that can also be used by other microorganisms at the rate k_8. In addition, we assume a natural degradation of the nutrient at the rate k_7. The nutrient equation is given by

$$\frac{dv}{dt} = k_8 g(u) - k_7 v - k_4 f(v) u,$$

where $g(u)$ is the production function that includes input from both external sources and active biomass, hence we assume the following conditions: $g(u) > 0$, $g'(u) > 0$ for all $u \geq 0$. Readers can consult, for example, the work [30, 31] and the references therein.

Allowing for the random movement of the active bacterial population and the nutrient with rates D_u and D_v, respectively, we now propose a multi-dimensional nonlinear reaction-diffusion partial differential equation describing the key properties of the population in response to a certain stimulus depending on the availability and sufficiency of the nutrient. Let $x \in \Omega \subset \mathbb{R}^m$, $(m \geq 1)$ be a simply connected bounded domain and $\partial\Omega$, the surface boundary enclosing Ω. We let $w(x,t) \geq 0$, $u(x,t) \geq 0$ and $v(x,t) \geq 0$ be the density of dormant population, density of active population and the concentration of the nutrient, respectively. Following the above-mentioned biological processes, and in particular, motivated by existing literature, [87, 117, 58], we propose the following generalised

diffusive model

$$\begin{aligned}
\frac{\partial w}{\partial t} &= k_1 q(a)u - k_2 p(b)w - k_3 w, \\
\frac{\partial u}{\partial t} &= k_4 Y f(v)u - k_3 u - k_1 q(a)u + k_2 p(b)w + D_u \nabla^2 u, \\
\frac{\partial v}{\partial t} &= k_8 g(u) - k_7 v - k_4 f(v)u + D_v \nabla^2 v, \\
\frac{\partial w}{\partial \tau} &= 0 \quad \frac{\partial u}{\partial \tau} = 0 \quad \frac{\partial v}{\partial \tau} = 0, \quad x \in \partial\Omega,
\end{aligned} \tag{2.2}$$

where $\partial\Omega$, is the surface boundary enclosing Ω with

$$w(x,0) = w_0(x) \geq 0, \quad u(x,0) = u_0(x) \geq 0 \quad v(x,0) = v_0(x) \geq 0.$$

We have also assumed density dependent nutrient production.

The model is rendered dimensionless by choosing the following scales:

$$w \sim \frac{k_3}{k_4}, \quad u \sim \frac{k_3}{k_4}, \quad v \sim \frac{k_3}{k_4 Y}, \quad x \sim \sqrt{\frac{D_u}{k_3}}, \quad t \sim \frac{1}{k_3}.$$

The corresponding dimensionless system takes the form

$$\begin{aligned}
\frac{\partial w}{\partial t} &= rq(a)u - sp(b)w - w, \\
\frac{\partial u}{\partial t} &= \nabla^2 u + (f(v) - 1)u - rq(a)u + sp(b)w, \quad x \in \Omega, t > 0, \\
\frac{\partial v}{\partial t} &= d_v \nabla^2 v + \alpha(\beta g(u) - v) - u f(v),
\end{aligned} \tag{2.3}$$

where

$$r = \frac{k_1}{k_3}, \quad s = \frac{k_2}{k_3}, \quad d_v = \frac{D_v}{D_u}, \quad \beta = \frac{k_8 Y}{k_7}, \quad \alpha = \frac{k_7}{k_3},$$

with ∇^2 representing the *Laplacian operator* with respect to x. System (2.3) is degenerate in the sense that the inactive population does not diffuse. In the next section, we consider the spatially independent model. Here, we wish to address if the observed plankton bloom in aquatic ecosystems are resource dependent or a result of cell-to-cell signalling. Later in Section 2.4, we establish the existence of travelling waves for the model (2.3).

2.3 Uniform steady state

Several spatially independent differential models of microbial quiescence are documented in the literature, see for example [58, 91, 14, 117, 87], to name a few. The authors in [117] proposed a resource-based model on microbial quiescence. Although random irregular inputs occur in natural environments, they assumed a constant rate of substrate influx,

constructed and studied a mathematical model where the transition between the two states is dependent on the essential resource levels; considering that active cells proliferate in an environment with a high nutrient and may die in a low nutrient environment. The transition rate functions are assumed to be smooth. Moreover, the hibernation rate does not increase when the resource is increased and the awakening rate does not decrease as the nutrient levels increase. In [87], the authors assumed the transition functions depend on the growth-limiting nutrient (since cells' metabolism changes according to the nutrient levels). For mathematical convenience, they assumed that there are threshold values for both switch functions: the reawakening rate is non-decreasing for the nutrient greater than some threshold value, and the hibernation rate is non-increasing for the nutrient less than some threshold value. Other researchers argued that populations could reactivate stochastically independent of environmental conditions. Here, our non-diffusive model takes the form

$$\begin{aligned}
\frac{dw}{dt} &= rq(a)u - sp(b)w - w,\\
\frac{du}{dt} &= (vh(v) - 1)u - rq(a)u + sp(b)w,\\
\frac{dv}{dt} &= \alpha(\beta g(u) - v) - uvh(v).
\end{aligned} \tag{2.4}$$

System (2.4) is appended with initial conditions

$$w(0) = w_0 \geq 0, \quad u(0) = u_0 \geq 0, \quad v(0) = v_0 \geq 0.$$

Adding all the equations in (2.4), we obtain

$$\begin{aligned}
\frac{d\eta}{dt} &= \alpha\beta g(u) - w - u - \alpha v\\
&\leq \beta_* - \alpha_m (w + u + v)\\
&= \beta_* - \alpha_m \eta,
\end{aligned} \tag{2.5}$$

where $\eta = w + u + v$ and $\alpha_m = \min\{1, \alpha\}$. With an assumption that $g(u)$ is a saturating function, then $\alpha\beta g(u) \leq \beta_*$ where $\beta_* > g(0)$. The application of the *Gronwall Inequality* [164], yields

$$\begin{aligned}
\eta(t) &\leq \frac{\beta_*}{\alpha_m}\left(1 - e^{-\alpha_m t}\right) + \eta_0 e^{-\alpha_m t}\\
&= \frac{\beta_*}{\alpha_m} + \left(\eta(0) - \frac{\beta_*}{\alpha_m}\right) e^{-\alpha_m t},
\end{aligned} \tag{2.6}$$

from which

$$\eta(t) \leq \frac{\beta_*}{\alpha_m}, \text{ whenever } \quad \eta(0) \leq \frac{\beta_*}{\alpha_m}.$$

Clearly, the solutions of the system (2.4) are attracted to the set

$$\Omega = \left\{(w,u,v) \in \mathbb{R}^3_+ : w+u+v \leq \frac{\beta_*}{\alpha_m}\right\}.$$

Assuming nonnegative initial conditions, we rewrite system (2.4) in the matrix form

$$\frac{d\boldsymbol{x}(t)}{dt} = \mathbb{M}\boldsymbol{x}(t) + \boldsymbol{z}(t),$$

where $\boldsymbol{x}(t) = (w(t), u(t), v(t))^t$

$$\mathbb{M} = \begin{pmatrix} -sp(b)-1 & rq(a) & 0 \\ sp(b) & -1-rq(a) & uh(v) \\ 0 & 0 & -\alpha - uh(v) \end{pmatrix}, \quad \boldsymbol{z}(t) = \begin{pmatrix} 0 \\ 0 \\ \alpha\beta g(u) \end{pmatrix}.$$

We note that $\mathbb{M}$ is a Metzler matrix (i.e., has nonnegative off-diagonal entries). Thus, $\mathbb{R}^3_+$ is invariant. The above, together with the existence and uniqueness of model (2.4)'s local solution, we have the following result which ensures the well-posedness of system (2.4) both mathematically and biologically.

Theorem 2.1. *Then, system (2.4) is a dynamical system on the compact set Ω.*

As highlighted earlier, in this Section 2.3 we aim to investigate various combinations of variables u_1 and u_2, i.e., observe the dynamics of the model when the microbial activity is either random as a result of paracrine signalling or a direct consequence of the change in nutrient levels. We restrict our work to switch functions satisfying $\mathcal{F}_1$ and $\mathcal{F}_2$. Assuming dormant cells do not die or proliferate, we have the following result.

Proposition 2.1. *System (2.4) admits the following equilibria:*

- *the microbial-free state $E_0 = (0, 0, \beta g(0))$, and*
- *a unique coexistence state $E^* = (w^*, u^*, v^*)$, where $w^* = \dfrac{rq(a^*)}{sp(b^*)}u^*$, and u^* satisfies $u^* - \alpha(\beta g(u^*) - v^*) = 0$ provided v^* exists and satisfies $f(v^*) - 1 = 0$.*

Proof. First, setting the right-hand side of equations (2.4) to zero, we get E_0 and E^* as the only equilibria points where v^* satisfies $f(v^*) - 1 = 0$. Next, defining $H_1(v^*) = f(v^*) - 1$, then $H_1(v^*)$ is a monotonically increasing function since $H_1'(v^*) = f'(v^*) \geq 0$, where we have used hypothesis $\mathcal{G}$. Furthermore, $\lim\limits_{v^*\to 0^+} H_1(v^*) = -1 < 0$, therefore, a unique solution v^* satisfying $H_1(v^*) = f(v^*) - 1$ exists.

Next, we consider $H_2(u^*) = u^* - \alpha(\beta g(u^*) - v^*) = 0$ for $v^* > 0$. Then $\lim\limits_{u^*\to 0^+} H_2(u^*) = \alpha(v^* - \beta g(0))$ and $H_2'(u^*) = 1 - \alpha\beta g'(u^*)$. We now have two cases to consider depending on the sign of $H_2'(u^*)$:

(*i*) Assume $1-\alpha\beta g'(u^*) < 0$, then $H_2(u^*)$ is a monotonically decreasing function of u^* and there exists a unique positive root for $H_2(u^*)$ provided $\beta g(0) < v^*$. Otherwise, there are no positive roots for $\beta g(0) > v^*$.

(*ii*) Assume $1-\alpha\beta g'(u^*) > 0$, then $H_2(u^*)$ is a monotonically increasing function of u^* and there exists a unique positive root for $H_2(u^*)$ provided $\beta g(0) > v^*$. Otherwise, there are no positive roots for $\beta g(0) < v^*$.

□

We notice that unlike the work in [87], here the third equilibrium on the boundary $u = 0$ does not exist since our model assumes $p(b) \neq 0$ for all b, see hypothesis $\mathcal{F}_2$. In particular, if $p(b) = 0$ then the initial state, $u = 0$, will not activate. See for instance [58] for further details. To study the stability of equilibria, we consider the Jacobian matrix of system (2.4) given by

$$\begin{pmatrix} -sp(b) & rq(a) + rq'(a)u - sp'(b)w & rq'(a)u - sp'(b)w \\ sp(b) & (f(v)-1) - rq(a) - rq'(a)u + sp'(b)w & uf'(v) - rq'(a)u + sp'(b)w \\ 0 & \alpha\beta g'(u) - f(v) & -\alpha - uf'(v) \end{pmatrix},$$

where the prime denotes differentiation with respect to the indicated variable, and variables a and b can be v or u. At E_0, we have

$$J(E_0) = \begin{pmatrix} -sp(b^0) & rq(a^0) & 0 \\ sp(b^0) & f(\beta g(0)) - 1 - rq(a^0) & 0 \\ 0 & \alpha\beta g'(0) - f(\beta g(0)) & -\alpha \end{pmatrix}.$$

Clearly, $-\alpha$ is one of the eigenvalues of $J(E_0)$. The remaining eigenvalues come from the reduced matrix

$$\begin{pmatrix} -sp(b^0) & rq(a^0) \\ sp(b^0) & f(\beta g(0)) - 1 - rq(a^0) \end{pmatrix},$$

whose trace is $(f(\beta g(0)) - 1) - rq(a^0) - sp(b^0)$ and the determinant given by

$$-sp(b^0)(f(\beta g(0)) - 1).$$

Under the hypotheses $\mathcal{F}_1$ and $\mathcal{F}_2$, with $(a, b) \geq 0$, we have the following result.

Proposition 2.2. *For any $a \in \{u, v\}$ and $b \in \{u, v\}$, the microbial-free equilibrium state E_0 is locally asymptotically stable provided $f(\beta g(0)) < 1$ and unstable if $f(\beta g(0)) > 1$.*

For later reference, it is important to note that Propositions 2.1 and 2.2, together with hypothesis $\mathcal{G}$ show that the condition $f(\beta g(0)) < 1$ is equivalent to $\beta g(0) < v^*$, and this refers to the population under starvation. Similarly, $f(\beta g(0)) > 1$ is equivalent to

$\beta g(0) > v^*$. In addition, this condition implies that the microbial population becomes extinct if the nutrient supply is less than some threshold value, $\beta g(0)$.

2.3.1 Conversion rate dynamics

In this section we consider the local stability of the coexistence equilibrium under different combinations of functions $q(a)$ and $p(b)$, i.e., we study the dynamics of the model when the microbial activity is either random as a result of paracrine signalling or a direct consequence of the change in nutrient levels. We restrict our work to switch functions satisfying $\mathcal{F}_1$ and $\mathcal{F}_2$. Neglecting dormant cell mortality and assuming they do not proliferate, we have the following result.

Case 1: Assuming that the switch from either hibernation or reawakening is dependent on the nutrient, i.e., $q = q(v)$, and $p = p(v)$, the Jacobian matrix at the co-existence equilibrium is

$$J(E^*) = \begin{pmatrix} -sp(v^*) & rq(v^*) & rq'(v^*)u^* - sp'(v^*)w^* \\ sp(v^*) & -rq(v^*) & u^*f'(v^*) - rq'(v^*)u^* + sp'(v^*)w^* \\ 0 & \alpha\beta g'(u^*) - f(v^*) & -\alpha - u^*f'(v^*) \end{pmatrix},$$

and the characteristic equation of the Jacobian is given by

$$Q(\lambda) = \lambda^3 + s_1\lambda^2 + s_2\lambda + s_3,$$

where the coefficients are given by

$$\begin{aligned} s_1 &= -\text{trace } J(E^*) = sp(v^*) + rq(v^*) + u^*f'(v^*) + \alpha, \\ s_2 &= (sp(v^*) + rq(v^*))(\alpha + u^*f'(v^*)) + (1 - \alpha\beta g'(u^*))(u^*f'(v^*) - rq'(v^*)u^* + sp'(v^*)w^*), \\ s_3 &= -\det J(E^*) = sp(v^*)u^*f'(v^*)\left\{1 - \alpha\beta g'(u^*)\right\}. \end{aligned}$$

Clearly, all coefficients are positive using hypothesis $\mathcal{G}$ provided $1 - \alpha\beta g'(u^*) > 0$. It remains to show that Δ_2 is positive. We have

$$\begin{aligned} \Delta_2 &= s_1s_2 - s_3 \\ &= sp(v^*)u^*f'(v^*)\left\{\alpha\beta g'(u^*) - f(v^*)\right\} + [sp(v^*) + rq(v^*) + (\alpha + u^*f'(v^*))]\times \\ &\quad [(sp(v^*) + rq(v^*))(\alpha + u^*f'(v^*)) - (\alpha\beta g'(u^*) - f(v^*))(u^*f'(v^*) - rq'(v^*)u^* + sp'(v^*)w^*)] \\ &= (sp(v^*) + rq(v^*))(\alpha + u^*f'(v^*))[sp(v^*) + rq(v^*) + \alpha + u^*f'(v^*)] \\ &\quad + \left\{1 - \alpha\beta g'(u^*)\right\}(u^*f'(v^*) - rq'(v^*)u^* + sp'(v^*)w^*)[rq(v^*) + \alpha + u^*f'(v^*)]. \end{aligned}$$

The trace as well as the second Hurwitz determinant are negative and positive, respectively. Therefore, the co-existence equilibrium is asymptotically stable, locally,

provided $1-\alpha\beta g'(u^*) > 0$. If we assume $1-\alpha\beta g'(u^*) < 0$, for the coexistence equilibrium E^* to exist we must have $f(\beta g(0)) < 1$. However, the microbial-free and coexistence equilibria are locally asymptotically stable and unstable, respectively, under this assumption.

Case 2: Assuming that the switch from either hibernation or reawakening is dependent on cell-to-cell interaction, i.e., $q = q(u)$, and $p = p(u)$, the Jacobian at E^* is given by

$$J(E^*) = \begin{pmatrix} -sp(u^*) & rq(u^*) + rq'(u^*)u^* - sp'(u^*)w^* & 0 \\ sp(u^*) & -rq(u^*) - rq'(u^*)u^* + sp'(u^*)w^* & u^*f'(v^*) \\ 0 & \alpha\beta g'(u^*) - f(v^*) & -\alpha - u^*f'(v^*) \end{pmatrix}.$$

Using the fact that at equilibrium $rq(u^*)u^* = sp(u^*)w^*$, the characteristic equation for $J(E^*)$ has the following coefficients,

$$\begin{aligned}
s_1 &= rq(u^*) + rq'(u^*)u^* + sw^*\left(\frac{p(u^*)}{u^*} - p'(u^*)\right) + (\alpha + u^*f'(v^*)), \\
s_2 &= (\alpha + u^*f'(v^*))\left(sp(u^*) + rq(u^*) + rq'(u^*)u^* - sp'(u^*)w^*\right) \\
&\quad - u^*f'(v^*)\left\{\alpha\beta g'(u^*) - f(v^*)\right\} \\
&= (\alpha + u^*f'(v^*))\left\{sp(u^*) + rq'(u^*)u^* + sw^*\left(\frac{p(u^*)}{u^*} - p'(u^*)\right)\right\} \\
&\quad + u^*f'(v^*)\left\{1 - \alpha\beta g'(u^*)\right\}, \\
s_3 &= sp(u^*)u^*f'(v^*)\left\{1 - \alpha\beta g'(u^*)\right\}.
\end{aligned}$$

Furthermore, we see that

$$\frac{p(u^*)}{u^*} - p'(u^*) > 0,$$

using Hypothesis $\mathcal{F}_1$ and [161, Proposition 4.1]. Assuming $sp(u^*) + rq'(u^*)u^* \geq 0$ and $1 - \alpha\beta g'(u^*) > 0$, then the trace given by $-s_1$ is negative, the second-Hurwitz determinant, $\Delta_2 = s_1s_2 - s_3$, is also positive and the equilibrium will be asymptotically stable locally. However, under $sp(u^*) + rq'(u^*)u^* < 0$, Δ_2 can be zero and there is a possibility that E^* can be unstable through a Hopf bifurcation leading to oscillatory solutions. This will be illustrated numerically in Fig. 2.2.

Case 3: Assuming that the switch from hibernation to reawakening is dependent on cell-to-cell interaction and switching from active to hibernation is dependent on the

nutrient, i.e., $q(u)$ and $p(v)$, then the Jacobian at the coexistence equilibrium is

$$J(E^*) = \begin{pmatrix} -sp(v^*) & rq(u^*) + rq'(u^*)u^* & -sp'(v^*)w^* \\ sp(v^*) & -rq(u^*) - rq'(u^*)u^* & u^*f'(v^*) + sw^*p'(v^*) \\ 0 & \alpha\beta g'(u^*) - f(v^*) & -\alpha - u^*f'(v^*) \end{pmatrix}.$$

The coefficients of the characteristic equation are

$$\begin{aligned} s_1 &= r(u^*q(u^*))' + sp(v^*) + (\alpha + u^*f'(v^*)), \\ s_2 &= (\alpha + u^*f'(v^*))\left[sp(v^*) + r(u^*q(u^*))'\right] + u^*f(v^*)f'(v^*) \\ &\quad + \{1 - \alpha\beta g'(u^*)\}(u^*f'(v^*) + sp'(v^*)w^*), \\ s_3 &= sp(v^*)u^*f'(v^*)\{1 - \alpha\beta g'(u^*)\}. \end{aligned}$$

Under assumption $\mathcal{F}_2$, $(u^*q(u^*))' \geq 0$. The trace given by $-s_1$ is negative. Assuming $1 - \alpha\beta g'(u^*) > 0$, all the coefficients of the characteristic equation are positive and the second-Hurwitz determinant given by $\Delta_2 = s_1s_2 - s_3$ is positive, hence, E^* is asymptotically stable, locally, when $q = q(u)$ and $p = p(v)$.

Case 4: Finally, assuming that the switch from hibernation to reawakening is dependent on the nutrient and switching from active to hibernation is dependent on cell-to-cell interaction, i.e., $q(v)$ and $p(u)$, we have

$$J(E^*) = \begin{pmatrix} -sp(u^*) & rq(v^*) - sp'(u^*)w^* & rq'(v^*)u^* \\ sp(u^*) & -rq(v^*) + sp'(u^*)w^* & u^*f'(v^*) - rq'(v^*)u^* \\ 0 & \alpha\beta g'(u^*) - f(v^*) & -\alpha - u^*f'(v^*) \end{pmatrix},$$

with the coefficients of the characteristic equation given by

$$\begin{aligned} s_1 &= s[p(u^*) - w^*p'(u^*)] + rq(v^*) + (\alpha + u^*f'(v^*)) \\ &= sw^*\left(\frac{p(u^*)}{u^*} - p'(u^*)\right) + sp(u^*) + (\alpha + u^*f'(v^*)), \\ s_2 &= s(\alpha + u^*f'(v^*))(p(u^*) - w^*p'(u^*)) + rq(v^*)(\alpha + u^*f'(v^*)) \\ &\quad + (u^*f'(v^*) - rq'(v^*)u^*)\{1 - \alpha\beta g'(u^*)\} \\ &= (\alpha + u^*f'(v^*))sw^*\left(\frac{p(u^*)}{u^*} - p'(u^*)\right) + sp(u^*)(\alpha + u^*f'(v^*)) \\ &\quad + (u^*f'(v^*) - rq'(v^*)u^*)\{1 - \alpha\beta g'(u^*)\}, \\ s_3 &= sp(u^*)u^*f'(v^*)\{1 - \alpha\beta g'(u^*)\}. \end{aligned}$$

Clearly the trace, $-s_1$, is negative where we have used Hypothesis $\mathcal{G}$. Assuming $1 - \alpha\beta g'(u^*) > 0$, the other coefficients are positive. In addition, we have that

$\Delta_2 = s_1 s_2 - s_3$, is positive.

We summarise the results for the uniform steady state in Proposition 2.3 and Table 2.1. In particular, the equilibria are either locally asymptotically stable (LAS) or may become unstable through Hopf bifurcation leading to oscillatory solutions (boom-and-bust). Numerical illustrations supporting the theoretical analysis for the uniform steady state are provided in Section 2.3.2.

Proposition 2.3. *Consider the nonlinear system (2.4).*

(i) Assume $1 - \alpha\beta g'(u^*) > 0$. *If* $p = p(v)$ *and* $q = q(v)$, *the co-existence equilibrium is locally asymptotically stable.*

(ii) Assume $1 - \alpha\beta g'(u^*) > 0$. *If* $p = p(u)$ *and* $q = q(u)$, *the co-existence equilibrium is locally asymptotically stable provided* $sp(u^*) + rq'(u^*)u^* \geq 0$.

(iii) Assume $1 - \alpha\beta g'(u^*) > 0$. *If* $p = p(v)$ *and* $q = q(u)$, *the co-existence equilibrium is locally asymptotically stable.*

(iv) Assume $1 - \alpha\beta g'(u^*) > 0$. *If* $p = p(u)$ *and* $q = q(v)$, *the co-existence equilibrium is locally asymptotically stable.*

Table 2.1: Summary of Propositions 2.1, 2.2 and 2.3. The equilibrium points are locally asymptotically stable (LAS), unstable or we see sustained oscillatory solutions (boom-and-bust).

Equil.	Case	Sufficient condition	Necessary condition	Dynamics
E_0	$p(u_2)$, $q(u_1)$		$f(\beta g(0)) > 1$	Unstable
			$f(\beta g(0)) < 1$	LAS
E^*	$p(v)$, $q(v)$		$1 - \alpha\beta g'(u^*) > 0$	LAS
E^*	$p(u)$, $q(u)$	$sp(u^*) + rq'(u^*)u^* \geq 0$	$1 - \alpha\beta g'(u^*) > 0$	LAS
		$sp(u^*) + rq'(u^*)u^* < 0$	$1 - \alpha\beta g'(u^*) > 0$	boom and bust
E^*	$p(v)$, $q(u)$		$1 - \alpha\beta g'(u^*) > 0$	LAS
E^*	$p(u)$, $q(v)$		$1 - \alpha\beta g'(u^*) > 0$	LAS

Remark 2.1. *A comment on the condition* $1 - \alpha\beta g'(u^*) < 0$ *is necessary. From the existence results in Proposition 2.1 and stability results summarised in Proposition 2.3 (and Table 2.1), this condition corresponds to a locally asymptotically stable bacteria-free state,* E_0, *and unstable coexistence equilibrium,* E^*, *irrespective of the dependence in the switch functions. In particular, this describes the dynamics of the model under poor-nutrient conditions.*

2.3.2 Numerical simulations

We recall the differential model (2.4). In this section, we propose a nonstandard-finite difference scheme to solve the system of equations (2.4). Since the pioneering monograph by Mickens on the subject [120], the nonstandard finite difference method has been applied successfully to solve several differential models in the applied sciences, see [7] for a latest review. We let $(w^n, u^n, v^n)^T$ denote an approximation of $(w(t_n), u(t_n), v(t_n))^T$ where $t_n = n\Delta t$, with $n \in \mathbb{N}$ and $\Delta t > 0$. First, we see that equation (2.5) has an exact scheme

$$\frac{\eta^{n+1} - \eta^n}{e^{\alpha_m \Delta t} - 1} \leq \frac{\beta_*}{\alpha_m} - \eta^{n+1}.$$

The above numerical scheme approximating equation (2.5) is called exact whenever the difference equation and the differential equation (2.5) have the same general solutions at the discrete point $t = t_n$. Also, with $\eta(t)$ being the solution of (2.5) we have that $\eta^n = \eta(t_n)$ [28].

Using this, we propose the following scheme

$$\begin{aligned}
\frac{w^{n+1} - w^n}{\psi(\Delta t)} &= rq(a^n)u^n - sp(b^n)w^{n+1} - w^{n+1}, \\
\frac{u^{n+1} - u^n}{\psi(\Delta t)} &= v^n h(v^n)u^n - u^{n+1} - rq(a^n)u^{n+1} + sp(b^n)w^{n+1}, \\
\frac{v^{n+1} - v^n}{\psi(\Delta t)} &= \alpha\left(\beta g(u^n) - v^{n+1}\right) - v^{n+1}h(v^n)u^{n+1},
\end{aligned} \tag{2.7}$$

for model (2.4), where $\psi(\Delta t) = e^{\alpha_m \Delta t} - 1$. The above equations can be rewritten in the form

$$\begin{aligned}
w^{n+1} &= \frac{w^n + r\psi(\Delta t)q(a^n)u^n}{1 + \psi(\Delta t) + s\psi(\Delta t)p(b^n)}, \\
u^{n+1} &= \frac{u^n + \psi(\Delta t)v^n h(v^n)u^n + s\psi(\Delta t)p(b^n)w^{n+1}}{1 + \psi(\Delta t) + r\psi(\Delta t)q(a^n)}, \\
v^{n+1} &= \frac{v^n + \psi(\Delta t)\alpha\beta g(u^n)}{1 + \alpha\psi(\Delta t) + \psi(\Delta t)h(v^n)u^{n+1}}.
\end{aligned} \tag{2.8}$$

Thus, assuming $w^n \geq 0,\ u^n \geq 0,\ \ v^n \geq 0$, then

$$w^{n+1} \geq 0, \quad u^{n+1} \geq 0, \quad \text{and} \quad v^{n+1} \geq 0,$$

for any step size $\Delta t > 0$. Therefore, the nonstandard finite difference scheme (2.7) is dynamically consistent with respect to the positivity of solutions and preservation of fixed points.

There is a vast amount of literature on the structure of the transition functions. For example, the work [58] discussed to a greater extent the functions $q(a)$ and $p(b)$. The authors considered the transition between active and quiescent state by awakening and

hibernation functions p and q, respectively, each being $\in (0,1)$ which can be thought of as probabilities of the population to switch states. There are several examples of species that undergo a quiescence state. Namely, seeds [67], cancer cells [67, 69, 68], to name a few. Furthermore, the work [14] on microbial dormancy was focused on batch cultures as a function of substrate-dependent mortality. In [90] they presented a multi-species model indicating that dormancy and environmental cues interact to influence the biodiversity of microbial communities. In the work, they assumed a negative correlation between cues for entrance into dormancy and reawakening from dormancy and used $1 - p(u_2)$ as the proportion of active cells entering the dormant state. We extend this discussion here to study the dynamics of model (2.4) under various assumptions on the switch functions. In particular, the asymptotic behaviour when the transition is either a response to the rate-limiting nutrient concentration level or a result of paracrine signalling.

We will now present numerical simulations, Figs. 2.1 – 2.4, to support the cases summarised in Proposition 2.3. Throughout, we assume that $f(v) = v$ and

$$g(u) = 1 + \frac{u^{\upsilon}}{1 + u^{\upsilon}}, \tag{2.9}$$

and take $\upsilon = 1$. As summarised in Table 2.1, it is the choice of switch functions and the switching rates that determine the dynamics of the model, in particular, in Case 2. Following [58], the dimensional hibernation function takes the form

$$q(a) = \frac{1}{1 + a^m}, \tag{2.10}$$

while the arousal function takes the modified version

$$p(b) = \frac{\delta + b^m}{1 + b^m}, \tag{2.11}$$

where m is a positive integer. The modified arousal function is important since no activation is possible using the simple Hill function $b^m/(1+b^m)$. In this context, δ defines the minimum concentration/density at which the switch can take place. In the numerical tests given in Fig. 2.1 – 2.4, we provide simulations for $\delta = 0.1$. For simulations not shown here, we highlight that smaller values of δ amplifies the oscillatory behaviour which disappears for larger values, see Fig 2.2. In fact, in the limit $\delta \to 0$, the state $b = 0$ will not be activated. The rest of the parameters, unless stated differently in the figure caption, are given as follows: $r = s = 1$ and $m = 5$ (for the Hill functions in (2.10) and (2.11)).

Also, under poor-nutrient conditions or unfavourable conditions for proliferation, $f(\beta) - 1 < 0$, the microbial population goes extinct irrespective of the dependence in the switch functions. That is, all trajectories will converge to the microbial-free equilibrium, see Figs. 2.1-2.4.

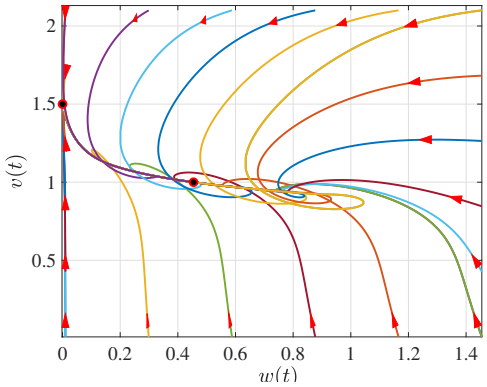

(a) Phase plane for $\beta > v^*$.

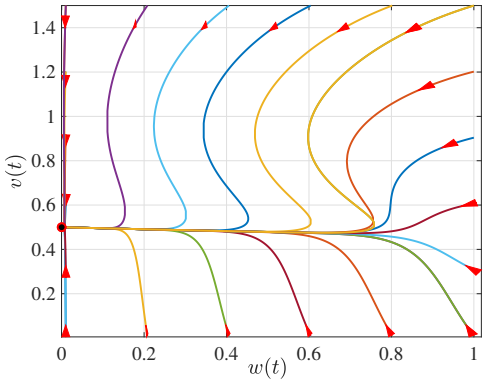

(b) Phase plane for $\beta < v^*$.

Figure 2.1: Case 1: In this case $p = p(v)$, $q = q(v)$ with $\alpha = 0.5$. In (a) $\beta = 1.1$ and all trajectories converge to the coexistence equilibrium point and in (b) $\beta = 0.5$ and all trajectories converge to the microbial-free equilibrium.

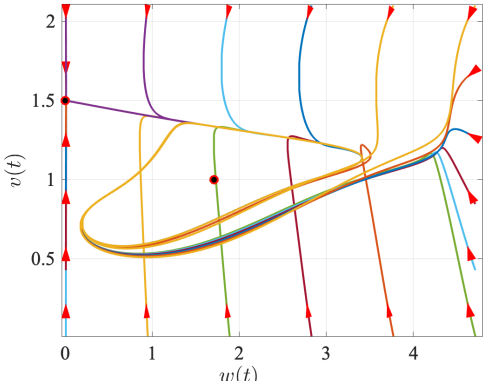

(a) Phase plane with $\beta > v^*$.

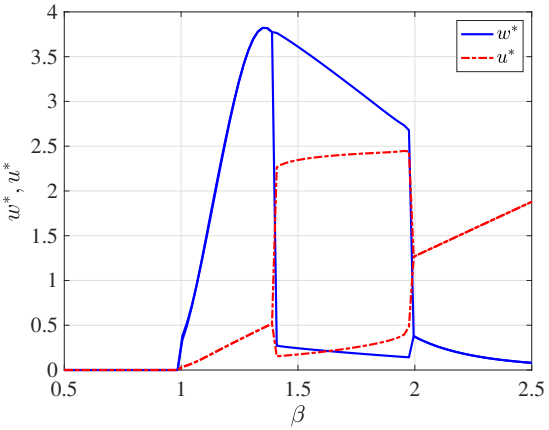

(b) Bifurcation with respect to β.

Figure 2.2: Case 2: In this case $p = p(u)$, $q = q(u)$ with $\alpha = 0.7$. The bifurcation figure shows the transition from stable state through Hopf bifurcation leading to oscillatory solutions. Figure (b) shows the minimal and maximal values of dormant (solid line) and active biomass (broken line).

Remark 2.2. *From here forthwith, we assume* $1 - \alpha\beta g'(u^*) > 0$ *and* $f(\beta) - 1 > 0$. *The first condition,* $1 - \alpha\beta g'(u^*) > 0$, *is necessary and of interest since it corresponds to the existence, uniqueness and local stability of* E^*. *Biologically, this condition implies that the biomass is sustained if the nutrient supply remains above a certain threshold value,* β.

Remark 2.3. *In boom-and-bust cases, hibernation is a result of cell-to-cell interaction, other than the availability of a nutrient. Thus, the dependence of switch functions on cell-to-cell interaction is of importance in explaining the occurrence of self-sustained oscillations in microbial populations, see Fig. 2.5.*

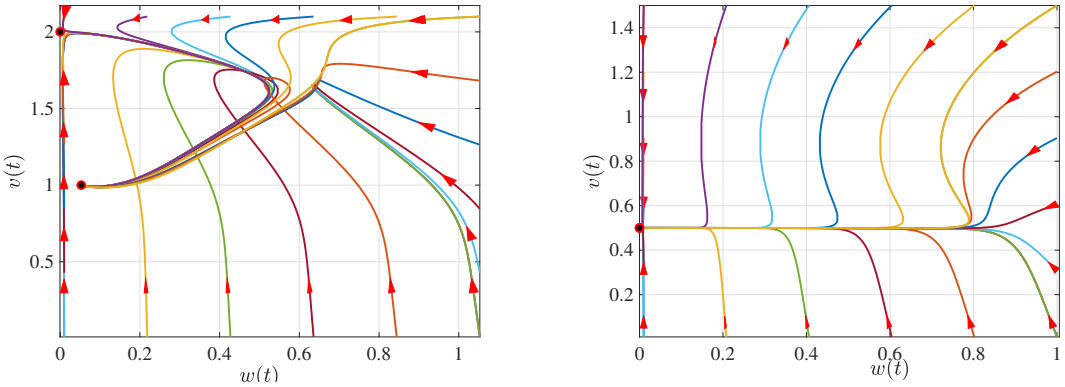

(a) Phase plane for $\beta > v^*$. (b) Phase plane for $\beta < v^*$.

Figure 2.3: Case 3: In this case $p = p(v),\ q = q(u)$ with $\alpha = 1.0$. In (a) $\beta = 2.0$ and all trajectories converge to the coexistence equilibrium point and in (b) $\beta = 0.5$ and all trajectories converge to the microbial-free equilibrium.

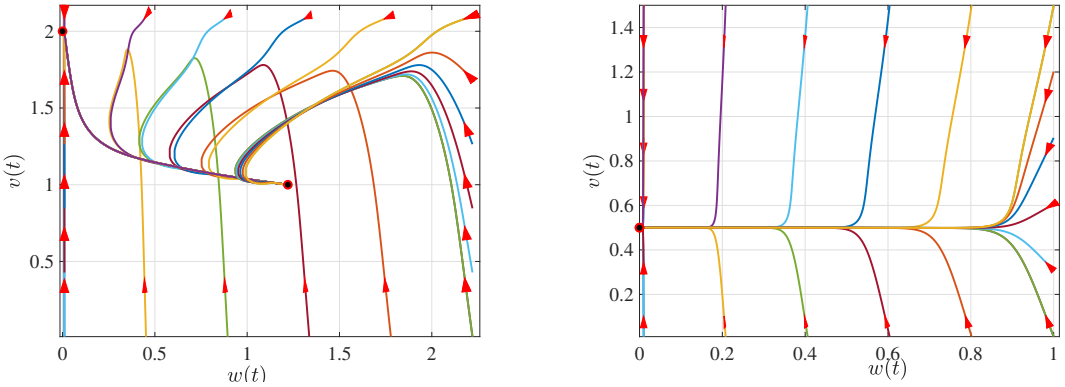

(a) Phase plane for $\beta > v^*$. (b) Phase plane for $\beta < v^*$.

Figure 2.4: Case 4: In this case $p = p(u),\ q = q(v)$ with $\alpha = 1.0$. In (a) $\beta = 2.0$ and all trajectories converge to the coexistence equilibrium point and in (b) $\beta = 0.5$ and all trajectories converge to the microbial-free equilibrium.

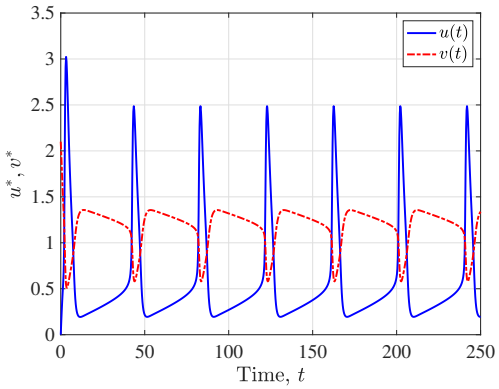

Figure 2.5: Illustration of self-sustained oscillations in microbial populations when $p = p(u)$ and $q = q(u)$ with $\alpha = 0.7$ and $\beta = 1.5$.

Remark 2.4. *It is worth making a remark regarding the model formulation vis-á-vis the existence of plankton blooms (oscillatory solution). If we neglect the dormant state, then we have a simple model*

$$\begin{aligned} \frac{du}{dt} &= (f(v)-1)u, \\ \frac{dv}{dt} &= \alpha(\beta g(u)-v) - uf(v), \end{aligned} \tag{2.12}$$

with two nonzero equilibrium as before. The local stability of both equilibria remains the same, with E^* locally asymptotically stable provided $f(\beta) > 1$. This result, including Proposition 2.3, is consistent with the findings in [58]. Particularly, this formulation is not capable of explaining the observed oscillatory behavior in plankton populations.

2.4 Travelling waves

From the simplest to the most complex biological levels of organisation, quiescence may occur in various phenomena and different names are given to describe diverse cases. For instance, mammals hibernate, genes become suppressed, tumor cells become dormant, and nerve cells rest. The previous section focused on the temporal nutrient-microbial interaction model with an assumption of homogeneous distribution. In practice, model (2.4) is not realistic, the space component is thereof very important since the active population direct their movement towards the highest concentration of the nutrient for uptake to occur, resulting in proliferation, see for example [111, 157]. The dispersal of active population and the limiting nutrient are considered.

2.4.1 Existence of traveling waves

In this section, we are interested in the case where the switch of a state depends on the availability of limiting nutrient. Other forms can also be considered. We recall the partial differential equation model (2.3), which we restate as follows

$$\boldsymbol{u}_t = D\boldsymbol{u}_{xx} + \boldsymbol{f}(\boldsymbol{u}), \quad x \in \mathbb{R},\ t > 0, \tag{2.13}$$

where

$$\boldsymbol{u} = (w,u,v)^t, \quad D = \operatorname{diag}(0,1,d_v), \quad \boldsymbol{f}(\boldsymbol{u}) = \begin{pmatrix} rq(v)u - sp(v)w \\ (f(v)-1)u - rq(v)u + sp(v)w \\ \alpha\left(\beta g(u) - v\right) - uf(v) \end{pmatrix}. \tag{2.14}$$

A traveling-wave solution for system (2.13) is a nonnegative and bounded solution in the form of $\boldsymbol{u}(x,t) = (w(x,t),u(x,t),v(x,t))^T = (w(z),u(z),v(z))^T$, $z = x + \zeta t$, where $\zeta > 0$ is referred to as the traveling-wave speed. We seek to find a traveling wave

which can be viewed as a heteroclinic orbit connecting the two equilibria, $\mathbf{1}$ and $\mathbf{0}$. We now assume constant conversion rates, and substituting $\boldsymbol{u}(x,t) = (w(z), u(z), v(z))^T$ into (2.13) we obtain

$$\begin{cases} \zeta w' = rqu - spw, \\ \zeta u' = u'' + (f(v) - 1)u - rqu + spw, \\ \zeta v' = d_v v'' + \alpha(\beta g(u) - v) - uf(v), \end{cases} \tag{2.15}$$

where the prime denotes differentiation with respect to z. The asymptotic conditions for (2.15) are given as follows

$$\begin{cases} w(-\infty) = w^*, \quad w(\infty) = 0, \\ u(-\infty) = u^*, \quad u(\infty) = 0, \\ v(-\infty) = v^*, \quad v(\infty) = \beta. \end{cases} \tag{2.16}$$

The existence and uniqueness of the oscillatory/monotone traveling waves have been studied, [33]. Below, we describe the needed results.

First, we study the eigenvalue problem of the wave profile at the bacteria-free state $\mathbf{0} = (0, 0, \beta)^t$. Linearising the equations at the bacteria-free point yields

$$\begin{cases} \zeta w' = rqu - spw, \\ \zeta u' = u'' + u(f(\beta) - 1) - rqu + spw, \\ \zeta v' = d_v v'' + \alpha(u\beta g'(0) - v) - uf(\beta). \end{cases} \tag{2.17}$$

We further reduce the number of equations in (2.17) to two. Indeed, together with boundary conditions (2.16) we use equation $(2.17)_1$ to express $w(z)$ in terms of $u(z)$, i.e.,

$$w(z) = \frac{rq}{\zeta} \int_{-\infty}^{z} u(\xi) e^{\frac{-sp}{\zeta}(z-\xi)} d\xi. \tag{2.18}$$

Substituting (2.18) into (2.17) leads to

$$\begin{aligned} \zeta u' &= u'' + u(f(\beta) - 1) - rqu + \frac{sprq}{\zeta} \int_{-\infty}^{z} u(\xi) e^{-\frac{sp}{\zeta}(z-\xi)} d\xi, \\ \zeta v' &= d_v v'' + \alpha(u\beta g'(0) - v) - uf(\beta). \end{aligned} \tag{2.19}$$

By substituting $v(z) = e^{\lambda z}$ into $(2.19)_1$, we have the characteristic equation

$$\lambda^2 - \zeta\lambda + (f(\beta) - 1) - rq + \frac{sprq}{\zeta(\lambda + sp/\zeta)} = 0, \tag{2.20}$$

or

$$P(\lambda) = \lambda^3 + a_2\lambda^2 + a_1\lambda + a_0, \tag{2.21}$$

with

$$\begin{aligned} a_2 &= \frac{sp}{\zeta} - \zeta, \\ a_1 &= (f(\beta) - 1) - sp - rq, \\ a_0 &= \frac{sp}{\zeta}(f(\beta) - 1). \end{aligned}$$

Now, we have two cases depending on the sign of a_1: $f(\beta) - 1 < sp + rq$ or $f(\beta) - 1 \geq sp + rq$. As we will see later in the discussion of Lemma 2.1, the case $f(\beta) - 1 > sp + rq$ does not guarantee the existence of $\zeta^* > 0$, and will not be considered further.

Lemma 2.1. *Assume $f(\beta) - 1 > 0$. Then there exists $\zeta^* > 0$ and $\lambda^* > 0$ such that*

$$P(\lambda^*) = 0, \quad \text{and} \quad \frac{\partial P}{\partial \lambda}\Big|_{\lambda=\lambda^*} = 0. \tag{2.22}$$

The result in Lemma 2.1 is similar to the discussion in [195, Section 3]. For completeness, we will provide an outline of the proof here. Since $f(\beta) - 1 > 0$, we see that (2.22) has one negative root and two roots with positive real parts. By calculation, to identify the conditions under which these two roots are positive real numbers, we have

$$\begin{aligned} P(0, \zeta) &= \frac{sp}{\zeta}(f(\beta) - 1) > 0, \\ P_1(\lambda) := \frac{1}{3}\frac{\partial P}{\partial \lambda} &= \lambda^2 + \frac{2}{3}\left(\frac{sp}{\zeta} - \zeta\right) + \frac{1}{3}\left((f(\beta) - 1) - sp - rq\right). \end{aligned}$$

We see that $P_1(\lambda)$ has a unique positive root

$$\lambda^* = \frac{1}{3}\frac{\zeta^2 - sp + \sqrt{\zeta^4 + sp[\zeta^2 + sp] - 3\zeta^2[f(\beta) - 1) - rq]}}{\zeta}, \tag{2.23}$$

provided $f(\beta) - 1) \leq rq$. Since $P(0, \zeta)$ is positive, then equation (2.21) has two positive roots if and only if $P(\lambda^*) < 0$, otherwise, there exists two complex roots with positive real parts if $P(\lambda^*) > 0$.

To obtain an equation for the minimal wave speed, we transform (2.21) to get an expression giving its discriminant, i.e., an expression in terms of the parameters. Suppose

$$\begin{aligned} P(\lambda) &= P_1(\lambda)Q_1(\lambda) + R_1(\lambda), \\ P_1(\lambda) &= R_1(\lambda)Q_2(\lambda) + R_2(\zeta, \beta), \end{aligned}$$

where $Q_1(\lambda)$, $R_1(\lambda)$ are the quotient and remainder terms when $P(\lambda)$ is divided by $P_1(\lambda)$, respectively. Similarly, $Q_2(\lambda)$, $R_2(\zeta, \beta)$ are the quotient and remainder terms of $P_1(\lambda)$ divided by $R_1(\lambda)$. Obviously, when $R_2(\zeta, \beta) = 0$, then $P(\lambda^*) = P_1(\lambda^*) = 0$. The sign of

$-R_2(\zeta,\beta)$ is determined by

$$\Delta(\zeta,\beta) = b_0\zeta^6 + b_1\zeta^4 + b_2\zeta^2 + b_3, \tag{2.24}$$

where

$$\begin{aligned}
b_0 &= (sp)^2 + 2sp(f(\beta) - 1 + rq) + (rq - (f(\beta) - 1))^2,\\
b_1 &= 2(sp)^3 + 2(sp)^2(4rq - (f(\beta) - 1)) + 2sp(5rq + 4(f(\beta) - 1)(rq - (f(\beta) - 1))\\
&\quad + 4(rq - (f(\beta) - 1))^3,\\
b_2 &= (sp)^4 + 2(sp)^3(rq - 4(f(\beta) - 1)) + (sp)^2((rq)^2 - 20rq(f(\beta) - 1) - 8(f(\beta) - 1)^2),\\
b_3 &= -4(sp)^4(f(\beta) - 1).
\end{aligned}$$

By the method of linearization, we have shown that system (2.15) admits the minimal wave speed, ζ^*, which is the unique root of (2.24). Thus, it remains to show the existence of traveling wave solution for system (2.15).

We state the main result for the existence of traveling wave solutions of system (2.13).

Theorem 2.2. *Assume $f(\beta) - 1 \leq rq$ and $f(\beta) - 1 > 0$. Then there exists a minimal wave speed $\zeta^* > 0$, which is a unique positive root of (2.24). When $\zeta \geq \zeta^*$, the system has a traveling wave solution satisfying boundary conditions (2.16). When $0 < \zeta < \zeta^*$, system (2.13) has no traveling wave solution satisfying conditions (2.16).*

Theorem (2.2) will be proved through several lemmas, see for example [195, 194, 182]. We will construct a pair of upper and lower solutions for the system (2.19) to show the existence of traveling wave solutions using an auxiliary system. To obtain this, we first investigate the distribution of roots of the characteristic equation (2.21) and set

$$l_1 = a_1 - \frac{a_2^2}{3}, \quad l_2 = \frac{2a_2^3}{27} - \frac{a_1a_2}{3} + a_0, \quad \triangle_0 = \frac{l_2^2}{4} + \frac{l_1^3}{27},$$

and introduce the following lemma from [194] and references therein.

Lemma 2.2. *The following hold:*

(i) If $\triangle_0 > 0$, then (2.21) has one real root and two complex conjugates;

(ii) if $\triangle_0 = 0$, then (2.21) has two real roots, with one having algebraic multiplicity 2;

(iii) if $\triangle_0 < 0$, then (2.21) has three distinct real roots.

From the above Lemma (2.2), we obtain the following results on the distribution of roots (2.21).

Lemma 2.3. *Assume $f(\beta) - 1 \leq rq$ and $f(\beta) - 1 > 0$. Then there exist a constant $\zeta^* > 0$ which is a unique root of (2.24) such that*

(a) if $0 < \zeta < \zeta^*$, (2.21) *has a negative real root and two complex conjugate roots with positive real parts;*

(b) if $\zeta = \zeta^*$, (2.21) *has a negative real root and a positive real multiple root;*

(c) $\zeta > \zeta^*$, (2.21) *has a negative real root and two different positive real roots.*

Proof. From equation (2.24), we notice that $b_0 > 0$, $b_1 > 0$ provided $f(\beta) - 1 \leq rq$ and $b_3 < 0$ since $f(\beta) - 1 > 0$. Using *Descarte*'s rule of signs, it follows that there is a unique $\zeta^* > 0$ such that $\Delta(\zeta^*, \beta) = 0$, and this implies

$$\Delta(\zeta, \beta) \begin{cases} < 0 & \text{if} \quad \zeta \in (0, \zeta^*), \\ = 0 & \text{if} \quad \zeta = \zeta^*, \\ > 0 & \text{if} \quad \zeta > \zeta^*. \end{cases} \tag{2.25}$$

Direct calculations show that $P(\lambda^*) = P_1(\lambda^*) = 0$ is valid when $\zeta = \zeta^*$ and $P(\lambda)$ is a decreasing function of ζ. Hence, we conclude that for $\zeta > \zeta^*$, $P(\lambda^*) < 0$ (we have two positive roots), for $\zeta \in (0, \zeta^*)$, $P(\lambda^*) > 0$, (we have two complex roots), and we have only one positive root if $\zeta = \zeta^*$. It follows from Lemma 2.2 and Descarte's rule of signs that conditions $(a) - (b)$ hold. □

In order to use the method of constructing lower and upper solutions, we begin with the following result.

Lemma 2.4. *Suppose that* $y \in C^2(\mathbb{R}, \mathbb{R})$ *and* y, y' *and* y'' *are bounded on* $\mathbb{R}$. *If*

$$\zeta y'(z) \geq y''(z) + (f(\beta) - 1 - rq)y(z), \quad \forall z \in \mathbb{R},$$

then $y(z) \geq 0$, $\forall z \in \mathbb{R}$.

Proof. Let

$$x(z) = \zeta y'(z) - y''(z) - (f(\beta) - 1 - rq)y(z), \quad z \in \mathbb{R}.$$

Then $x(z)$ is a nonnegative, continuous and bounded function on $\mathbb{R}$, and we have that $x(z)$ satisfies the linear equation

$$y''(z) - \zeta y'(z) + (f(\beta) - 1 - rq)y(z) + x(z) = 0, \quad z \in \mathbb{R}. \tag{2.26}$$

Using the theory of second-order linear ordinary differential equations, we obtain

$$y(z) = c_1 e^{\gamma_1 z} + c_2 e^{\gamma_2 z} \tag{2.27}$$

$$+ \frac{1}{\gamma_2 - \gamma_1} \left(\int_{-\infty}^{z} e^{\gamma_1 (z-\xi)} x(\xi) d\xi + \int_{z}^{\infty} e^{\gamma_2 (z-\xi)} x(\xi) d\xi \right), \tag{2.28}$$

where

$$\gamma_1 = \frac{\zeta - \sqrt{\zeta^2 - 4(f(\beta) - 1 - rq)}}{2} < 0, \quad \gamma_2 = \frac{\zeta + \sqrt{\zeta^2 - 4(f(\beta) - 1 - rq)}}{2} > 0$$

provided $f(\beta) - 1 \leq rq$.

Since $y(z)$ and $x(z)$ are bounded on $\mathbb{R}$, we have that $c_1 = c_2 = 0$. As a result, $y(z) \geq 0$, $\forall z \in \mathbb{R}$ since $x(z)$ is nonnegative on $\mathbb{R}$. □

Let $X = BUC(\mathbb{R}, \mathbb{R})$ be the *Banach* space of the functions that are uniformly continuous and bounded from $\mathbb{R}$ to $\mathbb{R}$. We define a continuous mapping $B(\phi)(z)$ as follows

$$B(\phi)(z) = \frac{sprq}{\zeta(\gamma_2 - \gamma_1)} \left\{ \int_{-\infty}^{z} e^{\gamma_1(z-\xi)} d\xi \int_{-\infty}^{\xi} e^{-\frac{sp}{\zeta}(\xi-\theta)} \phi(\theta) d\theta + \int_{z}^{\infty} e^{\gamma_2(z-\xi)} d\xi \int_{-\infty}^{\xi} e^{-\frac{sp}{\zeta}(\xi-\theta)} \phi(\theta) d\theta \right\}. \tag{2.29}$$

We see that the first and the second order derivatives of $B(\phi)(z)$ with respect to z are bounded on $\mathbb{R}$, moreover, $B(\phi)(z)$ is the unique bounded solution $\mathbb{R}$ to the linear ordinary differential equation

$$\zeta y'(z) = y''(z) + y(z)(f(\beta) - 1 - rq) + \frac{sprq}{\zeta} \int_{-\infty}^{z} \phi(\xi) e^{-\frac{sp}{\zeta}(z-\xi)} d\xi.$$

Clearly, any fixed point of B in X is a solution of equation $(2.19)_1$ [195].

Since it is challenging to construct upper and lower solutions for system (2.19), the authors in [194] proposed and constructed an auxiliary system to overcome the problem. As a result, we propose the auxiliary system given as

$$\begin{aligned} \zeta u' &= u'' + u(f(\beta) - 1) - rqu + \frac{sprq}{\zeta} \int_{-\infty}^{z} u(\xi) e^{-\frac{sp}{\zeta}(z-\xi)} d\xi - \alpha_2 u^2, \\ \zeta v' &= d_v v'' + \alpha(u\beta g'(0) - v) - uf(\beta), \end{aligned} \tag{2.30}$$

and assume $f(\beta) - 1 \leq rq$ with $f(\beta) - 1 > 0$.

Consider the case where $\zeta > \zeta^*$. To construct the upper and lower solutions, we let $\lambda_1 < \lambda_2$ be two positive roots of equation (2.21) and define

$$\begin{aligned} \underline{v}(\xi) &= \max\{v^0 - \sigma e^{\alpha_1 \xi}, 0\}, \\ \overline{u}(\xi) &= \min\{e^{\lambda_1 \xi}, u^0\}, \\ \underline{u}(\xi) &= \max\{e^{\lambda_1 \xi}\left(1 - Ee^{\varepsilon \xi}\right), 0\}, \end{aligned}$$

where $u^0 > \max\{1, (f(\beta) - 1)/\alpha_2\}$. The positive constants $\alpha_1, \sigma, \varepsilon, u^0, v^0$ and E will be

determined in the lemmas that follow.

Lemma 2.5. *Function $\overline{u}(\xi)$ satisfies the inequality*

$$\zeta\overline{u}' \geq \overline{u}'' + \overline{u}(f(\beta)-1) - rq\overline{u} + \frac{sprq}{\zeta}\int_{-\infty}^{z} \overline{u}(\xi)e^{-\frac{sp}{\zeta}(z-\xi)}d\xi - \alpha_2\overline{u}^2,$$

for any $\xi \neq \ln u^0/\lambda_1$.

Proof. Firstly, we assume that $\xi < \ln u^0/\lambda_1$. Therefore $\overline{u}(\xi) = e^{\lambda_1\xi}$. Since $\overline{u}(\xi)$ satisfies equation $(2.30)_1$, we have

$$\begin{aligned}
&\zeta\overline{u}' - \overline{u}'' - \overline{u}(f(\beta)-1) - rq\overline{u} - \frac{sprq}{\zeta}\int_{-\infty}^{z} \overline{u}(\xi)e^{-\frac{sp}{\zeta}(z-\xi)}d\xi + \alpha_2\overline{u}^2\\
&= e^{\lambda_1\xi}\left(\zeta\lambda_1 - \lambda_1^2 - (f(\beta)-1-rq) - \frac{sprq}{\zeta}\int_{-\infty}^{z} e^{\lambda_1\xi}e^{-\frac{sp}{\zeta}(z-\xi)}d\xi\right) + \alpha_2\left(e^{\lambda_1\xi}\right)^2\\
&= e^{\lambda_1\xi}P(\lambda_1) + \alpha_2\overline{u}^2\\
&= \alpha_2\overline{u}^2 \geq 0.
\end{aligned}$$

Secondly, we suppose that $\xi > \ln u^0/\lambda_1$ implying that $\overline{u}(\xi) = u^0$. Then we have

$$\begin{aligned}
&\zeta\overline{u}' - \overline{u}'' - \overline{u}(f(\beta)-1) - rq\overline{u} - \frac{sprq}{\zeta}\int_{-\infty}^{z} \overline{u}(\xi)e^{-\frac{sp}{\zeta}(z-\xi)}d\xi + \alpha_2\overline{u}^2\\
&= -u^0(f(\beta)-1-rq) - \frac{sprq}{\zeta}\int_{-\infty}^{z} u^0e^{-\frac{sp}{\zeta}(z-\xi)}d\xi + \alpha_2\left(u^0\right)^2\\
&= -u^0(f(\beta)-1) + \alpha_2\left(u^0\right)^2\\
&= u^0\left(\alpha_2u^0 - (f(\beta)-1)\right) > 0.
\end{aligned}$$

□

Lemma 2.6. *For $0 < \alpha_1 < \min\{\zeta/d_v, \lambda_1\}$ and $\sigma > \max\{v^0, \alpha v^0/(\zeta - d_v\alpha_1)\alpha_1\}$, the function $\underline{v}(\xi)$ satisfies*

$$\zeta\underline{v}' \leq d_v\underline{v}'' + \alpha(\overline{u}\beta g'(0) - \underline{v}) - \overline{u}f(\beta),$$

for any $\xi \neq 1/\alpha_1\ln(u^0/\sigma)$.

Proof. Since $u^0 > 1$, we have that $1/\alpha_1\ln(u^0/\sigma) < 0 < \ln u^0/\lambda_1$. When $v^0 - \sigma e^{\alpha_1\xi} < 0$, that is, if $\xi > 1/\alpha_1\ln(v^0/\sigma)$, then we have $\underline{v}(\xi) = 0$. Hence, we have that

$$\begin{aligned}
&-\zeta\underline{v}' + d_v\underline{v}'' + \alpha(\overline{u}\beta g'(0) - \underline{v}) - \overline{u}f(\beta).\\
&= \overline{u}\left(\alpha\beta g'(0) - f(\beta)\right) \geq 0,
\end{aligned}$$

provided $\alpha\beta g'(0) - f(\beta) \geq 0$. Thus, the lemma is true. Now, we consider the case where $\xi < 1/\alpha_1 \ln(v^0/\sigma)$. Then $\underline{v}(\xi) = v^0 - \sigma e^{\alpha_1 \xi}$, which leads to

$$\begin{aligned}
&- \zeta \underline{v}' + d_v \underline{v}'' + \alpha(\overline{u}\beta g'(0) - \underline{v}) - \overline{u} f(\beta) \\
&= \zeta \left(\sigma\alpha_1 e^{\alpha_1\xi}\right) - d_v \left(\sigma\alpha_1^2 e^{\alpha_1\xi}\right) + \alpha \left(e^{\lambda_1\xi}\beta g'(0) - v^0 + \sigma e^{\alpha_1\xi}\right) - e^{\lambda_1\xi} f(\beta) \\
&= \left[\zeta\sigma\alpha_1 - d_v\sigma\alpha_1^2 + \alpha\beta g'(0) e^{(\lambda_1-\alpha_1)\xi} - \alpha v^0 e^{-\alpha_1\xi} + \alpha\sigma - f(\beta) e^{(\lambda_1-\alpha_1)\xi}\right] e^{\alpha_1\xi} \\
&= \left[(\zeta - d_v\alpha_1)\sigma\alpha_1 + (\alpha\beta g'(0) - f(\beta))\, e^{(\lambda_1-\alpha_1)\xi} + \alpha\sigma - \alpha v^0 e^{-\alpha_1\xi}\right] e^{\alpha_1\xi} \\
&\geq \left[(\zeta - d_v\alpha_1)\sigma\alpha_1 - \alpha v^0 e^{-\alpha_1\xi}\right] e^{\alpha_1\xi} \\
&\geq \left[(\zeta - d_v\alpha_1)\sigma\alpha_1 - \alpha v^0\right] e^{\alpha_1\xi} \geq 0.
\end{aligned}$$

□

Lemma 2.7. *Let $\varepsilon < \alpha_1 < \min\{\lambda_1, \lambda_2 - \lambda_1\}/2$. Then for $E > 0$ sufficiently large, the function $\underline{u}(\xi)$ satisfies*

$$\zeta \underline{u}' \leq \underline{u}'' + \underline{u}(f(\beta) - 1 - rq) + \frac{sprq}{\zeta} \int_{-\infty}^{z} \underline{u}(\xi) e^{-\frac{sp}{\zeta}(z-\xi)} d\xi - \alpha_2 \underline{u}^2,$$

for any $\xi \neq 1/\varepsilon \ln(1/E)$.

Proof. Clearly, $\underline{v}(\xi) = 0$ if and only if $\xi \geq 1/\alpha_1 \ln(v^0/\sigma)$, $\underline{u}(\xi) = 0$ if and only if $\xi \geq 1/\varepsilon \ln(1/E)$, and $1/\varepsilon \ln(1/E) < 1/\alpha_1 \ln(v^0/\sigma)$ if and only if $E > (\sigma/v^0) e^{\alpha_1/\varepsilon}$. Assume $E > \max\{1, (\sigma/v^0)e^{\alpha_1/\varepsilon}\}$. When $\xi > 1/\varepsilon \ln(1/E)$, we have that $e^{\lambda_1\xi}\left(1 - Ee^{\varepsilon\xi}\right) < 0$ and $\underline{u}(\xi) = 0$, moreover, the inequality in Lemma 2.7 holds.

Now, we look at the case where $\xi < 1/\varepsilon \ln(1/E)$ which implies that $\xi < 0$ since $E > 1$. Then $\xi < 1/\alpha_1 \ln(v^0/\sigma)$, $\underline{v}(\xi) = v^0 - \sigma e^{\alpha_1\xi} > 0$ and $\underline{u}(\xi) = e^{\lambda_1\xi}\left(1 - Ee^{\varepsilon\xi}\right) > 0$. Let L and H be two linear operators defined by

$$L(\varphi)(z) := \varphi'' - \zeta\varphi' + \varphi(f(\beta) - 1 - rq), \quad \text{and} \quad H(\varphi)(z) := \frac{sprq}{\zeta} \int_{-\infty}^{z} \varphi(\xi) e^{-\frac{sp}{\zeta}(z-\xi)} d\xi.$$

It then follows that

$$\begin{aligned}
L(e^{\lambda\cdot})(z) &= \lambda^2 - \zeta\lambda + (f(\beta) - 1 - rq), \quad \forall z \in \mathbb{R}; \\
L(e^{\lambda\cdot})(z) + H(e^{\lambda\cdot})(z) &= \frac{P(\lambda)}{\zeta(\lambda + sp/\zeta)} e^{\lambda z}, \quad \forall z \in \mathbb{R}, \quad \lambda \geq 0.
\end{aligned}$$

□

Subsequently, it is sufficient to show that

$$
\begin{aligned}
&\underline{u}'' - \zeta\underline{u}' + \underline{u}(f(\beta) - 1 - rq) + \frac{sprq}{\zeta}\int_{-\infty}^{z} \underline{u}(\xi)e^{-\frac{sp}{\zeta}(z-\xi)}d\xi - \alpha_2\underline{u}^2 \\
&= e^{\lambda_1\xi}\left[\lambda_1^2 - \zeta\lambda_1 - E(\lambda_1+\varepsilon)^2e^{\varepsilon\xi} + \zeta E(\lambda_1+\varepsilon)e^{\varepsilon\xi} + \left(1 - Ee^{\varepsilon\xi}\right)(f(\beta) - 1 - rq)\right] \\
&+ e^{\lambda_1\xi}\left[\frac{sprq}{\zeta}e^{-\lambda_1\xi}\int_{-\infty}^{z} e^{\lambda_1\xi}\left(1 - Ee^{\varepsilon\xi}\right)e^{-\frac{sp}{\zeta}(z-\xi)}d\xi - \alpha_2 e^{\lambda_1\xi}\left(1 - Ee^{\varepsilon\xi}\right)^2\right] \\
&= e^{\lambda_1\xi}\left[\lambda_1^2 - \zeta\lambda_1 + (f(\beta) - 1 - rq) + \frac{sprq}{\zeta}e^{-\lambda_1\xi}\int_{-\infty}^{z} e^{\lambda_1\xi}e^{-\frac{sp}{\zeta}(z-\xi)}d\xi\right] \\
&+ e^{\lambda_1\xi}Ee^{\varepsilon\xi}\left[-(\lambda_1+\varepsilon)^2 + \zeta(\lambda_1+\varepsilon) - (f(\beta) - 1 - rq) - \frac{sprq}{\zeta}e^{-\lambda_1\xi}\int_{-\infty}^{z} e^{\lambda_1\xi}e^{-\frac{sp}{\zeta}(z-\xi)}d\xi\right] \\
&- \alpha_2 e^{\lambda_1\xi}\left(1 - Ee^{\varepsilon\xi}\right)^2 \\
&= e^{\lambda_1\xi}\left[-E(\lambda_1+\varepsilon)^2 + E\zeta(\lambda_1+\varepsilon) - E(f(\beta) - 1 - rq) - \alpha_2 e^{(\lambda_1-\varepsilon)\xi}\left(1 - Ee^{\varepsilon\xi}\right)^2\right]e^{\varepsilon\xi} \\
&- Ee^{\lambda_1\xi}\left[\frac{sprq}{\zeta}\int_{-\infty}^{z} e^{\lambda_1\xi}e^{-\frac{sp}{\zeta}(z-\xi)}d\xi\right]e^{\varepsilon\xi} \\
&= e^{\lambda_1\xi}\left[-EL(e^{(\lambda_1+\varepsilon)\cdot})(z) - \alpha_2 e^{(\lambda_1-\varepsilon)\xi}\left(1 - Ee^{\varepsilon\xi}\right)^2\right]e^{\varepsilon\xi} - Ee^{(\lambda_1+\varepsilon)\xi}H(e^{(\lambda_1+\varepsilon)\cdot})(z) \\
&= -e^{(\lambda_1+\varepsilon)\xi}\left[EL(e^{(\lambda_1+\varepsilon)\cdot})(z) + EH(e^{(\lambda_1+\varepsilon)\cdot})(z) + \alpha_2 e^{(\lambda_1-\varepsilon)\xi}\left(1 - Ee^{\varepsilon\xi}\right)^2\right] \\
&= -e^{(\lambda_1+\varepsilon)\xi}\left[E\frac{P(\lambda_1+\varepsilon)}{\zeta(\lambda_1+\varepsilon+sp/\zeta)} + \alpha_2 e^{(\lambda_1-\varepsilon)\xi}\left(1 - Ee^{\varepsilon\xi}\right)^2\right] \geq 0,
\end{aligned}
\tag{2.31}
$$

where we need to show that

$$
-E\frac{P(\lambda_1+\varepsilon)}{\zeta(\lambda_1+\varepsilon+sp/\zeta)} \geq \alpha_2 e^{(\lambda_1-\varepsilon)\xi}\left(1 - Ee^{\varepsilon\xi}\right)^2. \tag{2.32}
$$

Since $\xi < 0$ and $\lambda_1 - \varepsilon > 0$, we have

$$
\alpha_2 \geq \alpha_2\left(1 - Ee^{\varepsilon\xi}\right)^2 e^{(\lambda_1-\varepsilon)\xi}.
$$

Using the fact that $P(\lambda_1) = 0$ and $P(\lambda_1+\varepsilon) < 0$, inequality (2.32) is satisfied if

$$
E > -\frac{\zeta(\lambda_1+\varepsilon+sp/\zeta)}{P(\lambda_1+\varepsilon)}.
$$

Lemma 2.8. *For $\zeta = \zeta^*$, system (2.30) has a traveling wave solution $(w(z), u(z), v(z))$ satisfying boundary conditions (2.16).*

Proof. In the case where $\zeta = \zeta^*$, we choose a sequence $\{\zeta_m\}$ such that $\zeta_m \in (\zeta^*, \zeta^*+1]$ and $\lim_{m\to\infty}\zeta_m = \zeta^*$. Let $u_m(z)$ be the monotone solution of $(2.19)_1$ with $\zeta = \zeta_m$ subject to (2.16). Since each $u_m(z+y)$, $y \in \mathbb{R}$, is also a monotone solution, we then assume that $u_m(0) = \frac{1}{2}u^*$, for all $m \geq 1$. Clearly, we have that $|u_m(z)| \leq u^*$, for all $z \in \mathbb{R}$ and u_m

satisfies

$$\zeta_m u'_m = u''_m + u_m(f(\beta) - 1 - rq) + \frac{sprq}{\zeta_m}\int_{-\infty}^{z} u_m(\xi)e^{-\frac{sp}{\zeta_m}(z-\xi)}d\xi - \alpha_2 u_m^2, \quad \forall z \in \mathbb{R}. \tag{2.33}$$

Then $u_m(\cdot)$ is a fixed point of the mapping $B_m : X \to X$ defined using (2.29) with $\zeta = \zeta_m$, implying that there exists $d_1 = d_1(\zeta^*) > 0$ such that $|u'_m(z)| \leq d_1$, for all $z \in \mathbb{R}$. From equation (2.33), it then follows that there exists $d_2 = d_2(\zeta^*) > 0$ such that $|u''_m(z)| \leq d_2$, for all $z \in \mathbb{R}$. Differentiating both sides of equation (2.33) with respect to z, we obtain

$$\zeta_m u''_m = u'''_m + u'_m(f(\beta) - 1 - rq) + \frac{sprq}{\zeta}\left[u_m(z) - \frac{sp}{\zeta_m}\int_{-\infty}^{z} u_m(\xi)e^{-\frac{sp}{\zeta_m}(z-\xi)}d\xi\right] - 2\alpha_2 u_m u'_m, \tag{2.34}$$

consequently, there exist $d_3 = d_3(\zeta^*) > 0$ such that $|u'''_m(z)| \leq d_3$, for all $z \in \mathbb{R}$. Subsequently, $u_m(z), u'_m(z)$ and $u''_m(z)$ are uniformly bounded and equi-continuous sequences of functions with respect to the norm $|\cdot|$ on $\mathbb{R}$. By making use of the *Arzela–Ascoli's theorem*, then there exists a subsequence of $\{\zeta_m\}$ such that $\lim_{m\to\infty} \zeta_m = \zeta^*$, as well as $u_m(z), u'_m(z)$ and $u''_m(z)$ uniformly converge on every bounded interval, and therefore pointwise on $\mathbb{R}$ to $S(z), S_1(z)$ and $S_2(z)$, respectively. As a result, we have that $S(z)$ and $S_1(z)$ are differentiable, moreover, $S'(z) = S_1(z)$, $S''(z) = S'_1(z) = S_2(z)$, for all $z \in \mathbb{R}$. If we let $m \to \infty$ in equation (2.33), and using the theory of dominated convergence, we obtain

$$\zeta^* S_1(z) = S_2(z) + S(z)(f(\beta) - 1 - rq) + \frac{sprq}{\zeta^*}\int_{-\infty}^{z} S(\xi)e^{-\frac{sp}{\zeta^*}(z-\xi)}d\xi - \alpha_2(S(z))^2, \quad \forall z \in \mathbb{R}, \tag{2.35}$$

which is

$$\zeta^* S'(z) = S''(z) + S(z)(f(\beta) - 1 - rq) + \frac{sprq}{\zeta^*}\int_{-\infty}^{z} S(\xi)e^{-\frac{sp}{\zeta^*}(z-\xi)}d\xi - \alpha_2(S(z))^2, \quad \forall z \in \mathbb{R}. \tag{2.36}$$

Therefore, $S(z)$ is a solution to equation $(2.30)_1$ with $\zeta = \zeta^*$. Since $S(+\infty)$ and $S(-\infty)$ exist, then $S'(\pm\infty) = 0$ and $S''(\pm\infty) = 0$. In equation (2.36), if we let $z \to -\infty$, then $S(-\infty)\left((f(\beta) - 1 - rq) - \alpha_2 S(-\infty)\right) = 0$. Since we assume that $f(\beta) - 1 \leq rq$, then $S(-\infty) = 0$. Letting $z \to +\infty$, we obtain $S(\infty)\left(f(\beta) - 1 - rq\right) + rqS(\infty) - \alpha_2(S(\infty))^2 = 0$, that is, $S(\infty) = \dfrac{f(\beta) - 1}{\alpha_2}$. Therefore, we conclude that the traveling wave solution connecting $(0, 0, \beta)$ and (w^*, u^*, v^*) exists. □

It remains to show the there exist no monotone traveling wave solution for system (2.13) in the case where $0 < \zeta < \zeta^*$.

Lemma 2.9. *For $0 < \zeta < \zeta^*$, system (2.30) has no non-negative traveling wave solution $(w(z), u(z), v(z))$ satisfying boundary conditions (2.16).*

Proof. If we assume $0 < \zeta < \zeta^*$, then the characteristic equation (2.21) has one negative root and a pair of conjugate roots with positive real parts. Thus, there is a two-dimensional unstable manifold at $(0, 0, \beta)$. The critical point $(0, 0, \beta)$ is a spiral on the unstable manifold, hence a trajectory approaching $(0, 0, \beta)$ has $(w(\xi), u(\xi), v(\xi)) < 0$ for some ξ. However, this violates the requirement that traveling waves are non-negative, thus, system (2.15) with (2.16) admits no monotone traveling wave solution. □

Remark 2.5. *In [84], the authors apply the methods of Wazewski Theorem, LaSalle's Invariance Principle and Hopf bifurcation theory to prove the existence of traveling waves which is hard to apply for a three-state variable system (2.13). Moreover, we cannot employ the approach used in monotone wavefronts for cooperative systems [114, 54] since our system (2.13) is not cooperative, that is, it has similar interactions as predator-prey models. Therefore, the technique of constructing a pair of upper and lower solutions to show the existence of a minimal wave speed ζ^* is more applicable for (2.13). However, since we generalise the conversion rates, $p(v), q(v)$, the upper and lower solution technique is not mathematically tractable. In [194], the authors considered constant conversion rates to show the existence of traveling waves on an auxiliary system for a bacterial colony model with transitions between active bacteria and inactive bacteria, see the proof of Theorem (2.2). From the auxiliary system, the upper and lower solutions for the original system of equations are constructed. Nevertheless, it remains difficult to construct a pair of upper and lower solutions assuming general conversion rates. As a result, we will study the existence of traveling waves using general conversion rates, $p(v)$, $q(v)$, numerically.*

2.4.2 Numerical simulations

In this section, we present numerical simulations to illustrate the behaviour of the reaction-diffusion model. We will further discuss the effects of threshold value, β, and minimum activation concentration δ on the travelling wave speed. The proposed schemes build on scheme (2.7) with the central difference approximation used to discretise the second derivatives. The optimal time step and spatial step size are chosen according to the restriction specified for parabolic equations, i.e., $\dfrac{\Delta t}{(\Delta x)^2} < \dfrac{1}{2}$.

For the model under investigation, we wish to describe the growth rate (traveling wave speed) of the plankton population from an initially population-free state. These results could formulate the possible propagation modes of biofilms and plankton populations. To illustrate our results, all simulations are performed with all parameters selected as

before, i.e., the uniform steady-state computations. Unless stated differently under figure captions, we also choose $d_v = 1$ and $\delta = 1.1$.

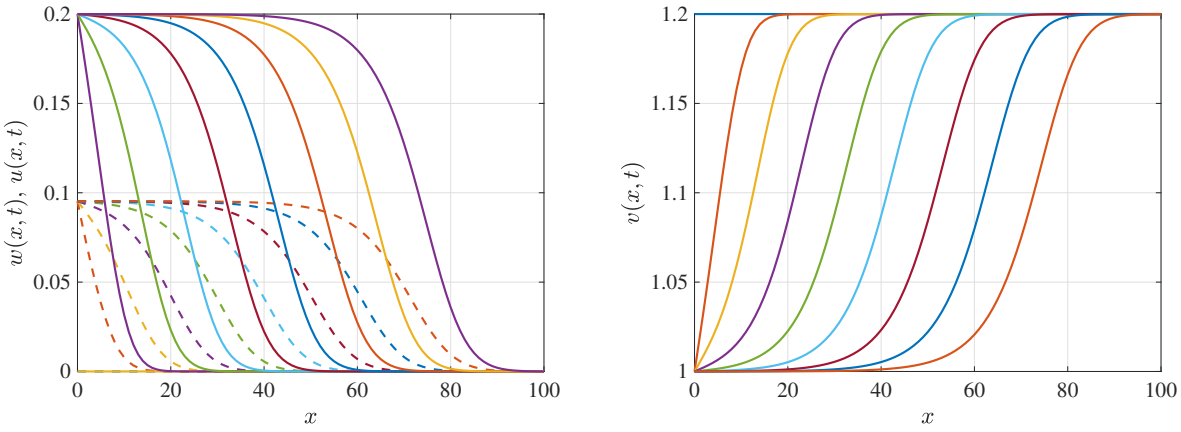

(a) (b)

Figure 2.6: Solution profiles at equally spaced time intervals for $\beta = 1.2$ and $\alpha = 0.5$. In (a) the solid line denotes density u and the broken line denotes density w.

In Figs. 2.6 – 2.8, we present simulations related to system (2.14) when α and β are varied. We observe that, numerically, there exists a traveling wave solution connecting the two equilibria $\mathbf{0} = (0, 0, \beta)$ and $\mathbf{1} = (w^*, u^*, v^*)$. All parameters are fixed as stated before unless indicated otherwise. In Fig. 2.6, we see that for $\beta = 1.2$ and $\alpha = 0.5$, corresponding to $1 - \alpha\beta g'(u^*) = 0.5833 > 0$ and $f(\beta) - 1 - rq(\beta) = -0.0867 < 0$, the traveling wave profile is monotonic. Whilst, in Fig. 2.7 we see non-monotonic traveling wave profiles with $1-\alpha\beta g'(u^*) = 0.8883 > 0$ and $f(\beta)-1-rq(\beta) = -0.0867 < 0$. Similarly, non-monotonic wave solutions are observed in Fig. 2.8 even when $f(\beta) - 1 - rq(\beta) = 0.3836 \not< 0$ and with $f(\beta) - 1 - sp(\beta) - rq(\beta) = -0.6280 < 0$.

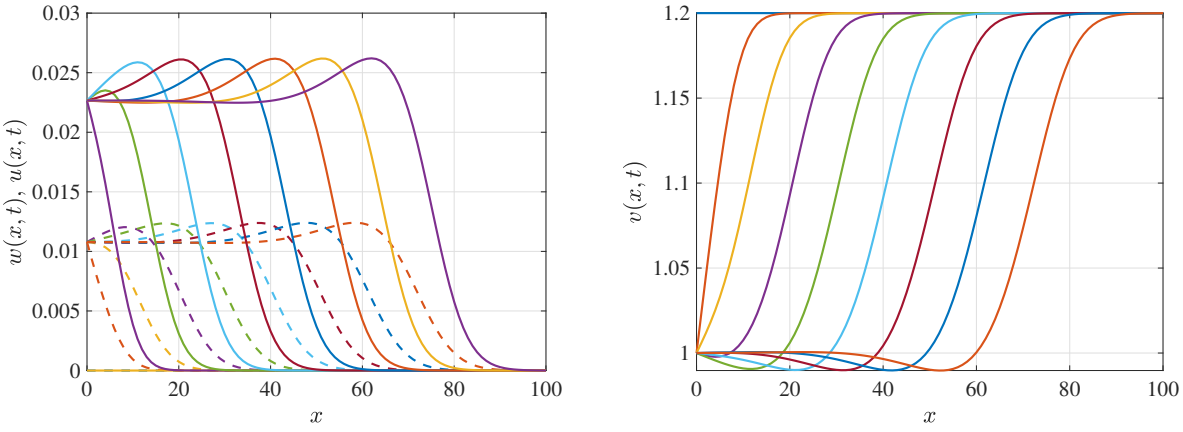

(a) (b)

Figure 2.7: Solution profiles at equally spaced time intervals for $\beta = 1.2$ and $\alpha = 0.1$. In (a) the solid line denotes density u and the broken line denotes density w.

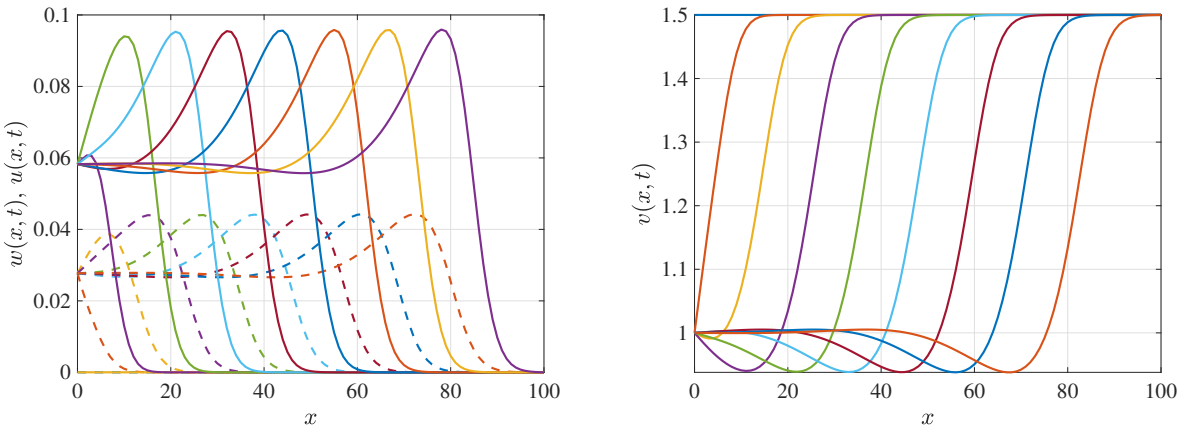

(a) (b)

Figure 2.8: Solution profiles at equally spaced time intervals for $\beta = 1.5$ and $\alpha = 0.1$. In (a) the solid line denotes density u and the broken line denotes density w.

In Fig. 2.9 we perform simulations to assess the effect of parameters on the wave speed. It is observed that the minimal wave speed increases as β and s increase, but decreases as r increases. On the other hand, the ratio of diffusivity coefficients, d_v, does not have an effect on the travelling wave speed.

2.5 Conclusions

Dormancy is a strategy used by microorganisms to cope with unfavorable environmental conditions. Typical models would normally ignore dormancy leading to notable model deficiencies. In practice, only a fraction of the population is active at any particular given time. In this work, we presented and analyzed ordinary differential equations and a reaction-diffusion model that include microbial population dormancy. Results for a uniform steady-state model predicted non-transient population oscillation when both switch functions are dependent on active population density. Clearly, as discussed in Remark 2.4, disregarding the dormant state does not lead to observed oscillations in the bacterioplankton population. Furthermore, the presented reaction-diffusion model predicted that the population gradually dies out if the nutrient supply is below some threshold value and that is referred to as a population under starvation. Whilst, if the nutrient levels remain above some critical value, the population is sustained in an environment. Thus, a nutrient has a high impact on the composition of the population. We have shown that the reaction-diffusion system of equations admits the minimal wave speed.

Deactivation and reactivation are complex processes. These results are theoretical predictions, thus, there is still a need for experiments to test these hypotheses. Future work will include the investigation of pattern formation in these communities.

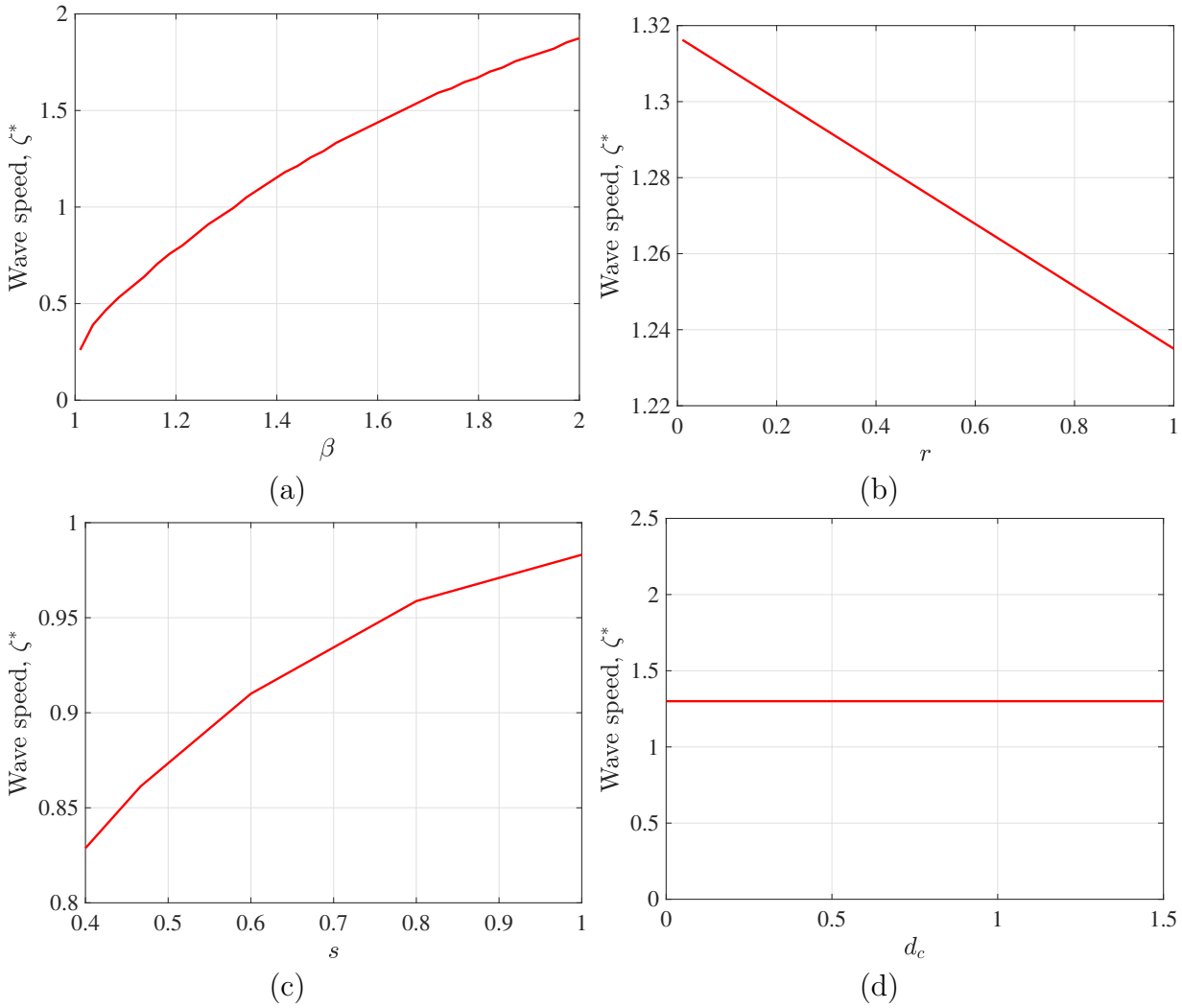

Figure 2.9: The dependence of the minimal wave speed, ζ^*, on the parameters β, r, s and d_v.

Chapter 3

Existence of traveling waves in the presence of a chemoattractant

3.1 Introduction

Mathematical models taking into account the consumption of a limiting nutrient in the presence of a chemo-attractant have been considered extensively in the literature. In particular, it has been observed in experiments that colonies of *E. coli* and *S. typhimurium* strains inoculated in the center of plates form high-density aggregates arranged in striking regular patterns [131]. Although the geometry of the pattern varies significantly, authors in [175] reported that the pattern-forming process is the same. In [131] *S. typhimurium* pattern was described in the form of *bacterial lawn* while the pattern forming mechanism exhibited by *E. coli* was referred to as a *swarm ring*. Their proposed mathematical semi-solid model assumes negligible nutrient consumption, which is supported by experiments.

While several mathematical and computational models have been constructed with the aim to give an adequate explanation of these patterns [104, 175, 131, 139], not much has been done to predict the rate of spatial spread of these highly symmetric shapes or the precise structure of the traveling pulses. To name a few, in the work [131, 159], the authors presented a bacteria-chemoattractant-nutrient interaction chemotaxis model to simulate the experimentally observed pulse waves [179]. Numerical simulations were provided to support their findings. In particular, most of these models emphasised on the motion of cell population in response to the chemoattractant concentration gradient - chemotaxis. An extensive literature survey on existing models incorporating the Patlak-Keller-Segel chemotaxis model with application to self-organization phenomena is found in [139]. For example, the work [128, 193] included the dynamics of the dormant cells in the absence of a chemo-attractant to investigate the asymptotic speed of the spread.

In this work, we consider the existence of traveling waves in a bacteria-chemoattractant interaction model when the dynamics of the active cells are influenced by the change in

chemo-attractant concentration. The model assumes that microorganisms may enter a quiescent phase to adapt or survive significant changes in environmental conditions. Our method in this chapter is mainly based on the work of [54, 192] and several earlier studies. Using the theory of monotone wavefronts for cooperative and partially degenerate reaction-diffusion systems, we establish the existence of traveling waves and show that the spreading speed coincides with the minimal wave speed for constant switch functions.

We begin by recalling the reaction-diffusion system from [175, 131] representing pattern-forming processes experimentally observed in both *E. coli* and *S. typhimurium*,

$$\begin{aligned}
\frac{\partial u}{\partial t} &= D_u \nabla^2 u - \nabla\left[\chi(u,v)\nabla v\right] + k_5 u(k_6 h(n) - u),\\
\frac{\partial v}{\partial t} &= D_v \nabla^2 v + k_8 n g(u) - k_4 u f(v), \quad x \in \Omega, t > 0,\\
\frac{\partial n}{\partial t} &= D_n \nabla^2 n - k_9 k_6 h(n) u,
\end{aligned} \tag{3.1}$$

see [175, 131] for further details. Under this setup, $x \in \Omega \subset \mathbb{R}^m$, $(m = 1, 2, 3)$, is a simply connected bounded domain and $\partial\Omega$, the surface boundary enclosing Ω, $u(x,t)$ denotes bacterial cell density, $v(x,t)$ the aspartate (chemo-attractant) concentration and $n(x,t)$ the succinate (main nutrient) concentration. Consumption of succinate is proportional to the population growth rate with proportionality constant k_9. The cell growth rate is given by $k_5 u h(n)$ and the production of aspartate per cell is given by $k_8 n g(u)$. Furthermore, $k_4 f(v)$ is the consumption of aspartate, where k_4 is the rate constant. Model (3.1) summarises a mechanism for *E. coli* in semi-solid medium experiments. They assumed that non-motile cells are dead, and thus not considered in the dynamics of the model. Chemotaxis is taken into account to represent the directed or biased movement of organism in response to the concentration gradient.

Motivated by the reaction-diffusion system (3.1), in this work, we assume that the nutrient concentration is large compared to the concentration of cells (negligible nutrient consumption) - which is consistent with the work of [131, Section 5.5], and include the dynamics of dormant cells. In addition, the response of bacteria to the availability of the chemoattractant is taken into account by tracking the dynamics of the dormant bacteria. Neglecting dormant cell mortality and assuming that they do not proliferate, the model considered in this chapter takes the form

$$\begin{aligned}
\frac{\partial w}{\partial t} &= k_1 q(v) u - k_2 p(v) w,\\
\frac{\partial u}{\partial t} &= D_u \nabla^2 u + k_5 u(k_6 - u) - k_1 q(v) u + k_2 p(v) w,\\
\frac{\partial v}{\partial t} &= D_v \nabla^2 v + k_8 g(u) - k_7 v - k_4 u f(v),
\end{aligned} \tag{3.2}$$

where we have introduced k_7 to denote the rate of natural degradation of the chemoat-

tractant. The effects of chemotaxis will be discussed in Chapter 4. To the best of our knowledge, this is the first time the model and analysis of (3.2) has been studied in the context of a monotone dynamical system. The model is rendered dimensionless by choosing the following scales

$$w \sim \frac{1}{k_6}, \quad u \sim \frac{1}{k_6}, \quad v \sim \frac{1}{k_6}, \quad x \sim \sqrt{\frac{D_b}{k_5 k_6}}, \quad t \sim \frac{1}{k_5 k_6},$$

to obtain

$$\begin{aligned} \frac{\partial w}{\partial t} &= rq(v)u - sp(v)w, \\ \frac{\partial u}{\partial t} &= \nabla^2 u + u(1-u) - rq(v)u + sp(v)w, \\ \frac{\partial v}{\partial t} &= d_v \nabla^2 v + \alpha(\beta g(u) - v) - \gamma u f(v), \end{aligned} \tag{3.3}$$

where $d_v = D_c/D_b$, $r = k_1/(k_5k_6)$, $s = k_2/(k_5k_6)$, $\alpha = k_7/(k_5k_6)$, $\beta = k_8/(k_6)$, $\gamma = k_4/k_5$ and ∇^2 denoting the *Laplacian operator* with respect to x. In this chapter, $v(x,t)$ denotes the concentration of the chemoattractant. We also assume $g(u) = 1 + g_1(u)$ such that $g_1(0) = 0$. The assumption $g(0) > 0$ takes into account the background production of the chemo-attractant in the system.

Various types of response functions have been proposed in the literature, see for example [117, 131], and the literature therein. In this work, we generalise $f(v)$, and assume it satisfies the following hypotheses: $f(v) = 0$ iff $v = 0$ and $f'(v) \geq 0$, for all v. Furthermore, we invoke assumptions on the transition functions $p(v)$ and $q(v)$.

$\mathcal{F}_1$: $p : \mathbb{R}_+ \to (0,1]$ is C^1, $p'(v) \geq 0$ for all v and $\lim_{v\to\infty} p(v) = 1$,

$\mathcal{F}_2$: $q : \mathbb{R}_+ \to (0,1]$ is C^1, $q'(v) \leq 0$ for all v and $\lim_{v\to\infty} q(v) = 0$.

The reaction-diffusion model is partially degenerate in the sense that one of the diffusion coefficients is zero. We remark that the proposed model (3.3) is generic and can be adopted for, e.g., cancer models. Dormancy has also an important bearing in the treatment of infections, see for example [23, 152]. Since spores are highly resistant to disinfectants, they stay dormant in wounds for periods longer that the applied disinfectant. This normally accounts for the recurrence of infections.

In the construction of traveling wave solutions of monotone degenerate reaction-diffusion equations, we recall the system of reaction-diffusion equations (1.10) given as

$$\boldsymbol{u}_t = D\boldsymbol{u}_{xx} + \boldsymbol{f}(\boldsymbol{u}), \quad x \in \mathbb{R},\ t > 0. \tag{3.4}$$

The system of equations generalised in (3.4) can be found in various sections of the applied sciences including mathematical epidemiology, chemical kinetics, and ecology, to name a few. In this work, we investigate the existence of traveling waves for system (3.4)

in the setting where it is cooperative and partially degenerate. A traveling wave solution of (3.4) is a solution of the form $\boldsymbol{u} = \boldsymbol{u}(\xi)$, with $\xi = x + \upsilon t$, such that if we substitute this solution into the system, we have the wave equation

$$D\boldsymbol{u}''(\xi) - \upsilon\boldsymbol{u}'(\xi) + \boldsymbol{f}(\boldsymbol{u}(\xi)) = 0,\ \xi \in \mathbb{R}. \tag{3.5}$$

This will be discussed in detail in Section 3.2.1.

This chapter is organised as follows: we begin in Section 3.2 where we summarise the traveling wave results in the absence of the quiescent stage, while Section 3.3 provides the full analysis of the bacteria-chemoattractant interaction model when the dynamics of the active cells are influenced by a change in chemo-attractant concentration (i.e., $p = p(v)$ and $q = q(v)$). We establish that there exists a traveling wave speed, $\upsilon^* > 0$, such that for every $\upsilon > \upsilon^*$ the model admits a nontrivial traveling wave solution. In the last section, we give concluding remarks.

3.2 Model without quiescence

Without quiescence, the model reduces to

$$\begin{aligned} \frac{\partial u}{\partial t} &= \nabla^2 u + u(1-u), \\ \frac{\partial v}{\partial t} &= d_v\nabla^2 v + \alpha(\beta g(u) - v) - \gamma f(v)u. \end{aligned} \tag{3.6}$$

The uniform steady-state model for system (3.6) has two equilibria: the bacteria-free equilibrium $E_0 = (0, \beta)$ and the co-existence equilibrium $E^* = (1, v^*)$, where v^* satisfies $H(v^*) = \alpha(\beta g(1) - v^*) - \gamma f(v^*) = 0$. We notice that $\lim\limits_{v^*\to 0^+} H(v^*) = \alpha\beta g(1) > 0$ and $H'(v^*) = -\alpha - \gamma f'(v^*) < 0$. Hence, a unique co-existence equilibrium, E^*, exists. Using the *Hartmann-Grobman theorem*, it is straightforward to show that E_0 is unstable and E^* is locally asymptotically stable.

Proposition 3.1. *The uniform steady state of system (3.6) has no periodic orbits.*

Proof. To prove this result, we use the *Dulac-Bendixon criterion*. Let $Z \subset X$ be open and simply connected in the first quadrant. Let $h_u(u, v) = u(1-u)$ and $h_v(u, v) = \alpha(\beta g(u) - v) - \gamma f(v)u$. We need to show that there exists a function $\phi : Z \to \mathbb{R}$, continuously differentiable on Z, such that

$$\frac{\partial(\phi h_u)}{\partial u} + \frac{\partial(\phi h_v)}{\partial v},$$

is either strictly negative or strictly positive everywhere on Z. Let $\phi(u, v) = \dfrac{1}{u^2}$. Taking Z to be open in the first quadrant, clearly, ϕ is continuously differentiable in Z.

Furthermore,

$$\frac{\partial(\phi h_u)}{\partial u} + \frac{\partial(\phi h_v)}{\partial v} = -\frac{1}{u^2}\left(1 + \alpha + \gamma f'(v)u\right) < 0.$$

Hence, the system has no periodic orbits in the open first quadrant. □

Remark 3.1. *In the next section, we investigate the existence of traveling waves for model (3.6). It is straightforward to observe that the bacteria population follows the well-known Fisher's reaction diffusion equation which admits a mono-stable traveling wave solution* $v(x,t) = v(x + \upsilon t) = v(\xi)$. *Assuming boundary conditions* $v(-\infty) = 0$ *and* $v(+\infty) = 1$ *for the Fisher's equation, we have the traveling wave speed* $\upsilon \geq 2$.

3.2.1 Traveling waves

We begin by recalling some useful results from [54]. Consider system (3.4). We denote the stability modulus of a square matrix A by

$$z(A) := \max\{Re\lambda : \det(\lambda I - A) = 0\}.$$

Let $A(\mu) = \mu^2 D + \boldsymbol{f}'(\mathbf{0})$ for any $\mu > 0$, and $\lambda_A(\mu)$ the stability modulus of $A(\mu)$. Since $\boldsymbol{f}'(\mathbf{0})$ is cooperative and irreducible, then $\lambda(\mu) > 0$ for all $\mu > 0$ such that $\Phi(\mu) = \dfrac{\lambda(\mu)}{\mu}$ can be defined. Then, by [54, Lemma 2.1] we define $\bar{\upsilon} = \inf_{\mu>0} \Phi(\mu) \geq 0$. We always assume $||\upsilon(\mu)|| = 1\ \forall \mu > 0$. We equip $\mathbb{R}^m$ with the *Euclidean* norm $||\cdot||$. Following [54], we can prove the existence of monostable traveling waves for system (3.4) by verifying the following conditions, denoted here as assumption $\mathcal{H}$.

1. $\boldsymbol{f}(\mathbf{0}) = \boldsymbol{f}(\mathbf{1}) = \mathbf{0}$ and there is no ν other than $\mathbf{0}$ and $\mathbf{1}$ such that $\boldsymbol{f}(\nu) = \mathbf{0}$ and $\mathbf{0} \leq \nu \leq \mathbf{1}$.

2. System (3.4) is cooperative.

3. $\boldsymbol{f}(\boldsymbol{u})$ is piecewise continuous differentiable in $\boldsymbol{u}$ for $\mathbf{0} \leq \boldsymbol{u} \leq \mathbf{1}$ and differentiable at $\mathbf{0}$, and the matrix $\boldsymbol{f}'(\mathbf{0})$ is irreducible with $z(\boldsymbol{f}'(\mathbf{0})) > 0$.

Assume assumption $\mathcal{H}$ holds. Let $\phi \in \mathcal{C}_{\mathbf{1}}$ and $\boldsymbol{u}(t,x;\phi)$ be the unique solution of (the integral form) (3.4) through ϕ. Then, there exists a real number $\upsilon^* \geq \bar{\upsilon} > 0$ such that the following statements are valid (see [54, Lemma 2.3]):

(i) If ϕ has a compact support, then $\lim_{t\to\infty, |x|\geq \upsilon t} \boldsymbol{u}(t,x;\phi) = 0$, for all $\upsilon > \upsilon^*$.

(ii) For any $\upsilon \in (0, \upsilon^*)$ and $r^* > 0$, there is a positive number R_{r^*} such that for any $\phi \in \mathcal{C}_{\mathbf{1}}$ with $\phi \geq r^*$ on an interval of length $2R_{r^*}$, there holds $\lim_{t\to\infty, |x|\leq \upsilon t} \boldsymbol{u}(t,x;\phi) = \mathbf{1}$.

(iii) If, in addition, $\boldsymbol{f}(\min\{\rho v(\mu^*), \mathbf{1}\}) \leq \rho \boldsymbol{f}'(\mathbf{0}) v(\mu^*)$, $\forall \rho > 0$, then $\upsilon^* = \bar{\upsilon}$.

Further, in [54] the authors obtained the minimal wave speed and its coincidence with the spreading speed through the following assumptions, denoted here as assumption $\mathcal{K}$.

1. $\boldsymbol{f}(\mathbf{0}) = \boldsymbol{f}(\mathbf{1}) = \mathbf{0}$ and there is no ν other than $\mathbf{0}$ and $\mathbf{1}$ such that $\boldsymbol{f}(\nu) = \mathbf{0}$ and $\mathbf{0} \leq \nu \leq \mathbf{1}$.

2. System (3.4) is cooperative.

3. $\boldsymbol{f}(\boldsymbol{u})$ is piecewise continuous differentiable in $\boldsymbol{u}$ for $\mathbf{0} \leq \boldsymbol{u} \leq \mathbf{1}$ and differentiable at $\mathbf{0}$ and the matrix $\boldsymbol{f}'(\mathbf{0})$ is irreducible with $z(\boldsymbol{f}'(\mathbf{0})) > 0$.

4. There exists $\kappa > 0$, $\sigma > 1$ and $r^* > 0$ such that $\boldsymbol{f}(\boldsymbol{u}) \geq \boldsymbol{f}'(\mathbf{0})\boldsymbol{u} - \kappa\|\boldsymbol{u}\|^\sigma \mathbf{1}$ for all $\mathbf{0} \leq \boldsymbol{u} \leq \mathbf{r}^*$.

5. For any $\rho > 0$, $\boldsymbol{f}(\min\{\rho v(\mu), \mathbf{1}\}) \leq \rho \boldsymbol{f}'(\mathbf{0}) v(\mu)$, $\forall \mu \in (0, \mu^*]$, where μ^* is the value of μ at which $\Phi(\mu)$ attains its infimum.

We recall the reaction-diffusion equation model (3.6), which we restate in the form (3.4) where

$$\boldsymbol{u} = (u, v)^t, \quad D = \operatorname{diag}(1, d_v), \quad \boldsymbol{f}(\boldsymbol{u}) = \begin{pmatrix} u(1-u) \\ \alpha(\beta - v) - \gamma f(v) u \end{pmatrix}, \tag{3.7}$$

and have assumed $g(u) =$ constant. Without loss of generality, we take $g(u) = 1$. For mathematical convenience, we make the change of variable $h = \beta - v$ which converts the system of equations (3.7) to

$$\boldsymbol{u} = (u, h)^t, \quad D = \operatorname{diag}(1, d_v), \quad \boldsymbol{f}(\boldsymbol{u}) = \begin{pmatrix} u(1-u) \\ -\alpha h + \gamma f(v^* - h) u \end{pmatrix}. \tag{3.8}$$

For this system, the only equilibria are: $\mathbf{0} = (0, 0)^t$ and $\mathbf{1}$= $(1, \beta - v^*)^t$. We aim to find a traveling wave that can be viewed as a heteroclinic orbit connecting the two equilibria, $\mathbf{0}$ and $\mathbf{1}$.

Theorem 3.1. *Systems (3.7) and (3.8) admit a traveling wave solution $\boldsymbol{u}(x + \upsilon t)$ for all $\upsilon \geq \bar{\upsilon}$ connecting $\mathbf{0}$ and $\mathbf{1}$.*

Proof. To prove this result, we need to verify that the reaction diffusion equation (3.7) with (3.8) satisfies assumption $\mathcal{H}$, or equivalently assumptions $\mathcal{K}_{1-3}$. The Jacobian matrix for $\boldsymbol{f}(\boldsymbol{u})$ is given by

$$\boldsymbol{f}'(\boldsymbol{u}) = \begin{pmatrix} (1-2u) & 0 \\ \gamma f(\beta - h) & -\alpha - \gamma u f'(\beta - h) \end{pmatrix},$$

so that

$$\boldsymbol{f}'(\mathbf{0}) = \begin{pmatrix} 1 & 0 \\ \gamma f(\beta) & -\alpha \end{pmatrix}.$$

We can deduce that system (3.7) with (3.8) is monotone cooperative since $\boldsymbol{f}(\boldsymbol{u})$ is differentiable and all off-diagonal entries of the Jacobian matrix, $\boldsymbol{f}'(\boldsymbol{u})$, are non-negative. It is clear that the solution $\boldsymbol{u}$ verifies $\mathbf{0} \leq \boldsymbol{u} \leq \mathbf{1}$, such that there are no other points other than $\mathbf{0}$ and $\mathbf{1}$ that verify $\boldsymbol{f}(\mathbf{0}) = \boldsymbol{f}(\mathbf{1}) = 0$. Moreover, the characteristic equation of $\boldsymbol{f}'(\mathbf{0})$ has one of the eigenvalues equal to 1. Hence, the stability modulus of $\boldsymbol{f}'(\mathbf{0})$, $z(\boldsymbol{f}'(\mathbf{0}))$, is strictly positive. Consequently, $\boldsymbol{f}'(\mathbf{0})$ is irreducible. □

Theorem 3.2. *Consider system (3.7) with (3.8). For each $\upsilon \geq \upsilon^* = \bar{\upsilon}$, the system has a non-decreasing traveling wave solution $\boldsymbol{u}(x + \upsilon t)$ connecting $\mathbf{0}$ and $\mathbf{1}$, while for $\upsilon < \upsilon^*$ there is no traveling wave solution connecting $\mathbf{0}$ and $\mathbf{1}$.*

Proof. Since assumptions $\mathcal{K}_{1-3}$ are already satisfied, we need to verify assumptions $\mathcal{K}_4$ and $\mathcal{K}_5$ to deduce that the spreading speed υ^* coincides with the minimal wave speed $\bar{\upsilon}$. In particular, we aim to find the minimal wave speed of the growing population. We assume f to be a linear function such that, $f(\beta - h) = \beta - h$.

Using the fact that $-hu \geq -\frac{1}{2}(h^2 + u^2) = -\frac{1}{2}||\boldsymbol{u}||_2^2$ and $-u^2 \geq -||\boldsymbol{u}||_2^2$, we deduce that

$$\boldsymbol{f}(\boldsymbol{u}) = \boldsymbol{f}'(\mathbf{0})\boldsymbol{u} - \begin{pmatrix} u^2 \\ \gamma uh \end{pmatrix} \geq \boldsymbol{f}'(\mathbf{0})\boldsymbol{u} - \kappa||\boldsymbol{u}||_2^2\mathbf{1},$$

with $\kappa = \max\{1, \frac{1}{2}\gamma\} > 0$, $\sigma = 2$, for $\mathbf{0} < \boldsymbol{u} < \mathbf{r}^* = \mathbf{1}$. Thus, $\mathcal{K}_4$ holds. For $\mu > 0$, let us define

$$A(\mu) = \mu^2 D + \boldsymbol{f}'(\mathbf{0}) = \begin{pmatrix} \mu^2 + 1 & 0 \\ \gamma\beta & \mu^2 d_v - \alpha \end{pmatrix}. \tag{3.9}$$

Clearly, the eigenvalues of $A(\mu)$ are $\lambda_1 = \mu^2 + 1$ and $\lambda_2 = \mu^2 d_v - \alpha$ which are positive and negative, respectively.

The positive eigenvector corresponding to the largest eigenvalue, λ_1, is

$$v_0 = \left(\frac{\lambda_1 - \lambda_2}{\gamma\beta}, 1\right)^t > \mathbf{0},$$

and we set $v(\mu) = \dfrac{v_0}{\|v_0\|}$ such that $\|v(\mu)\| = 1$. Now, let us consider the function $\Phi(\mu) = \dfrac{\lambda_1(\mu)}{\mu} > 0$ for $\mu > 0$, and set $\bar{\upsilon} = \inf\limits_{\mu>0} \Phi(\mu)$. We aim to show that the infimum $\bar{\upsilon}$ is reached for a positive value of μ^*. Since we have that $\Phi(\mu) > \mu$, therefore, $\lim\limits_{\mu\to\infty} \Phi(\mu) = +\infty$. Moreover, since $\lim\limits_{\mu\to 0} \lambda_1(\mu) > 0$, thus, we obtain $\lim\limits_{\mu\to 0^+} \Phi(\mu) = +\infty$. Furthermore,

$$\Phi'(\mu) = \frac{\lambda_1'(\mu)\mu - \lambda_1(\mu)}{\mu^2}, \text{ then } \quad \Phi'(\mu) = 0 \quad \text{whenever} \quad \lambda_1'(\mu)\mu - \lambda_1(\mu) = 0.$$

We have that

$$\Phi'(\mu) = \frac{\mu^2 - 1}{\mu^2}.$$

Solving for $\Phi'(\mu) = 0$, we deduce that there exists $\mu^* = 1$ at which $\Phi(\mu)$ attains its infimum, i.e., $\bar{v} = \dfrac{\lambda_1(\mu^*)}{\mu^*} = 2$. We compute

$$\begin{aligned}\boldsymbol{f}(\rho v(\mu)) &= \begin{pmatrix} \rho v_1(1-\rho v_1) \\ -\alpha\rho v_2 + \gamma(\beta - \rho v_2)\rho v_1 \end{pmatrix} \\ &= \rho \begin{pmatrix} 1 & 0 \\ \gamma\beta & -\alpha \end{pmatrix} v(\mu) + \rho \begin{pmatrix} -\rho v_1 & 0 \\ -\rho\gamma v_1 & 0 \end{pmatrix} v(\mu) \leq \rho \boldsymbol{f}'(\mathbf{0}) v(\mu).\end{aligned}$$

This completes the proof. □

We remark from the above result that the minimal speed for model (3.6) is given by $\bar{v} = 2\sqrt{k_3 k_4 D_b}$ in dimensional form which is consistent with the wave speed of *Fisher's* equation obtained in [174]. Numerical simulations will be provided to support these results in the next section.

3.2.2 Numerical simulations

We present one-dimensional numerical results for the reduced system (3.6) to support the results summarised in Theorems 3.1 and 3.2. We note that the proposed model is generic and can be used for other modelling scenarios, hence the selection of parameters is for illustration of the theoretical results only. All numerical simulations are obtained using MatLab's `PDEPE` solver. We assume the production function to be given by

$$g(u) = \frac{\sigma + 2u}{\sigma + u}, \tag{3.10}$$

and the response function, $f(v) = v$. With this selection, $E_0 = (0, \beta)^t$ and $E^* = (1, v^*)^t$ where $v^* = \dfrac{\alpha\beta g(1)}{\gamma + \alpha}$. Unless stated differently under the figure caption, we choose: $\gamma = 1$, $d_v = 0.05$, $\beta = 1$ and $\alpha = 0.5$. Fig. 3.1 illustrates the results in Theorems 3.1 and 3.2. Clearly, a comparison of Figs. 3.1 and 3.2 shows that the wave speed is independent of the model parameters α, β, and γ. This is supported by calculations of the wave speed in Fig. 3.3.

In Fig. 3.2, non-monotonic traveling wave profiles are observed in the chemo-attractant concentration profiles. The solution behaves like a stable oscillatory wave-front traveling from right to left. The predicted wave speed is calculated from Fig. 3.3 by using the slope of the contour lines. A comparison of theoretical and numerical wave speed supports the good convergence properties of the proposed method.

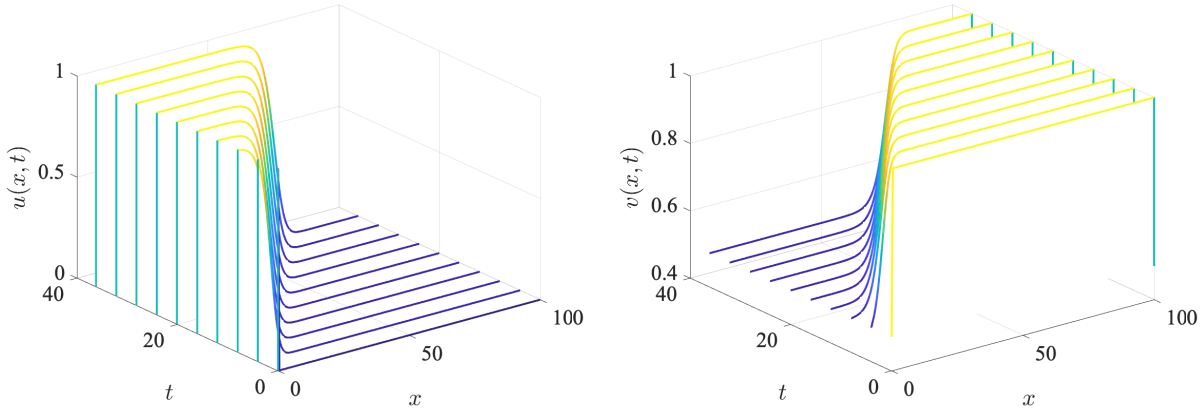

(a) $u(x,t)$. (b) $v(x,t)$.

Figure 3.1: Stable traveling wave profiles for $u(x,t)$ and $v(x,t)$ with $g(u) = 1$ in support of results in Theorems 3.1 and 3.2.

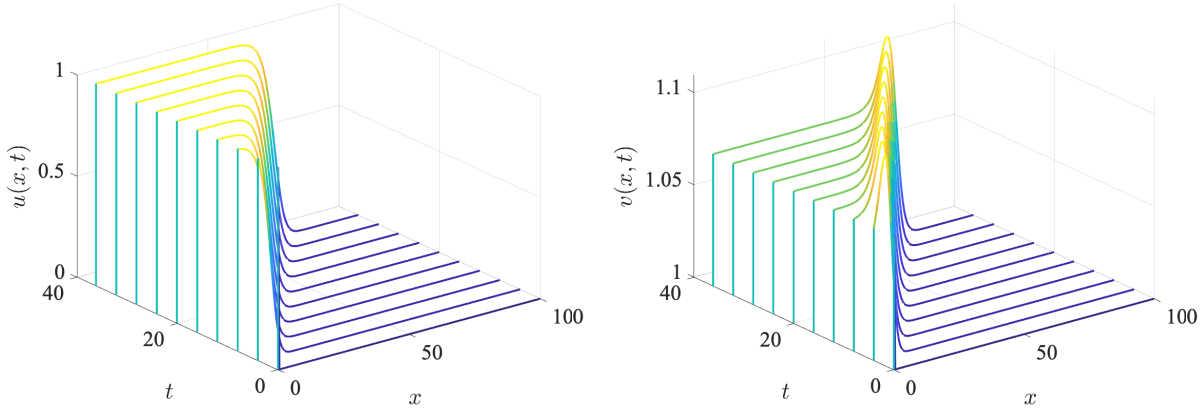

(a) $u(x,t)$. (b) $v(x,t)$.

Figure 3.2: Stable traveling wave profiles for $u(x,t)$ and $v(x,t)$ with $g(u)$ as given in (3.10). The parameters are modified to $\alpha = 2.5$ and $\delta = 1$.

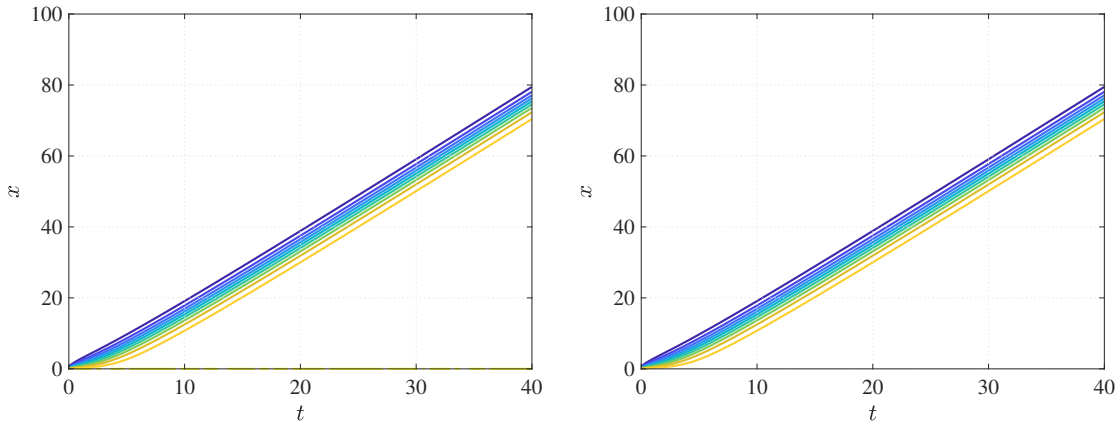

(a) Contour for Fig. 3.1(a). (b) Contour for Fig. 3.2(a).

Figure 3.3: Contour plots corresponding to Fig. 3.1 and Fig. 3.2. The slope of the contour plot gives the wave speed, $\bar{v} \approx 2$ for each case.

3.3 The full model

We are now interested in the case where bacteria switch states depending on the chemo-attractant concentration in the system. We begin by recalling the reaction-diffusion model (3.3), that is,

$$\begin{aligned}\frac{\partial w}{\partial t} &= rq(v)u - sp(v)w,\\ \frac{\partial u}{\partial t} &= \nabla^2 u + u(1-u) - rq(v)u + sp(v)w, \quad x \in \Omega, t > 0,\\ \frac{\partial v}{\partial t} &= d_v\nabla^2 v + \alpha(\beta g(u) - v) - \gamma f(v)u.\end{aligned} \tag{3.11}$$

We aim to investigate and observe the dynamics of the model when the microbial population transition from one state to another is a direct consequence of the change in chemo-attractant concentration. We restrict our work to switch functions satisfying $\mathcal{F}_1$ and $\mathcal{F}_2$. First, we consider the uniform steady-state model, i.e., ignore diffusion. We have the following result.

Proposition 3.2. *System (3.11) admits the following equilibria:*

- *the microbial-free state* $P^0 = (0, 0, \beta)$, *and*
- *a unique co-existence state* $P^* = (w^*, u^*, v^*)$, *where* $u^* = 1$, $w^* = \dfrac{rq(v^*)}{sp(v^*)}u^*$ *and* v^* *satisfies* $\alpha(\beta g(1) - v^*) - \gamma f(v^*) = 0$.

Proof. First, setting the right hand side of equations (3.11) to zero, we get P^0 and P^* as the only equilibria points where v^* satisfies $\alpha(\beta g(1) - v^*) - \gamma f(v^*) = 0$. Defining $H(v^*) = \alpha(\beta g(1) - v^*) - \gamma f(v^*)$, then $H(v^*)$ is a monotonically decreasing function since $H'(v^*) = -\alpha - \gamma f'(v^*) < 0$, where we have used the properties of functions f and g. Furthermore, $\lim\limits_{v^*\to 0^+} H(v^*) = \alpha\beta g(1) > 0$, hence, a unique solution v^* satisfying $H(v^*) = \alpha(\beta g(1) - v^*) - \gamma f(v^*)$ exists. □

To study the local stability of equilibria, we consider the general Jacobian matrix of system (3.11) given by

$$J(w,u,v) = \begin{pmatrix} -sp(v) & rq(v) & rq'(v)u - sp'(v)w \\ sp(v) & (1-u) - u - rq(v) & -rq'(v)u + sp'(v)w \\ 0 & \alpha\beta g'(u) - \gamma f(v) & -\alpha - \gamma u f'(v) \end{pmatrix}.$$

At the microbial-free state, P^0, we have

$$J(P^0) = \begin{pmatrix} -sp(\beta) & rq(\beta) & 0 \\ sp(\beta) & 1 - rq(\beta) & 0 \\ 0 & \alpha\beta g'(0) - \gamma f(\beta) & -\alpha \end{pmatrix}.$$

Clearly, $-\alpha$ is one of the eigenvalues of $J(P^0)$. The remaining eigenvalues are obtained from the reduced matrix

$$\begin{pmatrix} -sp(\beta) & rq(\beta) \\ sp(\beta) & 1 - rq(\beta) \end{pmatrix},$$

whose trace and determinant are given as $1 - (rq(\beta) + sp(\beta))$ and $-sp(\beta)$, respectively. Under the hypotheses $\mathcal{F}_1$ and $\mathcal{F}_2$, the microbial-free equilibrium state is unstable.

Next, we consider the local stability of the co-existence equilibrium, P^*. The Jacobian matrix at the co-existence equilibrium is

$$J(P^*) = \begin{pmatrix} -sp(v^*) & rq(v^*) & rq'(v^*) - sp'(v^*)w^* \\ sp(v^*) & -1 - rq(v^*) & -rq'(v^*) + sp'(v^*)w^* \\ 0 & \alpha\beta g'(1) - \gamma f(v^*) & -\alpha - \gamma f'(v^*) \end{pmatrix},$$

and the characteristic equation is given by

$$Q(\lambda) = \lambda^3 + s_1\lambda^2 + s_2\lambda + s_3,$$

where the coefficients are given by

$$\begin{aligned} s_1 &= -\text{trace } J(P^*) = sp(v^*) + rq(v^*) + 1 + (\alpha + \gamma f'(v^*)), \\ s_2 &= (\alpha + \gamma f'(v^*))(1 + rq(v^*) + sp(v^*)) + (\gamma f(v^*) - \alpha\beta g'(1))(sp'(v^*)w^* - rq'(v^*)) + sp(v^*), \\ s_3 &= -\det J(P^*) = sp(v^*)\left(\alpha + \gamma f'(v^*)\right). \end{aligned}$$

Clearly, s_1 and s_3 are unconditionally positive and s_2 is positive provided $\gamma f(v^*) - \alpha\beta g'(1) > 0$. It remains to check if Δ_2 is positive. We have

$$\begin{aligned} \Delta_2 &= s_1 s_2 - s_3 \\ &= (sp(v^*) + rq(v^*) + 1) \times s_2 + sp(v^*)(\alpha + \gamma f'(v^*))^2 \\ &+ (\alpha + \gamma f'(v^*))^2 (rq(v^*) + 1) + (\alpha + \gamma f'(v^*))(\gamma f(v^*) - \alpha\beta g'(1))(-rq'(v^*) + sp'(v^*)w^*), \end{aligned}$$

and it is unclear if the complete expression is positive. However, assuming $\gamma f(v^*) - \alpha\beta g'(1) \geq 0$, then the coefficients $s_i > 0$ for $i = 1, 2, 3$ and second-*Hurwitz* determinant, Δ_2, are positive and P^* becomes locally asymptotically stable. When $\gamma f(v^*) - \alpha\beta g'(1) < 0$, we cannot conclude on the sign of Δ_2 as the expression is not mathematically tractable. Therefore, we will proceed numerically, see Fig. 3.4.

3.3.1 Traveling waves

In this section, we make a simplifying reduction on the transfer functions p and q, i.e., we assume the switch functions are constants, which is consistent with Hypotheses $\mathcal{F}_1$

and $\mathcal{F}_2$. Furthermore, we take $\gamma f(v^*) - \alpha\beta g'(1) \geq 0$ so that P^* is locally asymptotically stable. As before, we assume $g(u) = 1$, and make the change of variable $h = \beta - v$ to rewrite the system in the form $\boldsymbol{u}_t = D\boldsymbol{u}_{xx} + \boldsymbol{f}(\boldsymbol{u})$, $x \in \mathbb{R}$, $t > 0$, that is,

$$\boldsymbol{u} = (w, u, h)^t, \quad D = \text{diag}(0, 1, d_v), \quad \boldsymbol{f}(\boldsymbol{u}) = \begin{pmatrix} rqu - spw \\ u(1-u) - rqu + spw \\ -\alpha h + \gamma f(\beta - h)u \end{pmatrix}. \tag{3.12}$$

Now we have the following result.

Theorem 3.3. *Consider system (3.11). Assuming $rq \leq 1$, for each $v \geq v^* = \bar{v}$, the system has a non-decreasing traveling wave solution $\boldsymbol{u}(x + vt)$ connecting $\mathbf{0}$ and $\mathbf{1}$, while for $v < v^*$ there is no traveling wave solution connecting $\mathbf{0}$ and $\mathbf{1}$.*

Proof. First, we need to verify that the reaction-diffusion equation (3.11) satisfies assumption $\mathcal{H}$, or equivalently assumptions $\mathcal{K}_{1-3}$. The Jacobian matrix for $\boldsymbol{f}(\boldsymbol{u})$ is given by

$$\boldsymbol{f}'(\boldsymbol{u}) = \begin{pmatrix} -sp & rq & 0 \\ sp & (1-2u) - rq & 0 \\ 0 & \gamma f(\beta - h) & -\alpha - \gamma u f'(\beta - h) \end{pmatrix},$$

so that

$$\boldsymbol{f}'(\mathbf{0}) = \begin{pmatrix} -sp & rq & 0 \\ sp & 1 - rq & 0 \\ 0 & \gamma f(\beta) & -\alpha \end{pmatrix}.$$

We can deduce that system (3.11) with (3.12) is monotone cooperative since $\boldsymbol{f}(\boldsymbol{u})$ is differentiable and all off-diagonal entries of the Jacobian matrix, $\boldsymbol{f}'(\boldsymbol{u})$, are non-negative. It is clear that the solution $\boldsymbol{u}$ verifies $\mathbf{0} \leq \boldsymbol{u} \leq \mathbf{1}$, such that there are no other points other than $\mathbf{0}$ and $\mathbf{1}$ that verify $\boldsymbol{f}(\mathbf{0}) = \boldsymbol{f}(\mathbf{1}) = 0$. Moreover, the characteristic equation of $\boldsymbol{f}'(\mathbf{0})$ has one of the eigenvalues equal to $-\alpha$. The remaining two eigenvalues are from the following sub-matrix

$$\begin{pmatrix} -sp & rq \\ sp & 1 - rq \end{pmatrix}.$$

The trace and determinant of the sub-matrix are given by $1 - (sp + rq)$ and $-sp$, respectively, which implies that one eigenvalue is real and positive. Hence, the stability modulus of $\boldsymbol{f}'(\mathbf{0})$, $z(\boldsymbol{f}'(\mathbf{0}))$, is strictly positive. Consequently, $\boldsymbol{f}'(\mathbf{0})$ is irreducible.

Next, we need to verify assumptions $\mathcal{K}_4$ and $\mathcal{K}_5$ to deduce that the spreading speed v^* coincides with the minimal wave speed $\bar{v}$. In particular, we aim to find the minimal wave speed of the growing population. We take $f(v) = v$, that is, $f(\beta - h) = \beta - h$.

Using the fact that $-uh \geq -\frac{1}{2}(h^2 + u^2) = -\frac{1}{2}||\boldsymbol{u}||_2^2$ and $-u^2 \geq -||\boldsymbol{u}||_2^2$, we deduce

that

$$\boldsymbol{f}(\boldsymbol{u}) = \boldsymbol{f}'(\mathbf{0})\boldsymbol{u} - \begin{pmatrix} 0 \\ u^2 \\ \gamma uh \end{pmatrix} \geq \boldsymbol{f}'(\mathbf{0})\boldsymbol{u} - \kappa||\boldsymbol{u}||_2^2\mathbf{1},$$

with $\kappa = \max\{1, \frac{1}{2}\gamma\} > 0$, $\sigma = 2$, for $\mathbf{0} < \boldsymbol{u} < \mathbf{r}^* = \mathbf{1}$. Thus, $\mathcal{K}_4$ holds.

For $\mu > 0$, let us define

$$A(\mu) = \mu^2 D + \boldsymbol{f}'(\mathbf{0}) = \begin{pmatrix} -sp & rq & 0 \\ sp & \mu^2 + 1 - rq & 0 \\ 0 & \gamma\beta & d_v\mu^2 - \alpha \end{pmatrix}. \tag{3.13}$$

Clearly, the first eigenvalue of $A(\mu)$ is $\lambda_1 = d_v\mu^2 - \alpha$ and the other eigenvalues can be obtained from the characteristic equation

$$\lambda^2 + \left[sp + rq - 1 - \mu^2\right]\lambda - sp\left[1 + \mu^2\right] = 0.$$

From the polynomial equation, we have the discriminant given by $\Delta = (sp + rq - 1 - \mu^2\ )^2 + 4sp\,(1 + \mu^2) > 0$. Consequently,

$$\lambda_2 = \frac{\sqrt{\Delta} - (sp + rq - 1 - \mu^2)}{2} > 0,$$

and

$$\lambda_3 = \frac{-\sqrt{\Delta} - (sp + rq - 1 - \mu^2)}{2} < 0.$$

Clearly, $\lambda_2 > \lambda_3$. Additionally, assuming $d_v \leq 1$, we have

$$\begin{aligned}
\lambda_2 - \lambda_1 &= \frac{\sqrt{\Delta} - (sp + rq - 1 - \mu^2)}{2} - (d_v\mu^2 - \alpha) \\
&\geq \frac{\sqrt{\Delta} - (sp + rq - 1) + \mu^2\,(1 - 2d_v)}{2}, \\
&\geq \frac{\sqrt{\Delta} - (sp + rq - 1 + \mu^2)}{2}, \quad \text{since} \quad \mu^2\,(1 - 2d_v) \geq -\mu^2, \\
&= \frac{\Delta - (sp + rq - 1 + \mu^2)^2}{2\left[\sqrt{\Delta} + (sp + rq - 1 + \mu^2)\right]} \\
&= \frac{2\left[sp + \mu^2(1 - rq)\right]}{\left[\sqrt{\Delta} + (sp + rq - 1 + \mu^2)\right]} \\
&= \frac{sp + \mu^2(1 - rq)}{\mu^2 - \lambda_3} > 0,
\end{aligned}$$

with $\lambda_3 < 0$ and $rq \leq 1$ such that $\lambda_2 > \max\{\lambda_1, \lambda_3\}$. The positive eigenvector corre-

sponding to the largest eigenvalue, λ_2, is

$$v_0 = \left(\frac{r(\lambda_2 - \lambda_1)}{\gamma\beta\,(sp + \lambda_2)}, \frac{\lambda_2 - \lambda_1}{\gamma\beta}, 1 \right)^t > \mathbf{0},$$

and we set $v(\mu) = \dfrac{v_0}{\|v_0\|}$ such that $\|v(\mu)\| = 1$. Now, let us consider the function $\Phi(\mu) = \dfrac{\lambda_2(\mu)}{\mu} > 0$ for $\mu > 0$, and set $\bar{v} = \inf\limits_{\mu>0} \Phi(\mu)$. We aim to show that the infimum $\bar{v}$ is reached for a positive value of μ^*. Since we have that $\Phi(\mu) > \mu - \dfrac{sp + rq}{\mu}$, therefore, $\lim\limits_{\mu\to\infty} \Phi(\mu) = +\infty$. Moreover, since $\lim\limits_{\mu\to 0} \lambda_2(\mu) > 0$, thus, we obtain $\lim\limits_{\mu\to 0^+} \Phi(\mu) = +\infty$. Furthermore,

$$\Phi'(\mu) = \frac{\lambda_2'(\mu)\mu - \lambda_2(\mu)}{\mu^2}, \text{ then } \quad \Phi'(\mu) = 0 \quad \text{whenever} \quad \lambda_2'(\mu)\mu - \lambda_2(\mu) = 0.$$

We have

$$\Phi'(\mu) = \mu \left(\frac{2\mu sp - \mu\,(sp + rq - (1 + \mu^2))}{\sqrt{\Delta}} + \mu \right) - \frac{\sqrt{\Delta} - (sp + rq - (1 + \mu^2))}{2},$$

and after some algebra, solving for $\Phi'(\mu) = 0$ is equivalent to finding the roots of the following third order polynomial,

$$x^3 + a_2 x^2 + a_1 x + a_0 = 0, \tag{3.14}$$

with $x = \mu^2$. The coefficients are given by

$$\begin{aligned} a_0 &= -(sp)^2 - 2sp(1 + rq) - (rq - 1)^2, \\ a_1 &= (sp + rq)^2 - 1, \\ a_2 &= 2(sp + rq) + 1. \end{aligned} \tag{3.15}$$

Coefficients a_2 and a_0 are strictly negative and positive, respectively. For any value of sp and rq this ensures $\Phi'(\mu) = 0$ changes sign only once on $(0, \infty)$. Hence, by *Descarte's* rule of signs, it follows there is a unique positive root $\mu^* \in (0, \infty)$ at which $\Phi(\mu)$ attains its infimum, i.e., $\bar{v} = \dfrac{\lambda_2(\mu^*)}{\mu^*}$ provided $rq \leq 1$.

Finally, we let $\mu \in (0, \mu^*]$ and $\rho > 0$. We compute

$$\begin{aligned}\boldsymbol{f}(\rho v(\mu)) &= \begin{pmatrix} rq\rho v_2 - sp\rho v_1 \\ \rho v_2(1-\rho v_2) - rq\rho v_2 + sp\rho v_1 \\ -\alpha\rho v_3 + \gamma(\beta - \rho v_3)\rho v_2 \end{pmatrix} \\ &= \rho \begin{pmatrix} -sp & rq & 0 \\ sp & 1-rq & 0 \\ 0 & \gamma\beta & -\alpha \end{pmatrix} v(\mu) + \rho \begin{pmatrix} 0 & 0 & 0 \\ 0 & -\rho v_2 & 0 \\ 0 & -\rho\gamma v_2 & 0 \end{pmatrix} v(\mu) \leq \rho \boldsymbol{f}'(\mathbf{0}) v(\mu).\end{aligned}$$

Hence, we deduce the existence of a wave-front $\boldsymbol{u}(x + \upsilon t)$ for each $\upsilon \geq \bar{\upsilon}$ connecting $\mathbf{0}$ and $\mathbf{1}$. □

Remarks concerning the above result will be meaningful. First, we note that the existence of the traveling wave was established for constant switch functions and constant production function $g(u)$. Secondly, to establish the minimal wave speed, we needed to make a specific choice for the response function $f(v)$, otherwise the analysis is not mathematically tractable. However, we note that the current approach is not applicable to establish the existence of travelling waves for variable switch functions since the system will not be cooperative.

In the case where we general switch functions, the system is non-cooperative and therefore, the theory on cooperative systems is not applicable. Most of the existing theoretical literature in this direction assumes cooperative, nondegenerate systems. In the case of competitive systems, a simple change of variable will change a competition into a cooperative system. See for example [114]. Recent results for non-cooperative systems can be found, for example, in [180] and [86]. However, [180]'s work is not applicable to non-degenerate systems, while the work by [86] on non-cooperative degenerate time-periodic systems is also not applicable as it is impossible to construct the upper and lower cooperative subsystems. We thus believe this remains an open problem, and here we will proceed numerically to the study existence of traveling waves for general nonlinear conversion rates, $p(v)$, $q(v)$.

3.3.2 Numerical simulations

We have proved in the previous section that the reaction diffusion system admits a non-negative heteroclinic orbit connecting P^0 and P^* when $rq \leq 1$. Numerical simulations to support the results and the effect of parameters will be investigated in this section. The system of equations (3.11) is integrated using MatLab's `PDEPE` solver. For all simulations, to ensure convergence, we choose 300 cells in space with both relative and absolute error tolerances set at 10^{-8}. We remark that the model was also solved for different parameters to ensure that the wave solution is not unstable relative to their small changes. Similar to

the simulations for the reduced model, we choose $f(v) = v$ and $g(u)$ as given in equation (3.10). Following [58], the hibernation function takes the form

$$q(v) = \frac{1}{1+v^m}, \tag{3.16}$$

while the arousal function takes the modified version

$$p(v) = \frac{\delta + v^m}{1+v^m}, \tag{3.17}$$

where m is a positive integer. The modified arousal function is important since no activation is possible using the simple Hill function $v^m/(1+v^m)$. In this context, δ, taken to be $\delta = 0.1$, defines the minimum concentration or density at which the switch can take place. Unless stated otherwise under the figure caption, we choose the baseline parameter values as follows

$$r = 1, \quad s = 1, \quad \beta = 2, \quad \alpha = 1.$$

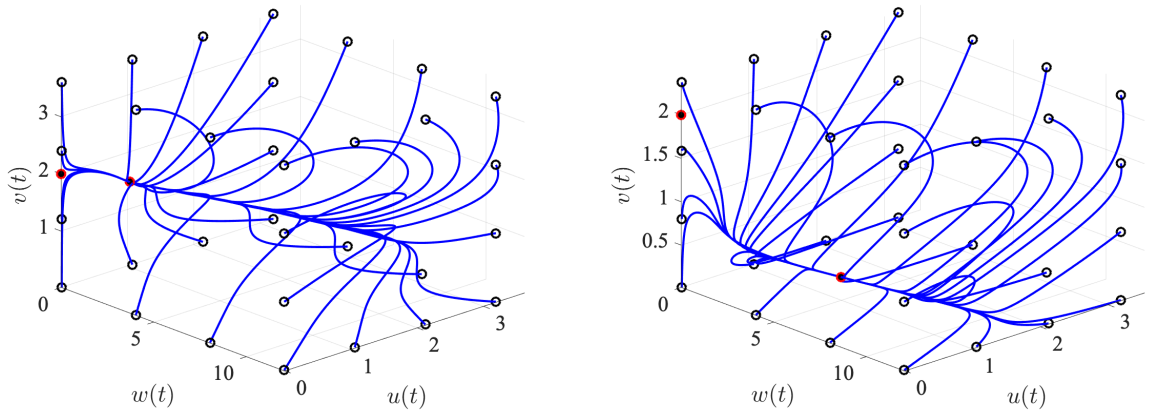

(a) $\gamma f(v^*) - \alpha\beta g'(1) > 0$ (b) $\gamma f(v^*) - \alpha\beta g'(1) < 0$

Figure 3.4: Illustration of the locally asymptotically stable P^*.

We begin with the numerical results for the uniform steady state with a focus on the nonzero equilibrium point P^*, see Fig. 3.4. If $\gamma f(v^*) - \alpha\beta g'(1) = 1 > 0$ with $\gamma = 1$, then $P^* = (0.1300, 1.00, 1.5000)^t$ is locally asymptotically stable. On the other hand, choosing $\gamma = 0.1$, then $\gamma f(v^*) - \alpha\beta g'(1) = -0.2273 < 0$, and $P^* = (0.0066, 1.00, 2.7273)^t$ remains locally asymptotically stable. The simulations in Fig. 3.4 were obtained using MatLab's `ode15s` solver.

Next, we consider the numerical solution of the reaction diffusion system (3.11). Since,

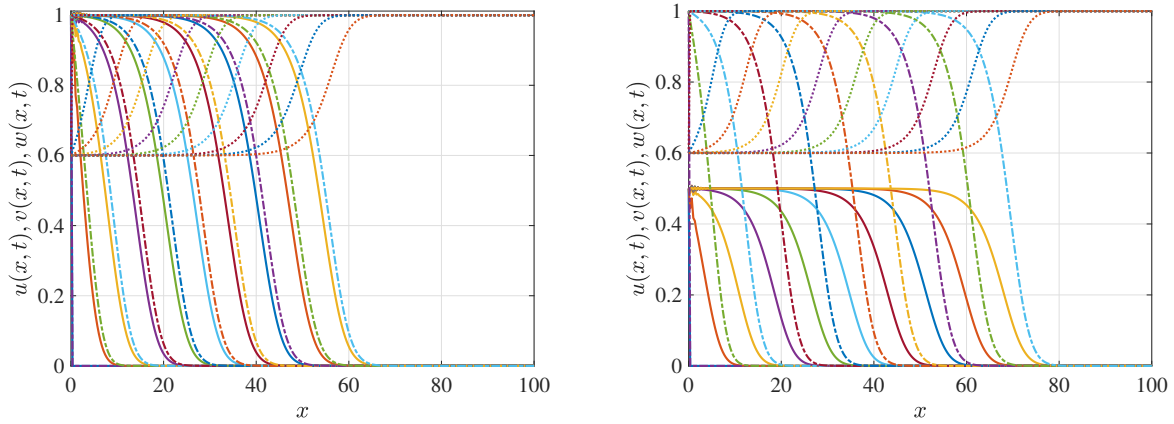

(a) $r = 1$. (b) $r = 0.5$.

Figure 3.5: Illustration of the existence of traveling wave for $r \leq 1$ with constant switch functions. The solid line is $w(x,t)$, the dash-dot line is $v(x,t)$, and the dotted line is $u(x,t)$ at equally spaced time intervals.

we are interested in traveling waves, the asymptotic conditions are

$$w(-\infty,t) = 0, \quad u(-\infty,t) = 0, \quad v(-\infty,t) = \beta,$$
$$w(\infty,t) = w^* = \frac{rq(v^*)}{sp(v^*)}, \quad u(\infty,t) = u^* = 1, \quad v(\infty,t) = v^* = \frac{\alpha\beta g(1)}{\gamma+\alpha}.$$

The numerical simulations will be performed on the truncated domain $x \in [0, 100]$, with the above asymptotic conditions at the end points. The asymptotic conditions as $x \to -\infty$ are taken as initial data for all values of x.

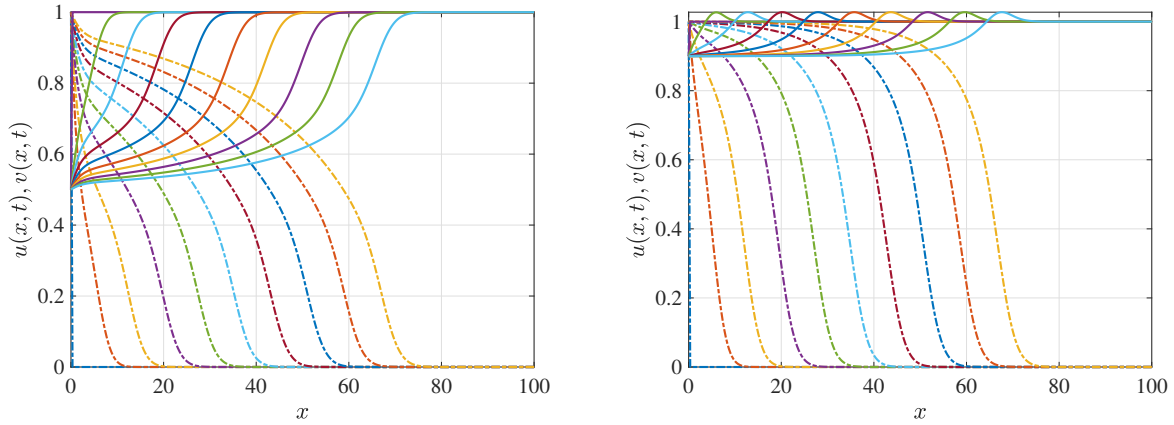

(a) $\alpha = 0.5$. (b) $\alpha = 1.5$.

Figure 3.6: Illustration of the existence of traveling wave for variable switch functions as given in equations (3.16) and (3.17). The broken line is $u(x,t)$ and the solid line is $v(x,t)$.

In Figs. 3.5 - 3.7 we support the results on the existence of the traveling waves for model (3.11). In particular, we illustrate the existence of wave solution connecting $\mathbf{0} = (0,0,\beta)^t$ and $\mathbf{1} = (w^*,u^*,v^*)^t$ through profiles at equally spaced time intervals.

From numerical results in Fig. 3.5, we see the system has a traveling wave solution $\boldsymbol{u}(x + vt)$ connecting $\mathbf{0}$ and $\mathbf{1}$. The monotone traveling wave exists and the spreading speed coincides with the minimal wave speed provided that $rq \leq 1$ with constant switch functions, in addition to a constant production function, $g(u)$.

In Fig. 3.6 we use switch functions as given in (3.16) and (3.17) with $g(u)$ as given by expression (3.10). It is clear that changing parameters, see in Fig. 3.6(b), the wave profiles may be non-monotonic under this setup. In particular, we see the appearance of a hump in the profiles, see also Fig. 3.2.

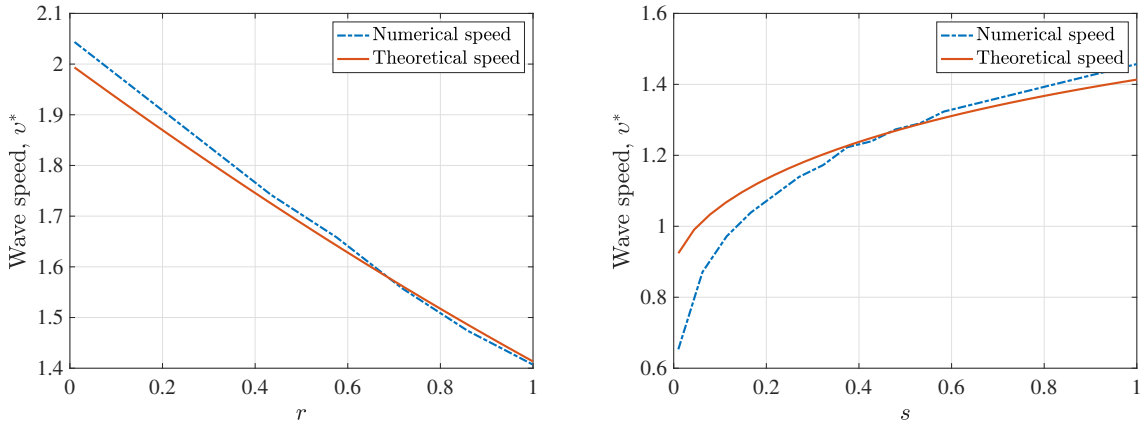

(a) Dependence of wave speed on r. (b) Dependence of wave speed on s.

Figure 3.7: Comparison of theoretical and numerical wave speeds under the setup of Theorem 3.3.

To illustrate theoretical results in comparison to numerical results, in Fig. 3.7 we present simulations comparing the wave speeds by varying s and r. Results in Fig. 3.7, in comparison with model results without quiescence clearly show that ignoring dormant cells overestimates the wave speed. The wave speed for the model with quiescence is less than 2, a constant speed which was obtained for the model with quiescence. Increasing the rate of deactivation, reduces the spreading speed, and increasing the rate of activation, increases the spreading speed.

3.4 Conclusions

Mathematical models can provide insights into the dynamics of the biology they represent. In this chapter, we considered solutions of a reaction-diffusion model describing the evolution of a bacterial colony with both active and dormant cells. We showed that the solution of the model converges to a traveling wave with a speed strongly dependent on the switching rates.

By using the theory of monotone wavefronts for cooperative and partially degenerate reaction-diffusion systems, the minimal wave speed is established for the model. In particular, the minimal wave speed plays a crucial role in the spread of the bacterial lawn.

Without quiescence, a closed form expression for the minimal wave speed was obtained to be: $v^* = 2\sqrt{k_3 k_4 D_b}$, while an implicit expression was obtained for the full model when the switch functions are constants. Numerical results indicate the importance of the quiescent stage in the speed of spread. Simulations show that the model admits non-monotonic traveling wave profiles when $g = g(u)$ and the switch functions are dependent on the chemo-attractant concentration.

As a final remark, it is worth mentioning that we have established that $\bar{v}$ is the minimal wave speed when the switch functions are considered constant. It remains to show a similar result when these are functions dependent on the chemo-attractant concentration. Using the current approach, a theoretical result for general switch functions ($p(v)$ and $q(v)$) remains mathematically not tractable and open. In addition, it remains to test the model within a physically relevant parameter regime supported by actual experimental data.

Chapter 4

Existence of stationary and oscillatory patterns

4.1 Introduction

Bacterial biofilms are multicellular communities embedded in a self-produced polymeric matrix comprised of polysaccharides, proteins and extracellular matrix [189]. Self organization and positioning of bacteria biofilms both in space and time, have been observed in natural environments and experimental studies leading to, for example, regularly repeating patterns, see [171, 150]. Biofilm formation occurs as a result of environmental cues such as starvation, chemical concentrations, or change in temperature. Cell density and signaling are two crucial components in the formation of a spatially organised biofilm [155]. Although cell signaling and distinct cell genes involved in the formation of biofilms differ between species, there exist other commonalities. Simple cells like the bacterium *E. coli* [171], *S. typhimurium* [191], to name a few, present regulated cellular anatomy resulting from the dynamic interactions between proteins and the cell membrane. However, as noted in [191], different bacteria present different patterns, in particular, during the formation stage. For example, *S. typhimurium* present structured lawn, while swarm ring appears for *E. coli*.

A review on cooperation in microbial populations can be found in [40]. The authors provided an ecological overview where ensembles of local subpopulations continuously emerge, grow and disappear again. The subpopulations vary in size from a few initial cells to billions in established communities. However, it has been reported that environmental noise such as the presence of toxins, triggered by the microbes themselves can be catastrophic. For example, pH changes caused by metabolic waste products such as lactic acid, acetate and hydrogen [52]. In their natural habitat, bacteria constantly compete with rivaling species found in the same ecological niche for survival and growth-limiting resources. Biological warfares occur where one species produces antibiotics or 'chemical

weapons' to suppress the growth or eradicate competing microorganisms. Some antimicrobial compounds do not only affect the competitors but also active against their own as well as identical bacteria [147, 65]. In some cases, however, such metabolic waste can be a resource for another species, allowing both polluters (waste producers) and detoxifiers (crossfeeders) to potentially benefit [63, 52]. On the other hand, the spreading of phages can change the fitness landscape [162, 176].

Bacterial communities exhibit a modified phenotype with regard to proliferation, gene expression and nutrient production, and can also show tolerance to unfavorable environmental conditions that individual cells fail to show [138]. The growth and survival of organisms often depend on their local interaction with their environment. Those interactions can either be negative or positive depending on the global or local cooperative modification of the environment. That is, instead of breaking down complex nutrients for their growth, microbes can exhibit negative local or global behaviour by engineering the environment in ways that are detrimental for their proliferation. It has been observed that bacteria modify the environmental pH to such a degree that they make their surroundings so acidic leading to the swift and complete extinction of the whole population. Termed 'ecological suicide' in their experiments, extinction of soil bacteria species *Paenibacillus sp.*, was observed in well-mixed batch culture in media containing glucose as the main carbon source. See also [149, 151] and references therein. The observation is that the denser the bacteria, the more waste is produced and thus, the risk of ecological suicide is higher at high population densities. This was observed in about 25% of soil microbes tested. In this case, low-density populations thrive while high density leads to ecological suicide. A study supporting the ability of bacteria to change media pH in their environment, indirectly rendering it more or less hospitable for other species, can be found in [46]. The authors in [149] observed that ecological suicide can also cause oscillations in the population size over time. Although these experiments are useful for providing insights into specific mechanisms of interactions, it is unclear to what extent findings from these studies scale up to predict the generic properties of large microbial communities or the interactions therein.

Despite the ubiquity of this environment-mediated population collapse, simple mathematical models to understand these processes are lacking in the literature. One of the simplest models is proposed in [136] to explain how microbes interacting through their chemical environment can achieve coexistence in a continuous growth setup. The authors observed that, in addition to consumption/degradation, facilitation and self-restraint interactions played a critical role in allowing species coexistence. Using pH as a model parameter, in [151] the authors proposed a simple deterministic model supported by experiments to understand how the bacteria manipulate their environment and also react to it. Motivated by the existing literature, we propose a spatial model comprising a general microbial population of inactive and active cells capable of producing waste products

modifying their environment to pH levels that could lead to either 'boom and bust' [58] or 'ecological suicide' [149]. While the proposed model is generic and can help to test hypotheses about these unknown processes, it is always important to bear in mind that they are only approximations of reality, and their predictions are subject to some uncertainty.

The rest of the chapter is organised as follows. The mathematical model under investigation is formulated in the next section. In Section 4.3 we study the reduced model which allows for the microbes to die or become dormant due to environmental stress. A full model tracking the density of dormant and active microbes is presented in Section 4.4. Numerical results and discussions related to the presented models are given in Sections 4.3 and 4.4. We discuss our findings and conclude in Section 4.5.

4.2 Model formulation

Mathematical models taking into account the consumption of a limiting nutrient in the presence of a chemoattractant have been considered extensively in the literature. See for example, [171, 128, 131, 30], and references therein. In [131], they summarised model mechanisms for *E. coli* experiments in a semi-solid medium. In addition, it is assumed that non-motile cells are dead, and not included in the analysis of the model dynamics. Chemotaxis was taken into account to represent the directed movement of organism in response to the concentration gradient. However, as indicated above, mathematical models including the negative feedback from the microbe's activities are lacking in the literature.

In this work, we consider an ecosystem comprising a general microbial population capable of modifying its environment to pH levels that are not hospitable to them. We begin by denoting $u(t)$, the density of active micro-organisms and $v(t)$ the concentration of the waste product in the surrounding environment. In the absence of $v(t)$, the bacteria growth follows a simple Logistic law

$$\frac{du}{dt} = k_5 u(k_6 - u), \tag{4.1}$$

where k_6 is the carrying capacity and $k_5 k_6$ is the growth rate, see also (3.2). The equation governing the change in concentration $v(t)$ is given by

$$\frac{dv}{dt} = k_8 g(u) - k_7 v - k_4 u f(v), \tag{4.2}$$

where k_7 denotes the rate of natural degradation of v, k_8 is the rate of production of v, see for example [46], and k_4 is the maximum rate of consumption of v. Thus, we allow for the consumption of metabolic waste, see for example [52] for further details. Moreover, we generalise the consumption function, $f(v)$, and assume it satisfies the following

hypotheses: $f(v) = 0$ if and only if $v = 0$ and $f'(v) \geq 0$, for all v. The production function $g(u)$ is assumed to saturate and includes input from both external sources and active microbes, hence we assume it satisfies the following conditions: $g(u) > 0$, $g'(u) > 0$ for all $u \geq 0$. Readers can consult for example, the work [30, 31],[149, Supplementary Information] and the references therein.

It has been reported that organisms that fail to adapt to this stress would either die or become dormant [66]. Motivated by the *Keller-Segel* model (1.3) and considering the above-mentioned ecological processes, we propose the model

$$\begin{aligned}
\frac{\partial w}{\partial t} &= k_1 q(v)u - k_2 p(v)w - k_3 w, \\
\frac{\partial u}{\partial t} &= D_u \nabla^2 u + D_{uv} \nabla \cdot (\chi(u,v)\nabla v) + k_5 u(k_6 - u) - k_1 q(v)u + k_2 p(v)w, \\
\frac{\partial v}{\partial t} &= D_v \nabla^2 v + k_8 g(u) - k_7 v - k_4 u f(v),
\end{aligned} \tag{4.3}$$

where ∇^2 is the *Laplacian operator* with respect to x, D_u and D_v are diffusion coefficients, D_{uv} represents the chemotaxis coefficient, and $w(t)$ denotes the density of dormant bacteria. The function $\chi(u,v)$ is the chemotaxis response functional, and we assume a system where microbes move from higher concentration of the toxins to lower concentration, known as negative chemotaxis [13]. The functions $q(v)$ and $p(v)$, each of them $\in (0,1)$, denote the hibernation and reawakening of bacteria in response to the concentration v, see for example [58], the literature therein and Section 1.3 for further discussion on these switch functions. In our work, we invoke assumptions on the transition functions $p(v)$ and $q(v)$.

$$\mathcal{P}_1 \ : \ p : \mathbb{R}_+ \to (0,1] \text{ is } C^1,\ p'(v) \leq 0 \text{ for all } v \text{ and } \lim_{v\to\infty} p(v) = 0,$$

$$\mathcal{P}_2 \ : \ q : \mathbb{R}_+ \to (0,1] \text{ is } C^1,\ q'(v) \geq 0 \text{ for all } v \text{ and } \lim_{v\to\infty} q(v) = 1,$$

which are different from hypotheses $\mathcal{F}_1$ and $\mathcal{F}_2$ in Section 2.2. Here we have assumed the concentration of energy source is large compared to the concentration of cells (negligible nutrient consumption) - which is consistent with the work of [131, Section 5.5]. The model is rendered dimensionless by choosing the following variables and scales

$$w \sim \frac{1}{k_6}, \quad u \sim \frac{1}{k_6}, \quad v \sim \frac{1}{k_6}, \quad x \sim \sqrt{\frac{D_b}{k_7}}, \quad t \sim \frac{1}{k_7},$$

to obtain

$$\begin{aligned}
\frac{\partial w}{\partial t} &= rq(v)u - sp(v)w - \mu w, \\
\frac{\partial u}{\partial t} &= \nabla^2 u + d\nabla \cdot (u\chi(v)\nabla v) + u(1-u) - rq(v)u + sp(v)w, \\
\frac{\partial v}{\partial t} &= d_v \nabla^2 v + \beta g(u) - v - \gamma u f(v),
\end{aligned} \tag{4.4}$$

where $d_v = D_c/D_b$, $d = [\chi]D_{bc}k_4/D_b$, $r = k_1/k_7$, $s = k_2/k_7$, $\beta = k_8/k_7$, $\gamma = k_4k_6/k_7$ and $\mu = k_3/k_7$. We consider a one-dimension spatial domain Ω. The notation $[*]$ refers to the scale for the given term.

First, we consider the homogeneous system of (4.4), i.e., ignore diffusion and chemotaxis. The system becomes

$$\begin{aligned} \frac{dw}{dt} &= rq(v)u - sp(v)w - \mu w, \\ \frac{du}{dt} &= u(1-u) - rq(v)u + sp(v)w, \\ \frac{dv}{dt} &= \beta g(u) - v - \gamma u f(v). \end{aligned} \tag{4.5}$$

System (4.5) is appended with the following initial conditions

$$w(0) = w_0 \geq 0, \quad u(0) = u_0 \geq 0, \quad v(0) = v_0 \geq 0. \tag{4.6}$$

Theorem 4.1. *System (4.5) defines a dynamical system on the biologically feasible region*

$$\Omega = \left\{ (w,u,v) \in \mathbb{R}^3_+ : w + u + v \leq \frac{2+\kappa}{\alpha_m}. \right\}$$

Proof. We show that for any initial data satisfying (4.6), the system possesses for all $t \geq 0$, a unique solution which lies in Ω.

First we show that Ω is a positively invariant set. In particular, no trajectories leave Ω by crossing one of its faces. On the contrary, let us assume there exists $t_1 > 0$ such that $w(t_1) = 0$ and $w'(t_1) < 0$ with $w(t) > 0$, $w(t) > 0$, $v(t) > 0$, for all $t \in (0, t_1)$. The first equation in (4.5) gives

$$\frac{dw}{dt}(t_1) = rq(v)u > 0,$$

which is a contradiction. Therefore, $w(t) \geq 0$ for all $t \geq 0$. Similarly for $t_2 > 0$, assuming $u(t_2) = 0$ and $u'(t_2) < 0$ with $u(t) > 0$, $w(t) > 0$ for all $t \in (0, t_2)$ then we have

$$\frac{du}{dt}(t_2) = sp(v)w > 0.$$

For $t_3 > 0$ with $v(t_3) = 0$ and $v'(t_3) < 0$ with $w(t) > 0$, $u(t) > 0$ for all $t \in (0, t_3)$, we have

$$\frac{dv}{dt}(t_3) = \beta g(u) > 0.$$

Therefore, in all cases the solution (w, u, v) remains in the region Ω for any initial data in Ω.

In the second step, we use the prior estimates together with the fact that the right hand of system (4.5) is a locally Lipschitz function. It follows from the second equation of

the system (4.5) that $u'(t) \leq u(t)\,(1-u(t))$, which implies that $\limsup_{t\to\infty} u(t) \leq 1$. Then for sufficiently large t, we have

$$\begin{aligned}\frac{d(w(t)+u(t)+v(t))}{dt} &= u(1-u)+\beta g(u)-v-\gamma u f(v)-\mu w\\ &\leq u(t)-u^2(t)+\beta g(u)+u(t)-u(t)-v(t)-\mu w(t)\\ &\leq \kappa+2u(t)-\alpha_m\left(w(t)+u(t)+v(t)\right),\end{aligned}$$

where $\alpha_m = \min\{1,\mu\}$. Since $g(u)$ is increasing and a saturating function, then $\beta g(u) \leq \kappa$. Hence, we have $\limsup_{t\to\infty}(w(t)+u(t)+v(t)) \leq \dfrac{2+\kappa}{\alpha_m}$. The above results show that the solution $(w(t),u(t),v(t))$ is nonnegative and uniformly bounded for any positive initial values. This complete the proof of the theorem. □

In the next sections we will study system (4.5) together with its submodels to gain insight into model (4.4) dynamics.

4.3 Reduced model

Observing that once active bacteria fail to adapt to the stress level $v(t)$, they would either die or become dormant (see for example [66]), we propose the following reduced model

$$\begin{aligned}\frac{du}{dt} &= u(1-u)-rq(v)u,\\ \frac{dv}{dt} &= \beta g(u)-v-\gamma u f(v).\end{aligned} \tag{4.7}$$

Under this setup, the term $rq(v)u$ represents the bacteria switching into dormant state, or bacterial mortality due to environmental stress. We remark that $1/(rq(v))$ describes the resistance or residence time of microbes under inhospitable conditions and it is dependent on the toxicity of the environment. The assumption on $q(0) > 0$ represents the existence of random switching or a result of paracrine signalling. Further details on the function $q(v)$ can be found in [58] or references therein.

4.3.1 Equilibria and their stability

Setting the right-hand side of $(4.7)_1$ to zero we see that $u = 0$ or $u = 1 - rq(v)$. That is, $u = 0$ together with the right-hand side of $(4.7)_2$ set to zero, we get the following boundary equilibrium $P^0 = (0, \beta g(0))$, representing the extinction state. Using the *Hartmann-Grobman Theorem*, P^0 is locally asymptotically stable provided $1 - rq(\beta g(0)) < 0$, otherwise it is unstable. Essentially we require that $r > 1/q(\beta g(0))$ for the population to derive itself to extinction.

On the other hand, assuming $u^* \neq 0$ or equivalently $u^* = 1 - rq(v^*)$, then from setting the right hand of $(4.7)_2$ to zero, v^* must satisfy the equation

$$H(v^*) = \beta g(u^*) - v^* - \gamma u^* f(v^*) = 0,$$

with $\lim_{v^* \to 0^+} H(v^*) = \beta g(rq(0) - 1) > 0$ and

$$H'(v^*) = -rq(v^*)[\beta g'(u^*) - \gamma f(v^*)] - \gamma u^* f'(v^*) - 1,$$

with $\lim_{v^* \to 0^+} H'(v^*) = -1 - \gamma f'(0)(1 - rq(0) < 0$. First we see that, if $\beta g'(u^*) - \gamma f(v^*) \geq 0$, then $H(v^*)$ is monotonically decreasing and a unique coexistence equilibrium point $P^* = (u^*, v^*)$ exists provided $1 - rq(v^*) > 0$.

On the other hand, if $\beta g'(u^*) - \gamma f(v^*) < 0$, together with $\lim_{v^* \to 0^+} H(v^*) > 0$ and $\lim_{v^* \to 0^+} H'(v^*) < 0$, in addition to $\lim_{v^* \to \infty} H'(v^*) = -1 - \gamma f'(1 - r) < 0$, then there exist at least one coexistence equilibrium point $P^* = (u^*, v^*)$ provided $1 - rq(v^*) > 0$. This will be illustrated numerically in Figs. 4.1 and 4.2.

Next we consider the local stability of the co-existence equilibrium, P^*, whose Jacobian is given by

$$J(u^*, v^*) = \begin{pmatrix} -u^* & -rq'(v^*)u^* \\ \beta g'(u^*) - \gamma f(v^*) & -1 - \gamma u^* f'(v^*) \end{pmatrix}.$$

The trace and determinant of $J(u^*, v^*)$ are given as

$$-u^* - 1 - \gamma u^* f'(v^*) < 0, \quad \text{and} \quad rq(v^*)u^*([\beta g'(u^*) - \gamma f(v^*)] + u^*[1 + \gamma u^* f'(v^*)]),$$

respectively. Clearly, we see that if $\beta g'(u^*) - \gamma f(v^*) \geq 0$, a unique co-existence equilibrium state exists and it is locally asymptotically stable. It is not clear what happens if $\beta g'(u^*) - \gamma f(v^*) < 0$. However, the following result rules out the possibility of Hopf bifurcation.

Proposition 4.1. *The uniform steady state system (4.7) has no periodic orbits.*

Proof. To prove this result, we apply the *Dulac-Bendixon criterion.* Let $Z \subset X$ be open and simply connected in the first quadrant. Let $h_u(u, v) = u(1 - u) - rq(v)u$ and $h_v(u, v) = \beta g(u) - v - \gamma u f(v)$. We need to show that there exists a function $\phi : Z \to \mathbb{R}$, continuously differentiable on Z, such that

$$\frac{\partial(\phi h_u)}{\partial u} + \frac{\partial(\phi h_v)}{\partial v}$$

is either strictly negative or strictly positive everywhere on Z. Let $\phi(u, v) = \frac{1}{u}$. Taking Z

to be open in the first quadrant, clearly ϕ is continuously differentiable in Z. Furthermore,

$$\frac{\partial(\phi h_u)}{\partial u} + \frac{\partial(\phi h_v)}{\partial v} = -\frac{1}{u}\left(u + 1 + \gamma u f'(v)\right) < 0.$$

Hence, the system has no periodic orbits in the open first quadrant. □

4.3.2 Numerical simulations

We have shown in the previous section that the system does not admit periodic orbits. Numerical simulations to support the results and the effect of parameter changes will be investigated in this section. We integrate the system of equations (4.7) using MatLab's `ode15s` solver. For all simulations, and to ensure convergence, we choose both relative and absolute error tolerances set at 10^{-8}. We remark that the model was also solved for different parameters to ensure that the solution is stable relative to their small changes.

Throughout this chapter, we choose $f(v) = v$ and

$$q(v) = \frac{\delta + v^m}{\sigma^m + v^m}, \tag{4.8}$$

with $m \geq 1$ and $\delta = 0.1 > 0$, satisfying the assumptions on $f(v)$ and hypothesis $\mathcal{P}_2$, respectively.

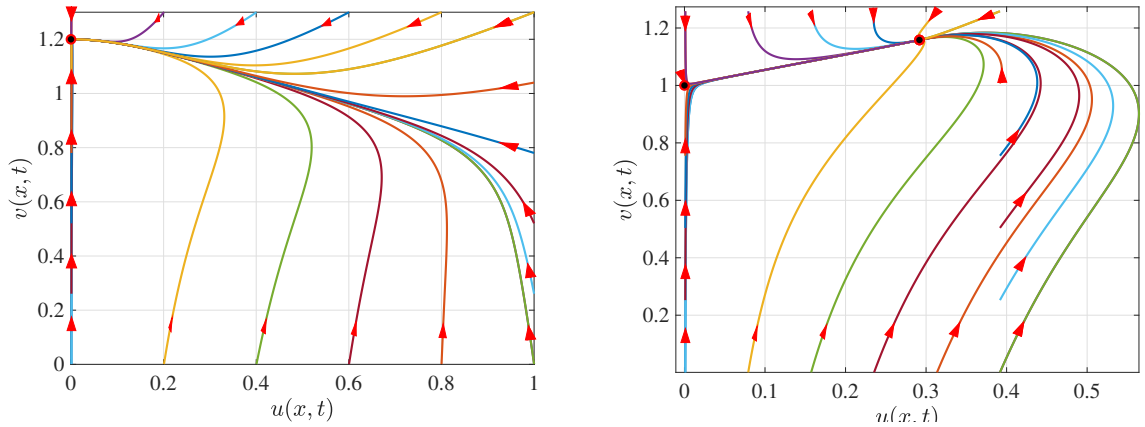

(a) $1 - rq(\beta g(0)) < 0$. (b) $\beta g'(u^*) - \gamma f(v^*) \geq 0$.

Figure 4.1: Phase planes corresponding to system (4.7). The parameters are chosen such that $r = 1.0$ with: $\beta = 1.2$, $\gamma = 1.0$ in figure (a), and $\beta = 1.0$, $\gamma = 0.2$ in figure (b).

Remark 4.1. *The initial investigation was centered on how microbial populations can drive themselves to extinction. It is clear from the proposed reduced model that this depends on the resistance of the population to the toxicity of the environment they reside in. The better the microbes can resist environmental toxic changes, the better they can avoid extinction. This can also be linked to the use of antibiotics as a treatment strategy*

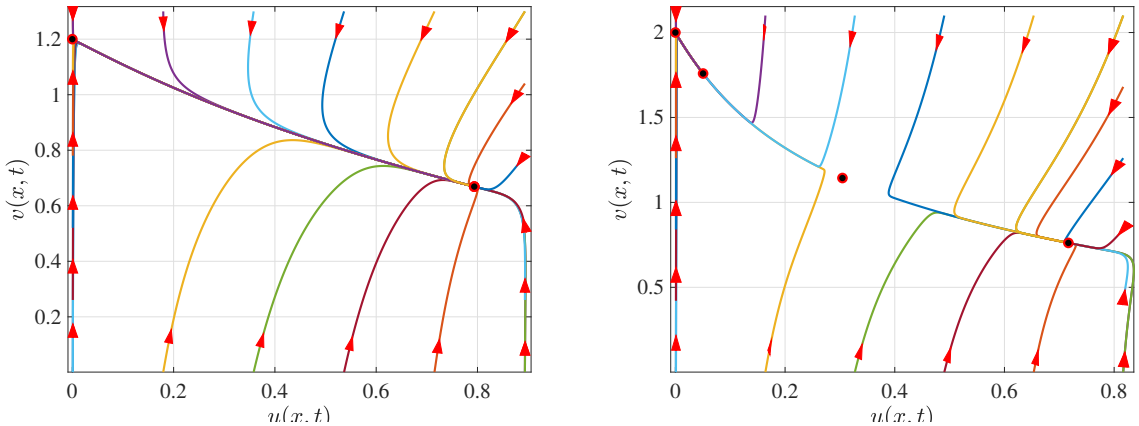

(a) $\beta g'(u^*) - \gamma f(v^*) < 0$. (b) $\beta g'(u^*) - \gamma f(v^*) < 0$.

Figure 4.2: Phase planes corresponding to system (4.7). The parameters are chosen such that $r = 1$ with: $\beta = 1.2$, $\gamma = 2.0$ in figure (a), and $\beta = 2.0$, $\gamma = 3.8$ in figure (b).

for infections as alluded to in [71]. It is crucial to understand antibiotic resistance before administering it.

In Fig. 4.1(a) we illustrate the stability of the extinction equilibrium point when the parameters are chosen such that $1 - rq(\beta g(0)) = -0.100 < 0$. In this case, a unique boundary equilibrium P^0 exists. If $1-rq(v^*) = 0.292 > 0$ together with $\beta g'(u^*)-\gamma f(v^*) = 0.368 \geq 0$, we have a unique coexistence equilibrium point $(u^*, v^*) = (0.2918, 1.1583)$ which is stable locally. This is illustrated in Fig. 4.1(b).

We further investigate the case $1 - rq(v^*) > 0$ together with $\beta g'(u^*) - \gamma f(v^*) < 0$. As illustrated in Fig. 4.2, we either have a unique coexistence equilibrium point which is locally asymptotically stable Fig. 4.2(a) or a bistable case Fig. 4.2(b). This is supported by experimental observations reported in [151, 136].

Remark 4.2. *The proposed reduced model (4.7) recovers the dynamics where bacteria acidify the environment inducing negative feedback on their survival. Under this setup, dormant cells are assumed to be dead [66]. The qualitative results indicated the nonexistence of a limit cycle, a conclusion which agrees with the discussion in [149, Fig. 2], and suggestion that the oscillations were a result of experimental conditions.*

4.3.3 Bifurcation analysis

We recall system (4.4) together with system (4.7). Assuming that once active bacteria fail to adapt to the stress level $v(t)$, they either die or become dormant, then system (4.4) is reduced to the following model

$$\begin{aligned} \frac{\partial u}{\partial t} &= \nabla^2 u + d\nabla \cdot (u\chi(v)\nabla v) + u(1-u) - rq(v)u, \\ \frac{\partial v}{\partial t} &= d_v \nabla^2 v + \beta g(u) - v - \gamma u f(v), \end{aligned} \tag{4.9}$$

where w can be obtained from

$$\frac{\partial w}{\partial t} = rq(v)u. \tag{4.10}$$

For convenience in the analysis, we rewrite system (4.9) in the form

$$\begin{aligned} \frac{\partial u}{\partial t} &= f(u,v) + \nabla^2 u + d\nabla \cdot (u\chi(v)\nabla v), \\ \frac{\partial v}{\partial t} &= g(u,v) + d_v \nabla^2 v, \end{aligned} \tag{4.11}$$

where

$$f(u,v) = u(1-u) - rq(v)u \quad \text{and} \quad g(u,v) = \beta g(u) - v - \gamma u f(v).$$

Without diffusion, the following generalised result holds.

Theorem 4.2. *With $f_u + g_v < 0$, assume $f_u g_v - f_v g_u > 0$ holds, then the steady state (u^*, v^*) of system (4.11) is stable in the absence of diffusion.*

With diffusion, the following result holds.

Theorem 4.3. *Assume $f_u + g_v < 0$ and $f_u g_v - f_v g_u > 0$ hold, the steady state (u^*, v^*) of system (4.11) loses stability if and only if $-g_u du^* \chi(v^*) + d_v f_u + g_v > 0$, and $(-g_u du^* \chi(v^*) + d_v f_u + g_v)^2 - 4d_v(f_u g_v - f_v g_u) > 0$, hold.*

Proof. Expanding system (4.11) at (u^*, v^*) using Taylor series and neglecting higher order terms gives the following linearised system of equations

$$\begin{aligned} \frac{\partial \bar{u}}{\partial t} &= f_u(u^*, v^*)\bar{u} + f_v(u^*, v^*)\bar{v} + \nabla^2 \bar{u} + du^* \chi(v^*)\nabla^2 \bar{v}, \\ \frac{\partial \bar{v}}{\partial t} &= g_u(u^*, v^*)\bar{u} + g_v(u^*, v^*)\bar{v} + d\,\nabla^2 \bar{v}. \end{aligned} \tag{4.12}$$

System (4.12) can be written in the matrix form:

$$\frac{\partial \omega}{\partial t} = J\omega + \mathcal{D}\nabla^2 \omega, \tag{4.13}$$

where $\omega = (\bar{u}, \bar{v})^t$ denotes vector solutions to the linear system (4.12), moreover,

$$\omega = \begin{pmatrix} \bar{u} \\ \bar{v} \end{pmatrix}, \; J = \begin{pmatrix} f_u & f_v \\ g_u & g_v \end{pmatrix}, \text{ and } \mathcal{D} = \begin{pmatrix} 1 & du^*\chi(v^*) \\ 0 & d_v \end{pmatrix}. \tag{4.14}$$

The dispersion relation given by the characteristic equation of the linearized system at (u^*, v^*) reads

$$|\lambda I + k^2 \mathcal{D} - J| = 0,$$

where $k \geq 0$ denotes the wave number [131]. Expanding the characteristic polynomial,

we obtain

$$\lambda^2 + \delta_1(k^2)\lambda + \delta_2(k^2) = 0, \tag{4.15}$$

where the trace and determinant of the Jacobian in (4.14) are given by

$$\delta_1(k^2) = (1 + d_v)k^2 - (f_u + g_v),$$

and

$$\delta_2(k^2) = d_v k^4 - k^2\left(-g_u d u^* \chi(v^*) + d_v f_u + g_v\right) + f_u g_v - f_v g_u,$$

respectively. The stability of the steady state (u^*, v^*) is determined by the eigenvalues, $\lambda = \lambda(k)$, of equation (4.15). The eigenvalues are given by

$$\lambda(k^2) = \frac{-\delta_1(k^2) \pm \sqrt{\delta_1(k^2)^2 - 4\delta_2(k^2)}}{2}.$$

When $k = 0$, the coefficients of (4.15) satisfy

$$\delta_1(0) = -(f_u + g_v) = u^* + (1 + \gamma u^* f'(v^*)) > 0, \tag{4.16}$$

$$\delta_2(0) = f_u g_v - f_v g_u = r q'(v^*) u^* \left\{\beta g'(u^*) - \gamma f(v^*)\right\} + u^*\left(1 + \gamma u^* f'(v^*)\right), \tag{4.17}$$

subsequently, the steady state (u^*, v^*) is stable linearly in the absence of spatial effects provided $\beta g'(u^*) - \gamma f(v^*) \geq 0$, which is consistent with the result in Section 4.3.1.

For values of $k \neq 0$, the coefficients of (4.15) satisfy

$$\delta_1(k^2) = \lambda_1(k^2) + \lambda_2(k^2) = (1 + d_v)k^2 + \delta_1(0), \tag{4.18}$$

$$\delta_2(k^2) = \lambda_1(k^2)\lambda_2(k^2) = d_v k^4 - k^2\left(-g_u d u^* \chi(v^*) + d_v f_u + g_v\right) + \delta_2(0). \tag{4.19}$$

We have that $\delta_1(k^2) > 0$ is always satisfied since $d_v > 0$ and $\delta_1(0) > 0$. Looking at

$$\delta_2(k^2) = d_v k^4 + k^2\left[\left\{\beta g'(u^*) - \gamma f(v^*)\right\} d u^* \chi(v^*) + d_v u^* + (1 + \gamma u^* f'(v^*))\right] + \delta_2(0),$$

if $\delta_2(k^2) < 0$ for some values of $k \neq 0$, then (u^*, v^*) becomes unstable due to inhomogeneous perturbations. The steady-state (u^*, v^*) is stable linearly in the absence of spatial effects provided $\beta g'(u^*) - \gamma f(v^*) \geq 0$, that is, $\delta_2(0) = f_u g_v - f_v g_u > 0$. Thus, if we assume $\beta g'(u^*) - \gamma f(v^*) \geq 0$, then

$$-g_u d u^* \chi(v^*) + d_v f_u + g_v > 0,$$

consequently, (u^*, v^*) remains stable. A condition that is of interest is $\beta g'(u^*) - \gamma f(v^*) < 0$

where a unique coexistence equilibrium, (u^*, v^*), exists. Subsequently, we assume that $\beta g'(u^*) - \gamma f(v^*) < 0$. Under this assumption, $\delta_2(0)$ and

$$-g_u d u^* \chi(v^*) + d_v f_u + g_v$$

might be positive and negative, respectively. Therefore, from Theorem 4.1 and Section 4.3.1, Ω is positively invariant and the co-existence equilibrium is locally asymptotically stable if $\beta g'(u^*) - \gamma f(v^*) \geq 0$, respectively. Using Proposition 4.1, we can conclude that P^* is globally asymptotically stable provided $\beta g'(u^*) - \gamma f(v^*) \geq 0$. In addition, we have that $\delta_2(k^2) < 0$ for some values of k if $\min(\delta_2(k^2)) < 0$, numerically shown in Fig. 4.4. When

$$k^2_{\min} = \frac{-g_u d u^* \chi(v^*) + d_v f_u + g_v}{2 d_v}, \tag{4.20}$$

we obtain

$$\min(\delta_2(k^2)) = -\frac{1}{4 d_v} \left(\left(-g_u d u^* \chi(v^*) + d_v f_u + g_v \right)^2 - 4 d_v \delta_2(0) \right).$$

Therefore, we have that $\min(\delta_2(k^2)) < 0$ when

$$\left(-g_u d u^* \chi(v^*) + d_v f_u + g_v \right)^2 - 4 d_v \delta_2(0) > 0,$$

which concludes the proof. □

Remark 4.3. *The first condition in Theorem (4.3) can be rewritten as*

$$d < \frac{d_v f_u + g_v}{g_u u^* \chi(v^*)},$$

and consequently, the only potentially destabilising mechanism is the presence of the cross-diffusion term, whereas the toxin linear diffusion acts as a stabiliser [172].

We have that the plot of $\delta_2(k^2)$ depends on d and as a result, we take d as the bifurcation parameter - see Figure 4.4. Furthermore, the marginal stability condition at some $k = k_c$ is $\min(\delta_2(k_c^2)) = 0$. We can write $\min(\delta_2(k^2)) = 0$ as

$$E_k d^2 + F_k d + G_k = 0,$$

where

$$E_k = \left(g_u u^* \chi(v^*) \right)^2, \quad F_k = -2 g_u u^* \chi(v^*) \left(d_v f_u + g_v \right), \quad G_k = \left(d_v f_u + g_v \right)^2 - 4 d_v \delta_2(0). \tag{4.21}$$

Bifurcation occurs at the critical value which is the root of equation (4.21) defined as a critical cross-diffusion coefficient,

$$d_c = \frac{-F_k \pm \sqrt{F_k^2 - 4E_kG_k}}{2E_k}.$$

Since $d > 0$, we let

$$d_c = \frac{-F_k + \sqrt{F_k^2 - 4E_kG_k}}{2E_k} = \frac{d_v f_u + g_v - 2\sqrt{d_v \delta_2(0)}}{g_u u^* \chi(v^*)}.$$

Solving equation (4.21) for d and substituting it into (4.20) we get the critical value

$$k_c^2 = \sqrt{\frac{\delta_2(0)}{d_v}}.$$

In Fig. 4.3, we show the bifurcation diagram. Below the solid line (i.e., in region IV), Turing pattern is expected while no pattern is expected in regions in I, II and III. Moreover, we observe that $\delta_2(k^2)$ can be negative provided $\beta g'(u^*) - \gamma f(v^*) < 0$, see Fig. 4.4.

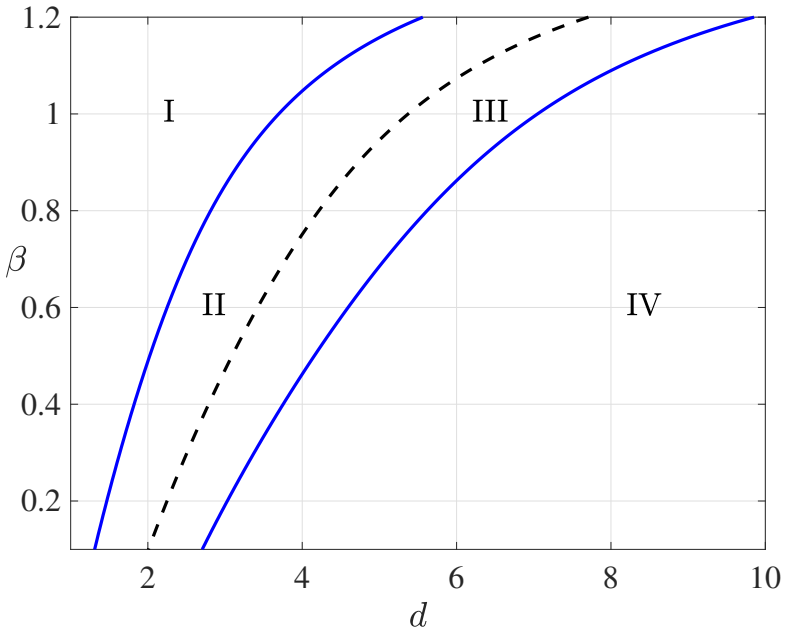

Figure 4.3: Bifurcation diagram for model in the d–β space.

Remark 4.4. *In Fig. 4.2(a) we have a locally asymptotically stable interior equilibrium point with* $\beta g'(u^*) - \gamma f(v^*) = -0.9651 < 0$. *For the same set of parameters, we observe that* $\delta_2(k^2)$ *can be negative leading to the occurrence of Turing instability; see Fig. 4.4.*

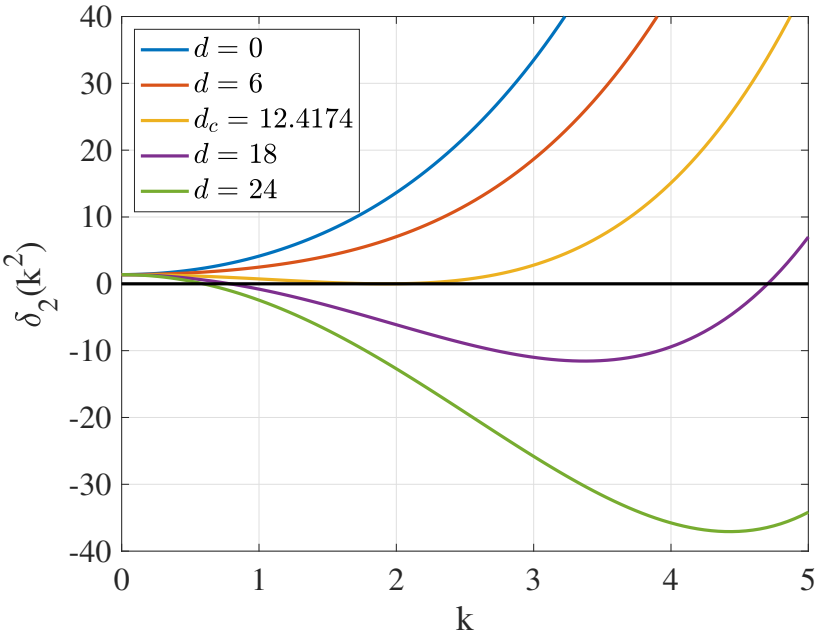

Figure 4.4: A plot of $\delta_2(k^2)$ for different values of d. The parameters are chosen as follows: $d_v = 0.1$, $r = 1.0$, $\beta = 1.2$, $\gamma = 2.0$ with $\beta g'(u^*) - \gamma f(v^*) = -0.9651 < 0$.

4.4 The full model

We are now interested in the case where bacteria switch states are dependent on the change in concentration $v(t)$ of the system. In addition, we assume dormant bacteria do not die. We begin by recalling the model system (4.5), that is,

$$\begin{aligned} \frac{dw}{dt} &= rq(v)u - sp(v)w, \\ \frac{du}{dt} &= u(1-u) - rq(v)u + sp(v)w, \\ \frac{dv}{dt} &= \beta g(u) - v - \gamma f(v)u, \end{aligned} \tag{4.22}$$

and present some mathematical results.

Proposition 4.2. *System (4.22) admits the following equilibria:*

- *the microbial-free state* $P^0 = (0, 0, \beta g(0))$, *and*
- *a unique co-existence state* $P^* = (w^*, u^*, v^*)$, *where* $u^* = 1$, $w^* = \dfrac{rq(v^*)}{sp(v^*)}$ *and* v^* *satisfies* $\beta g(1) - v^* - \gamma f(v^*) = 0$.

Proof. First, setting the right-hand side of equations (4.22) to zero, we get P^0 and P^* as the only equilibria points where v^* satisfies $\beta g(1) - v^* - \gamma f(v^*) = 0$. Defining $H(v^*) = \beta g(1) - v^* - \gamma f(v^*)$, then $H(v^*)$ is a monotonically decreasing function since $H'(v^*) =$

$-1-\gamma f'(v^*)<0$, where we have used the properties of functions f and g outlined in Section 4.2. Furthermore, $\lim_{v^*\to 0^+} H(v^*)=\beta g(1)>0$, hence, a unique solution v^* satisfying $H(v^*)=\beta g(1)-v^*-\gamma f(v^*)$ exists. □

To study the local stability of the two equilibria, we consider the general Jacobian matrix of system (4.22) given by

$$J(w,u,v)=\begin{pmatrix} -sp(v) & rq(v) & rq'(v)u-sp'(v)w \\ sp(v) & (1-u)-u-rq(v) & -rq'(v)u+sp'(v)w \\ 0 & \beta g'(u)-\gamma f(v) & -1-\gamma u f'(v) \end{pmatrix}.$$

At the microbial-free state, P^0, we have

$$J(P^0)=\begin{pmatrix} -sp(\beta g(0)) & rq(\beta g(0)) & 0 \\ sp(\beta g(0)) & 1-rq(\beta g(0)) & 0 \\ 0 & \beta g'(0) & -1 \end{pmatrix}.$$

Clearly, -1 is one of the eigenvalues of $J(P^0)$. The remaining eigenvalues are obtained from the reduced matrix

$$\begin{pmatrix} -sp(\beta g(0)) & rq(\beta g(0)) \\ sp(\beta g(0)) & 1-rq(\beta g(0)) \end{pmatrix},$$

whose trace is $(1-rq(\beta g(0)))-sp(\beta g(0))$ with the determinant given by $-sp(\beta g(0))$. Under the hypotheses $\mathcal{P}_1$ and $\mathcal{P}_2$, the microbial-free equilibrium state is unstable. This result, in comparison with the reduced model results, clearly supports the idea that microbial populations are capable of surviving hostile environments if they can switch state depending on the concentration $v(t)$.

4.4.1 Bifurcation analysis

The following linear stability analysis will be performed around the coexistence equilibrium (w^*,u^*,v^*). We call recall system (4.4) given by

$$\begin{aligned} \frac{\partial w}{\partial t} &= rq(v)u-sp(v)w-\mu w, \\ \frac{\partial u}{\partial t} &= \nabla^2 u+d\nabla\cdot(u\chi(v)\nabla v)+u(1-u)-rq(v)u+sp(v)w, \\ \frac{\partial v}{\partial t} &= d_v\nabla^2 v+\beta g(u)-v-\gamma u f(v). \end{aligned} \tag{4.23}$$

For convenience in the analysis, we rewrite system (4.23) in the form

$$\begin{aligned}\frac{\partial w}{\partial t} &= f(w,u,v),\\ \frac{\partial u}{\partial t} &= g(w,u,v) + \nabla^2 u + d\nabla\cdot(u\chi(v)\nabla v),\\ \frac{\partial v}{\partial t} &= h(w,u,v) + d_v\nabla^2 v.\end{aligned} \tag{4.24}$$

The linearized system of (4.24) can be written in the matrix form:

$$\omega_t = \mathcal{D}\Delta\omega + \mathcal{A}\omega, \tag{4.25}$$

where $\omega = (\bar{w},\bar{u},\bar{v})^t$ is a vector solution with

$$\omega = \begin{pmatrix}\bar{w}\\ \bar{u}\\ \bar{v}\end{pmatrix}, \quad \mathcal{D} = \begin{pmatrix}0 & 0 & 0\\ 0 & 1 & du^*\chi(v^*)\\ 0 & 0 & d_v\end{pmatrix}, \quad \mathcal{A} = \begin{pmatrix}f_w & f_u & f_v\\ g_w & g_u & g_v\\ 0 & h_u & h_v\end{pmatrix}.$$

The dispersion relation given by the characteristic equation of the linearized system at (w^*,u^*,v^*) reads

$$|\lambda I + k^2\mathcal{D} - \mathcal{A}| = 0,$$

where $k \geq 0$ denotes the wave number. The characteristic polynomial of system (4.25) reads

$$Q(\lambda) := s_3(k)\lambda^3 + s_2(k)\lambda^2 + s_1(k)\lambda + s_0(k) = 0, \tag{4.26}$$

where the coefficients are given by

$$\begin{aligned}s_3(k) &= 1,\\ s_2(k) &= k^2(d_v+1) - (f_w + g_u + h_v),\\ s_1(k) &= d_v k^4 - k^2\{-dh_u u^*\chi(v^*) + f_w(d_v+1) + h_v + d_v g_u\} + f_w h_v - g_v h_u + f_w g_u - f_u g_w\\ &\quad + g_u h_v,\\ s_0(k) &= -d_v f_w k^4 + k^2\{-f_w h_u d u^*\chi(v^*) + f_w(h_v + d_v g_u) - d_v f_u g_w\} + (f_w g_v - f_v g_w)h_u\\ &\quad + f_u g_w h_v - f_w g_u h_v,\end{aligned}$$

where

$$\begin{aligned}f_w &= -sp(v^*), & f_u &= rq(v^*), & f_v &= rq'(v^*) - sp'(v^*)w^*,\\ g_w &= sp(v^*), & g_u &= -1 - rq(v^*), & g_v &= -rq'(v^*) + sp'(v^*)w^*,\\ h_u &= \beta g'(1) - \gamma f(v^*), & h_v &= -1 - \gamma f'(v^*).\end{aligned}$$

The eigenvalues of the characteristic equation (4.26) determine the time evolution of perturbation.

According to the *Routh-Hurwitz criteria*, the stability conditions for system (4.23) are

$$s_i(k) > 0, \quad \text{for } i = 0, 1, 2; \quad \text{and } s_2(k)s_1(k) - s_0(k) > 0 \ \forall k. \tag{4.27}$$

A violation of any one of the conditions in (4.27) leads to diffusion-induced instability (Turing instability).

In the absence of cross and self-diffusion, we recover the model investigated in Section 3.3. For completeness, its results are summarised in this section. The coefficients of the corresponding characteristic equation are given by

$$\begin{aligned}
s_2(0) &= sp(v^*) + (1 + rq(v^*)) + (1 + \gamma f'(v^*)),\\
s_1(0) &= (1 + \gamma f'(v^*))(1 + rq(v^*) + sp(v^*)) + (\gamma f(v^*) - \beta g'(1))(-rq'(v^*) + sp'(v^*)w^*)\\
&\quad + sp(v^*),\\
s_0(0) &= sp(v^*)\left(1 + \gamma f'(v^*)\right).
\end{aligned}$$

Clearly, $s_0(0)$ and $s_2(0)$ are unconditionally positive and $s_1(0)$ is positive provided $\gamma f(v^*) - \beta g'(1) \leq 0$. Thus, the first assumption of *Routh-Hurwitz* is verified. It remains to check if $\Delta_2 = s_2(0)s_1(0) - s_0(0)$ is positive. We have

$$\begin{aligned}
\Delta_2 &= s_2(0)s_1(0) - s_0(0)\\
&= (sp(v^*) + rq(v^*) + 1) \times s_2(0) + sp(v^*)(1 + \gamma f'(v^*))^2\\
&\quad + (1 + \gamma f'(v^*))^2 (rq(v^*) + 1) + (1 + \gamma f'(v^*))(\gamma f(v^*) - \beta g'(1))(-rq'(v^*) + sp'(v^*)w^*).
\end{aligned}$$

It is unclear if the complete statement is positive. However, assuming $\gamma f(v^*) - \beta g'(1) \leq 0$, then the coefficient s_1 and the second-Hurwitz determinant, $\Delta_2 = s_2(0)s_1(0) - s_0(0)$, are positive. Under $\gamma f(v^*) - \beta g'(1) > 0$, Δ_2 can be zero, meaning that the polynomial $Q(\lambda)$ may have pure imaginary conjugate roots and one real root.

To prove a Hopf bifurcation, we choose β as the bifurcation parameter, then $Q(\lambda)$ has a pair of complex conjugate roots, $a \pm bi$ where $a, b \in \mathbb{R}$, which cross the real axis as β passes through β^*, then $\Delta(\beta)$ changes sign as β passes through β^*. Rewriting Δ, we have

$$\begin{aligned}
\Delta(\beta) &= -\beta g'(1)(-rq'(v^*) + sp'(v^*)w^*)\left[(1 + \gamma f'(v^*)) + (1 + sp(v^*) + rq(v^*))\right]\\
&\quad + (1 + sp(v^*) + rq(v^*))\left[sp(v^*) + (1 + \gamma f'(v^*))(1 + sp(v^*) + rq(v^*)) + (1 + \gamma f'(v^*))^2\right]\\
&\quad + \gamma f(v^*)(-rq'(v^*) + sp'(v^*)w^*)\left[(1 + \gamma f'(v^*)) + (1 + sp(v^*) + rq(v^*))\right].
\end{aligned}$$

For a Hopf bifurcation, we need an additional property to verify, the so-called transversal-

ity condition that indicates that the eigenvalues cross the $x-$axis with a non-zero velocity. In other words

$$\frac{da}{d\beta}(\beta^*) = a'(\beta^*) \neq 0. \tag{4.28}$$

Verifying (4.28) is equivalent to verifying $\Delta'(\beta^*) \neq 0$. We proceed to show numerically that $\Delta'(\beta^*) < 0$; see Fig. 4.5(b). We deduce that a Hopf bifurcation related to the bifurcation parameter, β, may occur at (P^*, β^*) provided conditions in Remark 4.5 are met.

Remark 4.5. *A Hopf bifurcation occurs if*

- *there exists a β^* such that $\Delta(\beta^*) = 0$, such Jacobian matrix at the coexistence state P^* has a pair of imaginary eigenvalues as well as one real negative eigenvalue,*
- *and $\Delta'(\beta^*) \neq 0$.*

The remark is supported numerically in Fig. 4.5 to illustrate the existence of a Hopf bifurcation and oscillatory solutions.

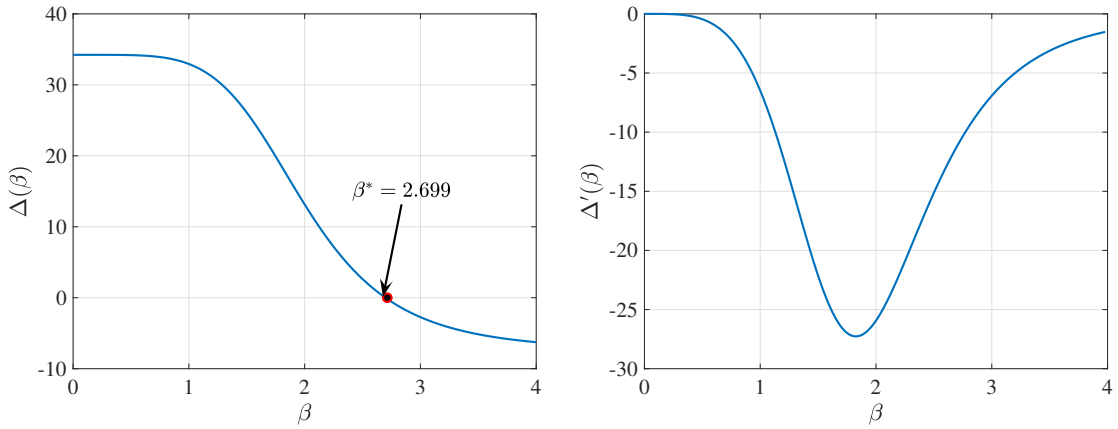

(a) Plot for $\Delta(\beta)$ with β. (b) Plot for $\Delta'(\beta)$ with β.

Figure 4.5: Illustrating the existence of Hopf bifurcation. There exists a $\beta^* = 2.699$ such that $\Delta(\beta^*) = 0$.

Similar to the previous reduced system (4.7), we integrate the equations (4.22) using MatLab's `ode15s` solver. In addition to the choice of $q(v)$ in (4.8), we also have

$$p(v) = \frac{\sigma^m}{\sigma^m + v^m}, \tag{4.29}$$

with $m \geq 1$ which satisfies hypothesis $\mathcal{P}_1$. In Figs. 4.5, 4.6, and 4.7 we illustrate the properties of model (4.22). Unless stated differently under the figure caption, the parameters are chosen as follows: $r = 1.0$, $s = 1.0$, $\gamma = 2.0$ and $\beta = 2.8$.

Microbial population oscillations have been observed in both the field and experiments, supported by mathematical models; see for example [149, 58] to name a few.

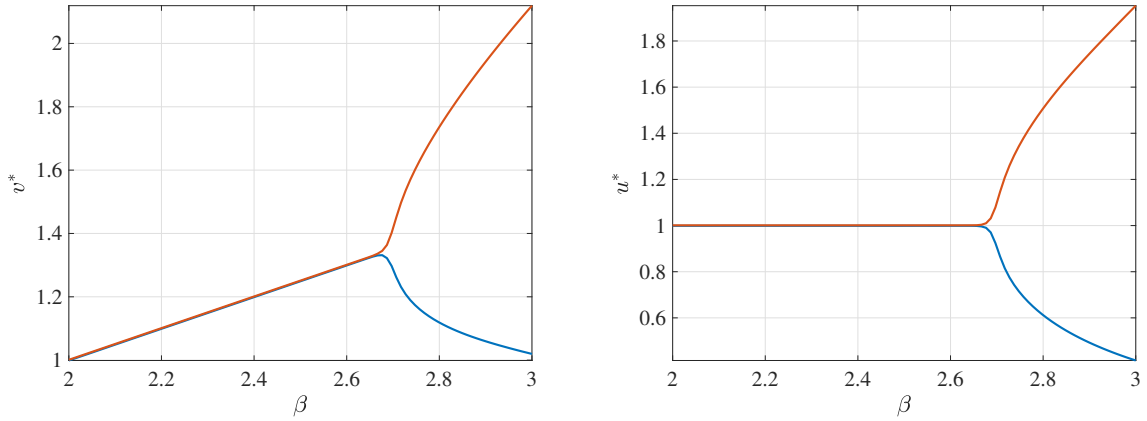

(a) Bifurcation on v^*. (b) Bifurcation on u^*.

Figure 4.6: Bifurcation with respect to β to illustrate the existence of population oscillations. The figure shows the minimal and maximal values of the concentration v (figure (a)) and active microbial population (figure (b)).

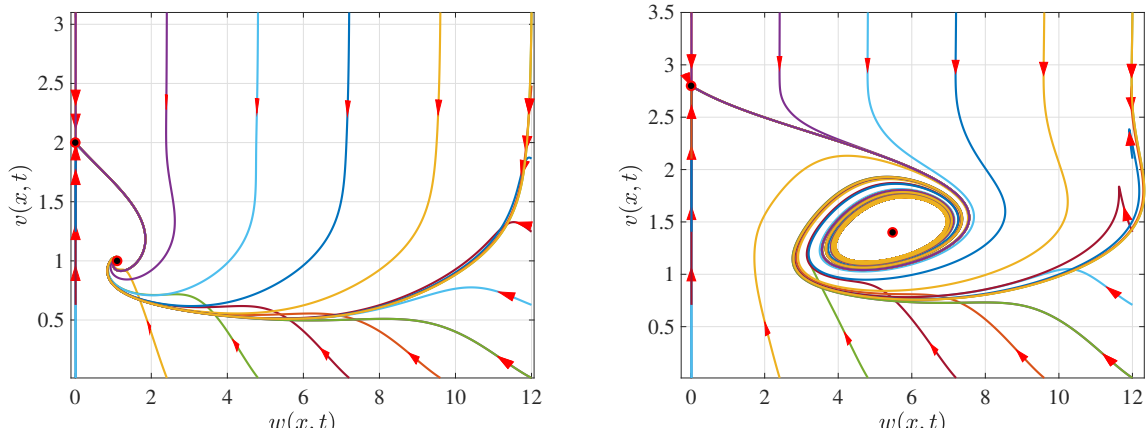

(a) $\beta = 2.0$. (b) $\beta = 2.8$.

Figure 4.7: Phase plane for model (4.22) illustrating the existence of oscillatory solutions and local stability.

Based on their experiments, the authors in [149] proposed a mathematical model consisting of two differential equations representing the change in bacterial density in response to the change in proton concentration (pH). An ad hoc function to account for a pH dependence of the bacterial growth was coupled to the standard *Logistic* growth model. The rate of change of proton concentration was assumed to depend on the rate of change of bacteria density to account for the observed non-monotonic time profiles. In this work, we proposed a generic model to account for the change in bacteria density in response to the change in its environment. We allow for the bacteria to switch state (active or dormancy) in response to their surroundings without going into the molecular details, see Section 4.4.

Similar to the experimental work of [149], coexistence and population oscillations were observed in the model proposed here. In particular, [149] population extinction was observed at low buffer levels, population oscillation at medium buffer levels and stable

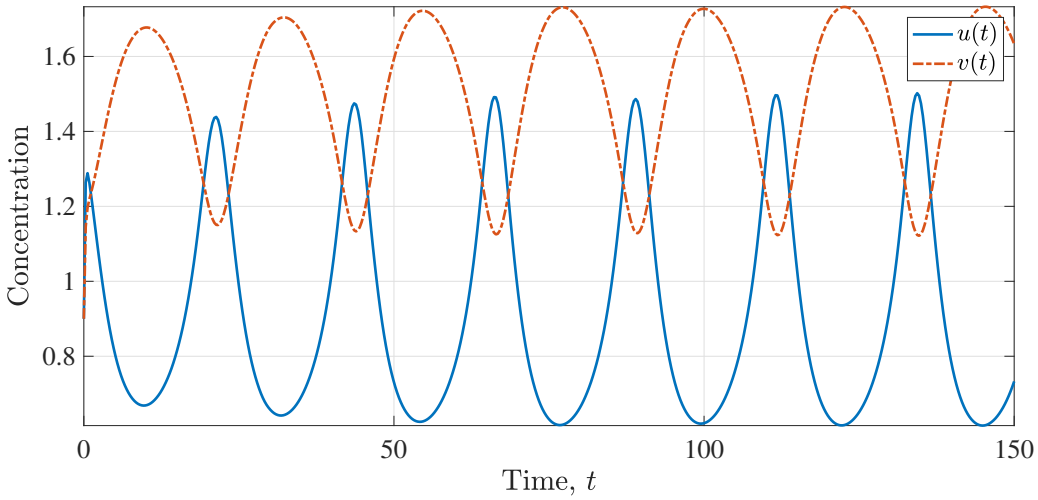

Figure 4.8: Time series solution of (4.22) corresponding to parameter selection: $r = 1.0$, $s = 1.0$, $\gamma = 2.0$, $\beta = 2.8$ and $\alpha = 1$.

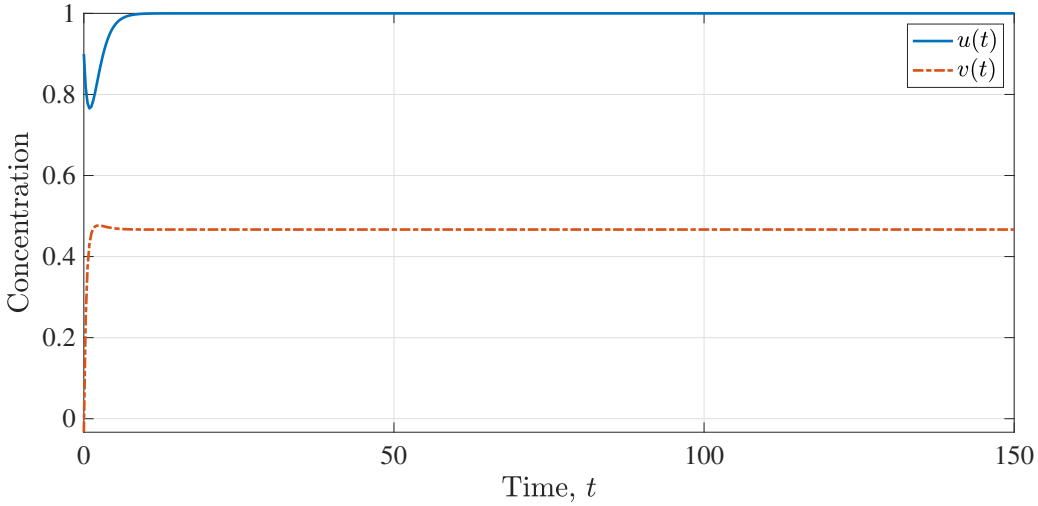

Figure 4.9: Time series solution of (4.22) corresponding to parameter selection: $r = 1.0$, $s = 1.0$, $\gamma = 2.0$, $\beta = 2.8$ and $\alpha = 0$.

coexistence at high buffer levels. This phenomenon is replicated here via the production term

$$g(u) = \alpha + \frac{u}{\sigma + u},$$

where a decrease in α is used to emulate an increase in buffer concentration as in experiments [149]. When $\alpha = 0$, representing high buffer levels, a stable coexistence state is observed; see Fig. 4.9. For medium buffer levels, $\alpha \neq 0$, both population oscillations and coexistence are observed; see Figs. 4.7 and 4.8.

Now we recall the characteristic equation (4.26). The *Routh Hurwitz* conditions are satisfied provided $\gamma f(v^*) - \beta g'(1) \leq 0$. Otherwise, there is a possibility that conditions (4.27) are violated.

In the absence of cross-diffusion, $d = 0$, the system is said to be stable if

$$s_1(k)s_2(k) - s_0(k) > 0,$$

and

$$s_i(k) > 0, \quad \text{for } i = 0, 1, 2; \quad \text{and } \forall k. \tag{4.30}$$

Note that $s_2(k) > 0$ since $s_2(0) = -f_w - g_u - h_v > 0$ as k and d_v are nonnegative numbers. Therefore, Turing instability cannot be induced through $s_2(k)$. Similarly,

$$\begin{aligned} s_0(k) &= -d_v f_w k^4 + k^2 \{f_w(h_v + g_u d_v) - d_v f_u g_w\} + s_0(0) \\ &= d_v sp(v^*)k^4 + k^2 \{sp(v^*)(1 + \gamma f'(v^*)) + d_v sp(v^*)\} + s_0(0) \end{aligned}$$

is positive since $s_0(0) > 0$. Once more Turing instability cannot be induced through $s_2(k)$ and $s_0(k)$. Now, we check the sign of $s_1(k)$. The coefficient $s_1(k)$ is given by

$$\begin{aligned} s_1(k) &= d_v k^4 - k^2 \{f_w(d_v + 1) + h_v + d_v g_u\} + s_1(0) \\ &= d_v k^4 + k^2 \{sp(v^*)(d_v + 1) + (1 + \gamma f'(v^*)) + d_v(1 + rq(v^*))\} + s_1(0). \end{aligned}$$

We know that $s_1(0)$ is positive provided $\gamma f(v^*) - \beta g'(1) \leq 0$, therefore, $s_1(k)$ is positive if $\gamma f(v^*) - \beta g'(1) \leq 0$. Otherwise, it is possible that $s_1(k)$ is negative. We then investigate the sign of $s_1(k)s_2(k) - s_0(k)$, which is a cubic polynomial function in k^2 given by

$$\begin{aligned} &d_v (d_v + 1) k^6 + k^4 \{d_v s_2(0) - (d_v + 1)(f_w(d_v + 1) + h_v + d_v g_u) + d_v f_w\} \\ &+ k^2 \{(d_v + 1)s_1(0) - s_2(0)(f_w(d_v + 1) + h_v + d_v g_u) - f_w(h_v + d_v g_u) + d_v f_u g_w\} \\ &+ (s_1(0)s_2(0) - s_0(0)), \end{aligned}$$

which is,

$$\begin{aligned} &d_v (d_v + 1) k^6 \\ &+ k^4 \{d_v s_2(0) + (d_v + 1) (sp(v^*)(d_v + 1) + (1 + \gamma f'(v^*)) + d_v(1 + rq(v^*)) - d_v sp(v^*)\} \\ &+ k^2 \{(d_v + 1)s_1(0) + s_2(0) (sp(v^*)(d_v + 1) + (1 + \gamma f'(v^*)) + d_v(1 + rq(v^*)))\} \\ &+ k^2 \{-sp(v^*)((1 + \gamma f'(v^*)) + d_v(1 + rq(v^*))) + d_v rq(v^*)sp(v^*)\} + \Delta_2. \end{aligned}$$

The polynomial above can be rewritten in the general form

$$P(k^2) := P_3(k^2)^3 + P_2(k^2)^2 + P_1(k^2) + P_0 = 0, \tag{4.31}$$

with coefficients given by

$$
\begin{aligned}
P_3 &= d_v\,(d_v+1)\,,\\
P_2 &= d_v s_2(0) + (d_v+1)\,((1+\gamma f'(v^*)) + d_v(1+rq(v^*))\,sp(v^*)(d_v^2+d_v+1),\\
P_1 &= (d_v+1)\left(s_1(0) + (sp(v^*))^2\right) + d_v rq(v^*)sp(v^*)\\
&\quad + [(1+rq(v^*)) + (1+\gamma f'(v^*))]\,[sp(v^*)(d_v+1) + (1+\gamma f'(v^*)) + d_v(1+rq(v^*))]\,,\\
P_0 &= \Delta_2.
\end{aligned}
$$

Clearly, coefficients P_3 and P_2 are positive since $d_v > 0$ and $s_2(0) > 0$ are positive. Assuming $\gamma f(v^*) - \beta g'(1) \leq 0$, then P_1 and P_0 are positive. As a result, equation (4.31), $P(k^2) = s_1(k)s_2(k) - s_0(k)$, is positive if $\gamma f(v^*) - \beta g'(1) \leq 0$. Since Turing instability occurs if the interior equilibrium point of the homogeneous system is stable, but becomes unstable in the presence of diffusion, then Turing instability cannot be induced through all the conditions, $s_2(k)$, $s_1(k)$, $s_0(k)$ and $s_1(k)s_2(k) - s_0(k)$ provided $\gamma f(v^*) - \beta g'(1) \leq 0$. Otherwise, if we assume $\gamma f(v^*) - \beta g'(1) > 0$, then either P_1 or P_0 could be negative which might lead $s_1(k)s_2(k) - s_0(k)$ to become negative.

Adding self and cross-diffusion terms, the dispersion relation is given by the characteristic equation (4.26) of the linearized system (4.25). Then, we have $s_2(k) > 0$ since $s_2(0) > 0$. We now check the signs of $s_1(k)$, $s_0(k)$ and $s_1(k)s_2(k) - s_0(k)$. Coefficient $s_1(k)$ is given as

$$
\begin{aligned}
s_1(k) &= d_v k^4 + s_1(0)\\
&\quad + k^2\left\{-d\,(\gamma f(v^*) - \beta g'(1))\,u^*\chi(v^*) + sp(v^*)(d_v+1) + (1+\gamma f'(v^*)) + d_v(1+rq(v^*))\right\}.
\end{aligned}
$$

We observe that provided $\gamma f(v^*) - \beta g'(1) \leq 0$, then $s_1(0)$ is positive. Thus, making $s_1(k) > 0$ under the same condition. Under the assumption that $\gamma f(v^*) - \beta g'(1) > 0$, we observe that there is a possibility that $s_1(k)$ becomes negative.

Similarly,

$$
\begin{aligned}
s_0(k) &= d_v sp(v^*)k^4 + s_0(0)\\
&\quad + k^2\left\{-sp(v^*)d(\gamma f(v^*) - \beta g'(1))u^*\chi(v^*) + sp(v^*)(1+\gamma f'(v^*)) + d_v sp(v^*)\right\}.
\end{aligned}
$$

Given that $\gamma f(v^*) - \beta g'(1) \leq 0$, then $s_0(0) > 0$ leading to $s_0(k)$ becoming positive. As a result, Turing instability cannot be induced through the coefficients of the characteristic equation (4.26). Similarly for $s_0(k)$, there is a possibility that the condition is violated given $\gamma f(v^*) - \beta g'(1) > 0$.

We then investigate the sign of $s_1(k)s_2(k) - s_0(k)$ and rewrite it in the form

$$
R(k^2) = R_3(k^2)^3 + R_2(k^2)^2 + R_1(k^2) + R_0 = 0, \tag{4.32}
$$

where the coefficients are given by

$$
\begin{aligned}
R_3 &= d_v\,(d_v+1)\,,\\
R_2 &= d_v s_2(0) + (d_v+1)\,(-d(\gamma f(v^*) - \beta g'(1))u^*\chi(v^*) + (1+\gamma f'(v^*)) + d_v(1+rq(v^*)))\\
&\quad + sp(v^*)(d_v^2 + d_v + 1),\\
R_1 &= (d_v+1)s_1(0) - d(\gamma f(v^*) - \beta g'(1))u^*\chi(v^*)\,(s_2(0) + sp(v^*)) + sp(v^*)(d_v+1)s_2(0)\\
&\quad + [(1+rq(v^*)) + (1+\gamma f'(v^*))]\,(s_2(0) - sp(v^*)) + d_v rq(v^*)sp(v^*),\\
R_0 &= \Delta_2.
\end{aligned}
$$

Clearly, R_3 is positive since $d_v > 0$. Assuming $\gamma f(v^*) - \beta g'(1) \leq 0$, then R_1, R_2 and R_0 become positive, otherwise, there is a possibility that the coefficients become negative.

Remark 4.6. *We observe that if we assume $\gamma f(v^*) - \alpha\beta g'(1) \leq 0$, then all inequalities (4.27) are satisfied. Thus, under this assumption the Turing instability cannot be induced through $s_0(k)$, $s_1(k)$, $s_2(k)$ or $s_1(k)s_2(k) - s_0(k)$. Provided $\gamma f(v^*) - \alpha\beta g'(1) > 0$, the interior equilibrium point can be unstable through a Hopf bifurcation. Therefore, the first case is of no interest whereas the second case possibly gives interesting results; see Figs 4.10 - 4.11 below.*

In Figs. 4.10 and 4.11, we see that conditions $s_1(k)$, $s_0(k)$ and $s_1(k)s_2(k) - s_0(k)$ are violated when $\gamma f(v^*) - \beta g'(1) = 1.5000 > 0$.

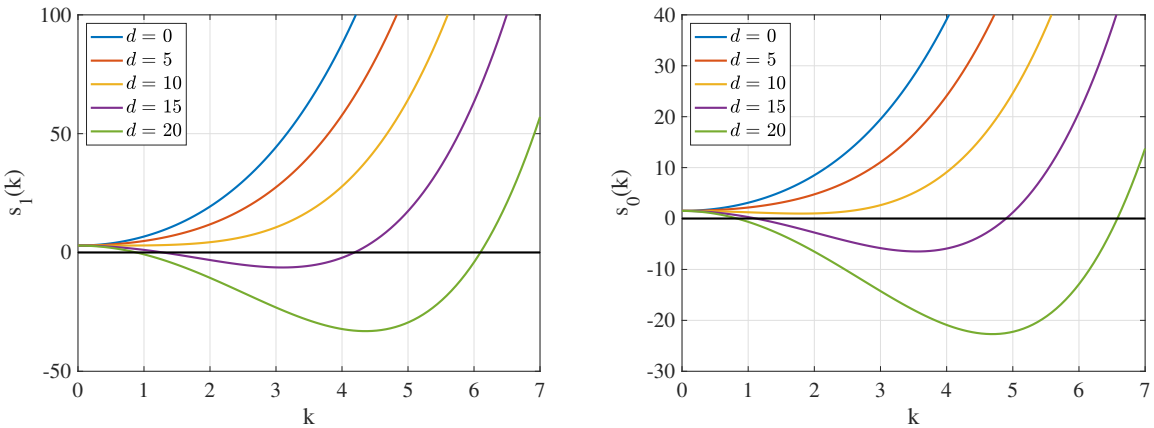

(a) $s_1(k)$ (b) $s_0(k)$

Figure 4.10: (a) A plot of $s_1(k)$ for different values of d. (b) A plot of $s_0(k)$ for different values of d. The parameters are chosen as follows: $r = 1.0$, $s = 1.0$, $\gamma = 2.0$ and $\beta = 2$ with $\gamma f(v^*) - \beta g'(1) = 1.5000 > 0$.

Remark 4.7. *We note that for the same set of parameters as in Figs. 4.10 - 4.11 with $\gamma f(v^*) - \beta g'(1) = 1.5000 > 0$, we have a locally asymptotically stable interior equilibrium point. See Fig. 4.7(a). From Figs 4.10 -4.11, we observe that the inequalities (4.27) can be violated.*

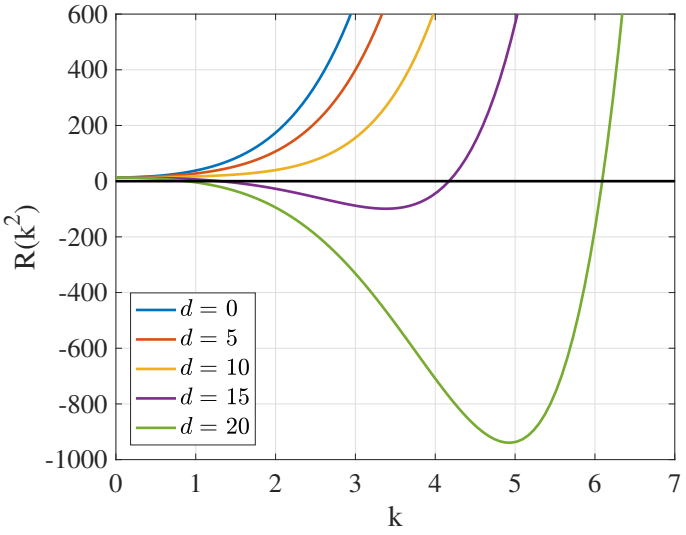

Figure 4.11: A plot of $R(k^2)$ for different values of d.

The minimum Turing point and the corresponding criteria are given by the following relations

$$\frac{\partial R}{\partial k^2} = 0, \quad \text{and} \quad \frac{\partial^2 R}{\partial^2 k^2} > 0, \tag{4.33}$$

[61]. From the above relation, a direct calculation gives

$$\frac{\partial R}{\partial k^2} = 0 \Rightarrow k^2 = k_m^2 = \frac{-R_2 + \sqrt{R_2^2 - 3R_1R_3}}{3R_3}, \tag{4.34}$$

and from the expression, we must have either

$$R_1 < 0 \quad \text{or} \quad R_2 < 0. \tag{4.35}$$

The second criteria of (4.33) given by

$$\frac{\partial^2 R}{\partial^2 k^2} = 6R_3k^2 + 2R_2$$

is positive, which shows that at the point $k^2 = k_m^2$ the equation (4.32) has a minimum value. Consequently, the condition where we will have $R(k_m^2) < 0$ is if

$$2R_2^3 - 9R_1R_2R_3 - 2\left(R_2^2 - 3R_1R_3\right)^{3/2} + 27R_0^2R_3 < 0. \tag{4.36}$$

The relations (4.35) and (4.36) are necessary and sufficient conditions, respectively, for instability. However, they are not enough to show Turing instability. The growth of each plane wave mode is determined by the real part of the roots of (4.26), i.e., λ. Turing instability occurs if the $\Re(\lambda)$ becomes positive for at least one wave number $k = k_c$,

and the uniform steady state is destablised leading to wave patterns with critical wave number k_c. If the imaginary part, $\Im(\lambda|_{k=k_c})$ of the unstable mode is zero, then the first critical mode corresponds to a stationary plane wave and Turing instability occurs. In this case, the characteristic equation (4.26) has three real roots provided that

$$\left[2\left(s_2(k)\right)^3 - 9s_2(k)s_1(k) + 27s_0(k)\right]^2 - 4\left[\left(s_2(k)\right)^2 - 3s_1(k)\right]^3 \leq 0. \tag{4.37}$$

The above inequality (4.37) is true if

$$\left(s_2(k)\right)^2 - 3s_1(k) \geq 0.$$

The above inequalities are illustrated in Fig. 4.12.

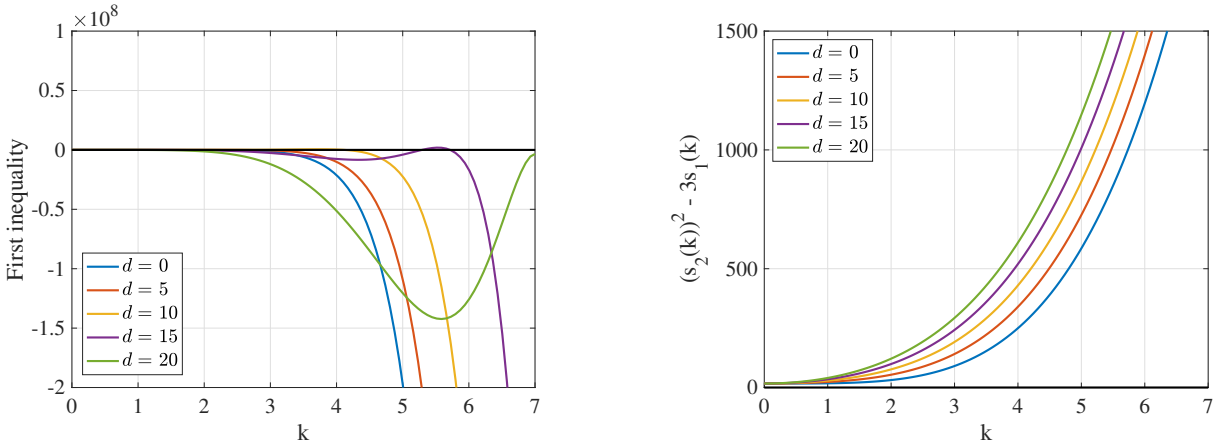

Figure 4.12: Numerical illustration that conditions (4.37) and inequality $\left(s_2(k)\right)^2 - 3s_1(k) \geq 0$ are satisfied.

4.5 Conclusions

Understanding bacterial responses to physiological conditions is an important priority for combating opportunistic infections. The proposed model has the underpinnings of antibiotic resistance. For example, in [71] they studied the dynamics of *E. faecalis* communities exposed to antibiotics revealing scenarios where increasing population size or delaying drug exposure can promote population collapse. In [151], the authors showed that the way microbes modify their environment and react to it sets the interactions within single-species populations and also between different species.

Microbial growth and survival depend on the environment and interactions within. These populations are capable of changing their environment by producing chemicals, thereby changing the pH of their environment. The proposed model takes into account

the dynamics of bacteria transitioning from one state to another depending on the concentration levels of the toxin in their surroundings. Our results support the observed rapid eradication, also named 'ecological suicide', of microbial population as a result of a change in their environment [149]. In addition, we observed the occurrence of self-sustained oscillations in the microbial population mediated by the change in concentration levels of the toxin. In Fig. 4.8, we see that as the toxin concentration levels increase, the number of active cells decline which support the negative interaction between active microbe density and toxin concentrations. We can conclude that as the toxin concentration levels increase, causing the deterioration of the environment, this leads to ecological suicide. Our results support the experimental observations in [149] showing ecological suicide as a result of environmental deterioration leading to oscillatory dynamics.

The role of interactions between genotypes and their consequences for the spatial structure and functional outcomes are increasingly being studied to better understand the ecology and evolution of microbial communities. Therefore, it is of great importance to investigate the phenotypic variation and microbial population processes that occur in order to understand the emergence and consequences of interactions in spatially structured microbial communities [47].

As reported in [150], organisms are not randomly dispersed but can be found in spatial aggregates at many scales, leading to spatial heterogeneity. They further argued that generic factors intrinsic to the populations such as interactions between the organisms play a major role in the emergence of these patterns. Regular spatial patterns and heterogeneity can be observed in different microbial ecosystems. Experimental observations ranged from bistability, successive growth, extended suicide, and stabilization. In future work, we will explore the variety of spatial patterns that could possibly emerge from the system and the ecological consequences that follow.

Chapter 5

Coupled finite volume - nonstandard finite difference methods

5.1 Introduction

The mathematical theory connecting continuous and discrete dynamical systems from numerical schemes has been expanded in the literature; see for example [164]. The main important elements to consider when constructing or designing numerical methods to approximate solutions for continuous dynamical systems are convergence, rate of convergence as well as stability. In turn, the intrinsic properties of dynamical systems that ideally should be preserved if the numerical methods are to produce reliable simulations providing qualitative observations and useful insights into the exact solutions include: fixed points and their stability, limit cycles, and as well as attracting sets [12].

Dynamic consistency (DC) of a system is defined with respect to its specific properties and normally these properties will differ from one system to another. Suppose a differential equation and/or its solutions have property P. Then, we say a discrete model is dynamically consistent with a differential equation, with respect to the property P, if it has and/or its solutions also have property P [127]. Positivity, boundedness and monotonicity of solutions, correct number and stability of fixed-points and other special solutions are important properties associated with the mathematical modeling of phenomena in the natural and engineering sciences [123, 127]. Our interest and focus in DC is its use as a fundamental principle to limit possible forms of the nonstandard finite difference (NSFD) schemes [127]. It is well known that using standard numerical integration techniques; for example, the explicit Euler and/or Runge-Kutta (RK) methods, to solve initial-value problems often leads to numerical instabilities for cases of models and discretization parameters [173, 101, 120, 125]. Although these instabilities such as oscillations and chaos can be removed using small time steps, an extra cost for computing or examining the long-term behavior of a dynamical system can be crucial [32]. Conse-

quently, it is an objective to design robust numerical approximations using numerical methods that have no scheme-dependent instabilities for realistic values of the model parameters. To achieve this aim, the nonstandard framework of Mickens [124, 120, 125] is used. Numerical methods constructed using the Mickens framework generally are known to preserve some important features of the continuous model they are approximating; see [124, 120, 125]. Since the pioneering work by Mickens on the subject [120], the nonstandard finite difference method has been proposed and applied successfully as a very efficient tool for approximating to solve different models of differential equations arising from the applied sciences, [9, 12, 125, 121] and [7] for the latest review.

To describe the concept of a discrete dynamical system which is a numerical approximation of a continuous dynamical system, we denote the first-order system of ordinary differential equations (1.11) and rewrite it as

$$\frac{dU}{dt} = \boldsymbol{f}(U, \pi), \tag{5.1}$$

where $\boldsymbol{f} : \mathbb{R}^m \to \mathbb{R}^m$, $\boldsymbol{u} = U(t) : [0, +\infty) \to \mathbb{R}^m$ with initial conditions $U_0 \in \mathbb{R}^m$ and $\pi = (\pi_1, \pi_2, ...)$ denoting the parameters of the system. To transform a continuous system (5.1) to a discrete system, we discretise the continuous variable $t \in [0, +\infty)$ such that $t \in (t_0, t_1, ..., t_n)$ where $n \in \mathbb{N}$ and $U(t)$ is represented by the discrete values U_n [119]. The transformation leads to a difference equation given of the form

$$Y(U_{n+1}, U_n) = 0, \tag{5.2}$$

where $Y : \mathbb{R}^m \times \mathbb{R}^m \to \mathbb{R}^m$. We can also write U_{n+1} in terms of U_n in the following explicit form

$$U_{n+1} = G(U_n, \pi, \Delta t), \tag{5.3}$$

where Δt denotes the time step size with $G : \Omega \subseteq \mathbb{R}^m \times \mathbb{R}^m \to \mathbb{R}^m$.

There are various discretisation methods used to approximate differential equations such as the $Runge - Kutta$ and $Forward - Euler$ methods with the latter being one of the classical methods. The standard discretisation is given as

$$\frac{dU}{dt} \to \frac{U_{n+1} - U_n}{\Delta t}, \tag{5.4}$$

where U_{n+1} is approximated by $U(t+n\Delta t)$. In [126] the author showed that these classical $forward - Euler$ and $Runge - Kutta$ methods lead to numerical instabilities making the transformations inconsistent with the original continuous system. Consequently, in [125] the nonstandard finite difference method based on the concept of dynamical consistency was proposed so as to prevent instabilities observed in other methods [122].

Definition 5.1. *[44] A finite difference method is called a nonstandard finite difference scheme if at least one of the following conditions is satisfied:*

- *The classical denominator Δt, of the discrete derivative is replaced by a non-negative function $\phi(\Delta t)$ satisfying the requirement $\phi(\Delta t) = \Delta t + \mathcal{O}([\Delta t]^2)$;*
- *Nonlinear terms that occur in the right-hand side of (5.1) are approximated in a non-local way.*

The first order differential equation (5.1) and the difference equation (5.4) are said to be dynamically consistent when the difference equation (5.4) preserves essential properties such as the equilibria and their stability, bifurcations as well as the chaos of the original continuous system of equations [121, 119].

The performance of nonstandard finite difference methods in comparison to other finite difference methods can be illustrated through its qualitative stability or dynamic consistency analysis. Topological dynamic consistency is a stronger result and further investigation can be found in [10, 11, 12], and references therein.

5.2 Nonstandard finite difference method

We recall the differential model (4.22). In this section, we propose a nonstandard finite difference scheme to solve the system of equations. We let $(w^n, u^n, v^n)^T$ denote an approximation of $(w(t_n), u(t_n), v(t_n))^T$ where $t_n = n\Delta t$, with $n \in \mathbb{N}$ and $\Delta t > 0$.

We propose the following scheme constructed via the non-local approximation (cf. [120]) of the nonlinear terms

$$\begin{aligned}
\frac{w^{n+1} - w^n}{\phi(\Delta t)} &= rq(v^n)u^n - sp(v^n)w^{n+1} - \mu w^{n+1}, \\
\frac{u^{n+1} - u^n}{\phi(\Delta t)} &= \left(1 - u^{n+1}\right) u^n - rq(v^n)u^{n+1} + sp(v^n)w^{n+1}, \\
\frac{v^{n+1} - v^n}{\phi(\Delta t)} &= \beta g(u^n) - v^{n+1} - \gamma v^{n+1} h(v^n) u^{n+1},
\end{aligned} \tag{5.5}$$

where $f(v) = vh(v)$ and the denominator function of the discrete derivatives is chosen according to

$$\eta'(t) \leq (2 + \kappa) - \alpha_m \eta, \tag{5.6}$$

where $\eta(t) = w(t) + u(t) + v(t)$, $\alpha_m = \min\{1, \mu\}$ and $\phi(\Delta t) = \Delta t + \mathcal{O}(\Delta t^2)$ with κ defined as in Section 4.2 . In particular, we see that (5.6) has an exact scheme (see [120])

$$\frac{\eta^{n+1} - \eta^n}{1 - \exp(-\alpha_m \Delta t)} \leq \frac{2 + \kappa}{\alpha_m} - \eta^{n+1}, \tag{5.7}$$

such that $\phi(\Delta t) = 1 - e^{-\alpha_m \Delta t}$. By exact scheme, we mean that the discrete solution η^n coincides with the continuous solution $\eta(t_n)$. In compact form, we can write system (5.5) in the form

$$y^{n+1} = F(\Delta t)\,(y^n)\,, \quad y(0) = y_0,$$

where $y^n = (w^n, u^n, v^n)$ and

$$F(\Delta t)(y^n) = \begin{pmatrix} \dfrac{w^n + \phi rq(v^n)u^n}{1 + \phi\mu + \phi sp(v^n)} \\ \dfrac{u^n + \phi u^n + \phi sp(v^n)w^{n+1}}{1 + \phi u^n + \phi rq(v^n)} \\ \dfrac{v^n + \phi\beta g(u^n)}{1 + \phi + \phi\gamma h(v^n)u^{n+1}} \end{pmatrix}. \tag{5.8}$$

Using standard techniques [12], we now verify the dynamic consistency of the scheme. For consistency, F must satisfy the following requirements:

$$F(0)(y) = y, \quad \frac{dF(0)}{d\Delta t}(y) = F(y).$$

Clearly, the first condition is satisfied. We have that $\dfrac{dF(0)}{d\Delta t}(y)\Big|_{\Delta t=0}$ is given by

$$\begin{pmatrix} \dfrac{rq(v)u - sp(v)w - \mu w}{(1 + \phi\mu + \phi sp(v))^2} \\ \dfrac{u(1-u) - rq(v)u + sp(v)w}{(1 + \phi u + \phi rq(v))^2} \\ \dfrac{\beta g(u) - v - \gamma uvh(v)}{(1 + \phi + \phi\gamma h(v)u)^2} \end{pmatrix}_{\Delta t=0} = \begin{pmatrix} rq(v)u - sp(v)w - \mu w \\ u(1-u) - rq(v)u + sp(v)w \\ \beta g(u) - v - \gamma u f(v) \end{pmatrix}.$$

The above system (5.8) can be rewritten in the explicit form

$$A(\Delta t, y^n)y^{n+1} = B(\Delta t, y^n)y^n + \psi(0, 0, 1 + \beta g(0))^t, \tag{5.9}$$

where matrices $A(\Delta t, y^n)$ and $B(\Delta t, y^n)$ are given by

$$\begin{pmatrix} 1 + \phi\mu + \phi sp(v^n) & 0 & 0 \\ 0 & 1 + \phi u^n + \phi rq(v^n) & 0 \\ 0 & 0 & 1 + \phi + \phi\gamma h(v^n)u^{n+1} \end{pmatrix}$$

and

$$\begin{pmatrix} 1 & \phi rq(v^n) & 0 \\ \phi sp(v^n) & 1 + \phi & 0 \\ 0 & 0 & 1 + \phi\beta g(u^n) \end{pmatrix},$$

respectively. We see that $A(\Delta t, y^n)$ is an *M-matrix* since it is a diagonal matrix. Hence,

its inverse, $A(\Delta t, y^n)^{-1}$, is non-negative. We have that $B(\Delta t, y^n) \geq 0$, which is sufficient for the scheme to preserve the positivity of solutions. We conclude that scheme (5.5) defines a discrete dynamical system on the same domain as the continuous model (4.22). See [8] and references therein for more details. Setting $y^{n+1} = y^n$, we see that the scheme preserves the same fixed points, $E_0 = (0, 0, \beta g(0))$ and $E^* = (w^*, u^*, v^*)$ as the continuous model (4.22).

Following (5.8) and (5.9), then $F(\Delta t)(y) = A^{-1}(\Delta t, y)B(\Delta t, y)$ so that

$$\frac{dF(\Delta t)}{dy}(y) = \begin{pmatrix} \dfrac{1}{1+\phi\mu+\phi sp(v)} & \dfrac{\phi rq(v)}{1+\phi\mu+\phi sp(v)} & J_{1,3} \\ \dfrac{\phi sp(v)}{1+\phi u+\phi rq(v)} & \dfrac{1+\phi}{1+\phi u+\phi rq(v)} - \dfrac{\phi\left(u+\phi u+\phi sp(v)w\right)}{\left(1+\phi u+\phi rq(v)\right)^2} & J_{2,3} \\ 0 & \dfrac{\phi\beta g'(u)}{1+\phi+\phi\gamma h(v)u} - \dfrac{\left(v+\phi\beta g(u)\right)\phi\gamma h(v)}{\left(1+\phi+\phi\gamma h(v)u\right)^2} & J_{3,3} \end{pmatrix},$$

where

$$\begin{aligned} J_{1,3} &= \frac{\phi rq'(v)u}{1+\phi\mu+\phi sp(v)} - \frac{\left(w+\phi rq(v)u\right)\phi sp'(v)}{\left(1+\phi\mu+\phi sp(v)\right)^2}, \\ J_{2,3} &= \frac{\phi sp'(v)w}{1+\phi u+\phi rq(v)} - \frac{\phi rq'(v)\left(u+\phi u+\phi sp(v)w\right)}{\left(1+\phi u+\phi rq(v)\right)^2}, \\ J_{3,3} &= \frac{1}{1+\phi+\phi\gamma h(v)u} - \frac{\phi\gamma h'(v)u\left(v+\phi\beta g(u)\right)}{\left(1+\phi+\phi\gamma h(v)u\right)^2}. \end{aligned}$$

We proceed to show that all eigenvalues of the Jacobian matrix evaluated at the fixed points lie in a unit circle.

Evaluating $\dfrac{dF(\Delta t)}{dy}(y)$ at the bacteria-free equilibrium, we obtain

$$\frac{dF(k)}{dy}(0, 0, \beta g(0)) = \begin{pmatrix} \dfrac{1}{1+\phi\mu+\phi sp(\beta g(0))} & \dfrac{\phi rq(\beta g(0))}{1+\phi\mu+\phi sp(\beta g(0))} & 0 \\ \dfrac{\phi sp(\beta g(0))}{1+\phi rq(\beta g(0))} & \dfrac{1+\phi}{1+\phi rq(\beta g(0))} & 0 \\ 0 & \dfrac{\phi\beta g'(0)}{1+\phi} - \dfrac{\beta g(0)\phi\gamma h(\beta g(0))}{(1+\phi)} & \dfrac{1}{1+\phi} \end{pmatrix}.$$

Now, we need to verify that all the eigenvalues of the Jacobian matrix at E_0 lie inside a unit circle. First, we see that $\dfrac{1}{1+\phi}$ is the first eigenvalue of the matrix $\dfrac{dF(\Delta t)}{dy}(0, 0, \beta g(0))$ which is strictly less than one. The remaining eigenvalues are obtained from the reduced matrix

$$J_r = \begin{pmatrix} \dfrac{1}{1+\phi\mu+\phi sp(\beta g(0))} & \dfrac{\phi rq(\beta g(0))}{1+\phi\mu+\phi sp(\beta g(0))} \\ \dfrac{\phi sp(\beta g(0))}{1+\phi rq(\beta g(0))} & \dfrac{1+\phi}{1+\phi rq(\beta g(0))} \end{pmatrix}.$$

To show whether the remaining eigenvalues lie in a unit circle, we use the well-known

Jury's conditions for $J_r \in \mathbb{R}^2 \times \mathbb{R}^2$. In this case, we need to show that

$$(i) \quad 1-\det(J_r) > 0, \quad (ii) \quad 1-\text{trace}(J_r)+\det(J_r) > 0, \quad (iii) \quad 0 < J_{11} < 1,\ 0 < J_{22} < 1.$$

The left hand side of the first condition, $1 - \det(J_r) > 0$, is equivalent to

$$\phi[2\phi sp(\beta g(0))rq(\beta g(0)) + \mu(1 + \phi rq(\beta g(0))) + (sp(\beta g(0)) + rq(\beta g(0)) - 1)],$$

which is strictly positive provided $sp(\beta g(0)) + rq(\beta g(0)) - 1 > 0$. The left hand side of the second condition is equivalent to

$$\phi^2[\mu(rq(\beta g(0)) - 1) - sp(\beta g(0))],$$

which is strictly positive provided $\mu(rq(\beta g(0)) - 1) - sp(\beta g(0)) > 0$. The last condition is clearly not satisfied if $rq(\beta g(0)) - 1 < 0$, that is, there is a possibility that the fixed point E_0 lies inside a unit circle if $rq(\beta g(0)) - 1 > 0$.

Similarly, for the stability of E^*, we proceed to evaluate $\dfrac{dF(\Delta t)}{dy}(y)$ at the co-existence fixed point and we obtain the characteristic equation

$$\lambda^3 + s_2\lambda^2 + s_1\lambda + s_0 = 0, \tag{5.10}$$

where the roots of equation (5.10) lie inside the unit circle provided

$$|s_0 + s_2| < 1 + s_1, \quad \text{and} \quad |s_1 - s_0 s_2| < 1 - s_0^2. \tag{5.11}$$

A theoretical verification of these conditions results in an overlong expression, thus we proceed numerically. In the results shown in Fig. 5.1, we choose $r = 1$, $s = 1$,$\gamma = 0.1$, $\beta = 1.1$, $\delta = 0.2$ with $\gamma f(v^*) - \beta g'(1) \leq 0$. Clearly, for $\Delta t > 0$, conditions (5.11) are satisfied provided $\gamma f(v^*) - \beta g'(1) \leq 0$ and we conclude that all eigenvalues lie in a unit circle. Hence, the coexistence fixed point for the discrete model (5.5) is locally asymptotically stable provided $1 - \alpha\beta g'(b^*) \leq 0$.

In addition, in Fig. 5.2 we observe that provided $\gamma f(v^*) - \beta g'(1) > 0$, there is a possibility that E^* can be unstable through a Hopf bifurcation leading to oscillatory solutions and this is also illustrated in Fig. 4.7. In Fig. 5.2 we choose $r = 1$, $s = 1$,$\gamma = 2$, $\delta = 0.2$ with $\gamma f(v^*) - \beta g'(1) > 0$. It is clear that when $\beta = 2.8$ the first condition of (5.11) is not satisfied but when $\beta = 2$, E^* remains locally asymptotically stable.

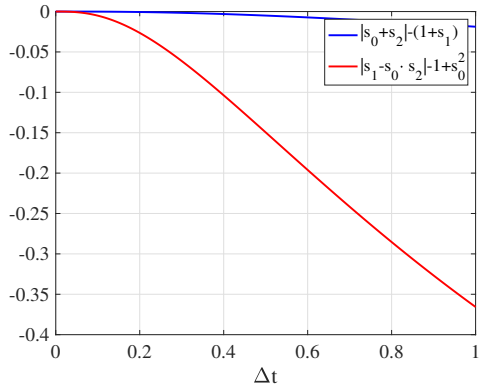

Figure 5.1: Numerical illustration for the local stability of the co-existence fixed point E^* provided $\gamma f(v^*) - \beta g'(1) = -0.1250 < 0$.

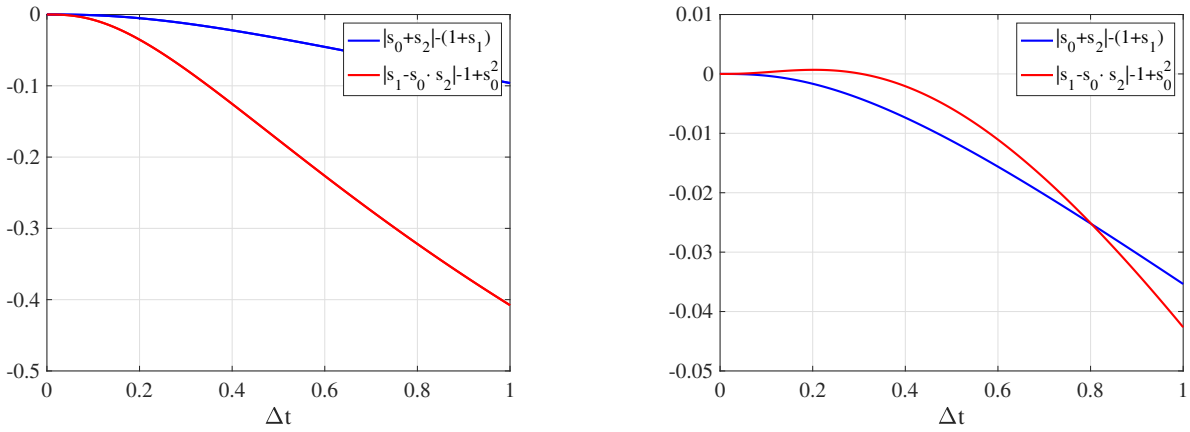

(a) $\beta = 2.0$ (b) $\beta = 2.8$

Figure 5.2: Numerical illustration for: (a) the local stability of the co-existence fixed point E^* when $\gamma f(v^*) - \beta g'(1) = 1.5000$ and (b) possibility of Hopf bifurcation when $\gamma f(v^*) - \beta g'(1) = 2.1000$.

5.3 Finite volume method

In this section, we follow an approach to derive a scheme by making use of the finite volume method for the nonlinear system (4.23). The finite volume method is a discretization method that uses a numerical technique to transform the partial differential equations of various types (elliptic, parabolic or hyperbolic, for instance) representing conservation laws over differential volumes into discrete algebraic equations over finite volumes; it has been extensively used in several engineering fields, such as fluid mechanics, heat and mass transfer or petroleum engineering [53, 130]. In this section, we construct a scheme for the system of equations (4.23) by coupling nonstandard finite difference methods and finite volume methods. Firstly, we recall $(4.23)_2$, given by

$$\frac{\partial u}{\partial t} = \nabla^2 u - d\nabla \cdot (u\chi(v)\nabla v) + u(1-u) - rq(v)u + sp(v)w. \tag{5.12}$$

We first discretise only a portion of the above equation given by

$$\frac{\partial u}{\partial t} = \nabla^2 u + u(1-u), \tag{5.13}$$

using the following nonstandard finite difference scheme

$$\frac{1}{\rho_1(\Delta t)}\left[u_m^{n+1} - u_m^n\right] = \frac{1}{\psi^2(\Delta x)}\left[u_{m+1}^n - 2u_m^n + u_{m-1}^n\right] + u_m^n - \frac{u_m^{n+1}}{3}[u_{m+1}^n + u_m^n + u_{m-1}^n], \tag{5.14}$$

where m denotes the spatial discretisation index, $\psi(\Delta x) = 2\sin\left(\dfrac{\Delta x}{2}\right)$ and $\phi(\Delta t) = e^{\Delta t} - 1$ satisfying the asymptotic relations $\psi(\Delta x) = \Delta x + \mathcal{O}(\Delta x^2)$ and $\phi(\Delta t) = \Delta t + \mathcal{O}(\Delta t^2)$, respectively [120]. When considering the nonlinear diffusion term $(u\chi(v)v_x)_x$, we employ the discretisation in [29] to obtain

$$\frac{1}{\psi^2(\Delta x)}\left[u_m\chi(v_m)v_{m+1} - [u_m\chi(v_m) + u_{m-1}\chi(v_{m-1})]v_m + u_{m-1}\chi(v_{m-1})v_{m-1}\right]. \tag{5.15}$$

Furthermore, for the spatially independent system of (4.23), we propose the following scheme constructed via a non-local approximation (cf. [120]) of the nonlinear terms

$$\begin{aligned}
\frac{w^{n+1} - w^n}{\phi(\Delta t)} &= rq(v^n)u^n - sp(v^n)w^{n+1},\\
\frac{u^{n+1} - u^n}{\phi(\Delta t)} &= u^n(1-u^{n+1}) - rq(v^n)u^{n+1} + sp(v^n)w^{n+1},\\
\frac{v^{n+1} - v^n}{\phi(\Delta t)} &= \beta g(u^n) - v^{n+1} - \gamma v^{n+1}h(v^n)u^{n+1}.
\end{aligned} \tag{5.16}$$

Combining schemes (5.12), (5.15) and $(5.16)_2$, we propose the following scheme for equation $(4.23)_2$

$$\begin{aligned}
\frac{1}{\phi(\Delta t)}\left[u_m^{n+1} - u_m^n\right] = \frac{1}{\psi^2(\Delta x)}\left[u_{m+1}^n - 2u_m^n + u_{m-1}^n\right] + u_m^n - \frac{u_m^{n+1}}{3}[u_{m+1}^n + u_m^n + u_{m-1}^n]\\
-\frac{d}{\psi^2(\Delta x)}\left[u_m^n\chi(v_m^n)v_{m+1}^n - [u_m^n\chi(v_m^n) + u_{m-1}^n\chi(v_{m-1}^n)]v_m^n + u_{m-1}^n\chi(v_{m-1}^n)v_{m-1}^n\right]\\
-rq(v_m^n)u_m^{n+1} + sp(v_m^n)w_m^{n+1}.
\end{aligned} \tag{5.17}$$

In an explicit form, the scheme is written as

$$u_m^{n+1} = \frac{(1-2\theta)u_m^n + \phi(\Delta t)u_m^n + \theta\left[u_{m+1}^n + u_{m-1}^n\right] + \phi(\Delta t)sp(v_m^n)w_m^{n+1}}{1 + \frac{\phi(\Delta t)}{3}\left(u_{m+1}^n + u_m^n + u_{m-1}^n\right) + \phi(\Delta t)rq(v_m^n)}$$
$$+ d\theta\frac{\left[u_m^n\chi(v_m^n) + u_{m-1}^n\chi(v_{m-1}^n)\right]v_m^n}{1 + \frac{\phi(\Delta t)}{3}\left(u_{m+1}^n + u_m^n + u_{m-1}^n\right) + \phi(\Delta t)rq(v_m^n)}$$
$$- d\theta\frac{\left[u_m^n\chi(v_m^n)v_{m+1}^n + u_{m-1}^n\chi(v_{m-1}^n)v_{m-1}^n\right]}{1 + \frac{\phi(\Delta t)}{3}\left(u_{m+1}^n + u_m^n + u_{m-1}^n\right) + \phi(\Delta t)rq(v_m^n)},$$

where $\theta = \dfrac{\phi(\Delta t)}{\psi^2(\Delta x)}$.

Looking at the cross diffusion term and formulating a finite volume approximation for this term, we consider the following sub-equation of (5.12),

$$\frac{\partial u}{\partial t} - d\frac{\partial}{\partial x}\left(u\chi(v)\frac{\partial v}{\partial x}\right) = 0. \tag{5.18}$$

Equation (5.18) can be written as a nonlinear hyperbolic conservation law, $u_t - \varphi_x = 0$ with a flux, $\varphi = u\chi(v)v_x$. Here, the region of integration is taken to be a control volume Ω_m, which we associate with the coordinate x_m, represented by $x_{m-\frac{1}{2}} \leq x \leq x_{m+\frac{1}{2}}$. The integral form is written as

$$\int_{x_{m-1/2}}^{x_{m+1/2}} u_t dx - \int_{x_{m-1/2}}^{x_{m+1/2}} \varphi_x dx = 0. \tag{5.19}$$

The last term in equation (5.19) can be evaluated to obtain

$$\int_{x_{m-1/2}}^{x_{m+1/2}} \varphi_x dx = \varphi(u_{m+1/2}, v_{m+1/2}) - \varphi(u_{m-1/2}, v_{m-1/2}).$$

Moreover, we have that u_m^n approximates the average over the m^{th} interval at time t^n, that is,

$$u_m^n = \frac{1}{\Delta x}\int_{x_{m-1/2}}^{x_{m+1/2}} u(x,t^n)dx = \frac{1}{\Delta x}\int_{\Omega_m} u(x,t^n)dx.$$

However, defining $\mathcal{E}$ as the numerical flux function, we have

$$\mathcal{E}(u_m^n, u_{m+1}^n) = du_{m+1/2}^n\chi(v_{m+1/2}^n)\frac{v_{m+1}^n - v_m^n}{\Delta x}.$$

Similarly,

$$\mathcal{E}(u_{m-1}^n, u_m^n) = du_{m-1/2}^n\chi(u_{m-1/2}^n, v_{m-1/2}^n)\frac{v_m^n - v_{m-1}^n}{\Delta x}.$$

As a result, the finite volume scheme for the conservation law is

$$\frac{u_m^{n+1}-u_m^n}{\Delta t}+\frac{1}{\Delta x}\left[\mathcal{E}(u_m^n,u_{m+1}^n)-\mathcal{E}(u_{m-1}^n,u_m^n)\right]=0,$$

explicitly written as

$$u_m^{n+1}=u_m^n-\frac{\Delta t}{\Delta x}\left[\mathcal{E}(u_m^n,u_{m+1}^n)-\mathcal{E}(u_{m-1}^n,u_m^n)\right].$$

Instead of the discretization (5.15), employed above in equation (5.17), we propose the following coupled nonstandard - finite volume scheme where the nonlinear diffusive term is discretised as follows

$$\begin{aligned}\frac{1}{\phi(\Delta t)}\left[u_m^{n+1}-u_m^n\right]=&\frac{1}{\psi^2(\Delta x)}\left[u_{m+1}^n-2u_m^n+u_{m-1}^n\right]+u_m^n-\frac{u_m^{n+1}}{3}[u_{m+1}^n+u_m^n+u_{m-1}^n]\\&+\frac{d}{\psi^2(\Delta x)}\left[u_{m+1/2}^n\chi(v_{m+1/2}^n)\left(v_{m+1}^n-v_m^n\right)-u_{m-1/2}^n\chi(v_{m-1/2}^n)\left(v_m^n-v_{m-1}^n\right)\right]\\&-rq(v_m^n)u_m^{n+1}+sp(v_m^n)w_m^{n+1},\end{aligned}\tag{5.20}$$

where the denominator Δx is replaced with the non-negative function $\psi(\Delta x)$.

Next, we recall equation $(4.23)_3$

$$\frac{\partial v}{\partial t}=d_v\nabla^2 v+\beta g(u)-v-\gamma u f(v).\tag{5.21}$$

Following the Gauss-Seidel approach, we approximate the remaining kinetic terms of equation $(4.23)_3$. Hence, we obtain the following scheme

$$\frac{1}{\phi(\Delta t)}\left[v_m^{n+1}-v_m^n\right]=\frac{d_v}{\psi^2(\Delta x)}\left[v_{m+1}^n-2v_m^n+v_{m-1}^n\right]+\beta g(u_m^n)-v_m^{n+1}-\gamma v_m^{n+1}h(v_m^n)u_m^{n+1},\tag{5.22}$$

$$v_m^{n+1}=\frac{v_m^n(1-2d_v\theta)+d_v\theta\left[v_{m+1}^n+v_{m-1}^n\right]+\phi(\Delta t)\beta g(u_m^n)}{(1+\phi(\Delta t)+\gamma\phi(\Delta t)h(v_m^n)u_m^{n+1})}.$$

The scheme for equation $(4.23)_1$ is given by

$$\frac{w_m^{n+1}-w_m^n}{\phi(\Delta t)}=rq(v_m^n)u_m^n-sp(v_m^n)w_m^{n+1}.\tag{5.23}$$

In explicit form, equation (5.23) is rewritten as

$$w_m^{n+1}=\frac{w_m^n+\phi(\Delta t)rq(v_m^n)u_m^n}{1+\phi(\Delta t)sp(v_m^n)}.$$

To summarise, the coupled nonstandard finite difference and finite volume scheme for system (4.23) is given by

$$\begin{aligned}
w_m^{n+1} &= \frac{w_m^n + \phi rq(v_m^n)u_m^n}{1+\phi sp(v_m^n)},\\
u_m^{n+1} &= \frac{\phi u_m^n + u_m^n\,(1-2\theta) + \theta\left[u_{m+1}^n + u_{m-1}^n\right] + \phi sp(v_m^n)w_m^{n+1}}{\left[1+\frac{\phi}{3}[u_{m+1}^n + u_m^n + u_{m-1}^n] + \phi rq(v_m^n)\right]}\\
&\quad + \frac{d\theta\left[u_{m+1/2}^n\chi(v_{m+1/2}^n)\left(v_{m+1}^n - v_m^n\right) - u_{m-1/2}^n\chi(v_{m-1/2}^n)\left(v_m^n - v_{m-1}^n\right)\right]}{\left[1+\frac{\phi}{3}[u_{m+1}^n + u_m^n + u_{m-1}^n] + \phi rq(v_m^n)\right]},\\
v_m^{n+1} &= \frac{v_m^n(1-2d_v\theta) + d_v\theta\left[v_{m+1}^n + v_{m-1}^n\right] + \phi\beta g(u_m^n)}{(1+\phi+\phi h(v_m^n)u_m^{n+1})}.
\end{aligned} \tag{5.24}$$

If we let $\bar{u}_m^n = \dfrac{u_{m+1}^n + u_m^n + u_{m-1}^n}{3}$ and define $\kappa_m^n = u_m^n\chi(v_m^n)$, then

$$\begin{aligned}
w_m^{n+1} &= \frac{w_m^n + \phi rq(v_m^n)u_m^n}{1+\phi sp(v_m^n)},\\
u_m^{n+1} &= \frac{\phi u_m^n + u_m^n\,(1-2\theta) + \theta\left[u_{m+1}^n + u_{m-1}^n\right] + \phi sp(v_m^n)w_m^{n+1} + d\theta v_m^n\left[\kappa_{m+1/2}^n + \kappa_{m-1/2}^n\right]}{[1+\phi\bar{u}_m^n + \phi rq(v_m^n)]}\\
&\quad + \frac{d\theta\left[\kappa_{m+1/2}^n v_{m+1}^n + \kappa_{m-1/2}^n v_{m-1}^n\right]}{[1+\phi\bar{u}_m^n + \phi rq(v_m^n)]},\\
v_m^{n+1} &= \frac{v_m^n(1-2d_v\theta) + d_v\theta\left[v_{m+1}^n + v_{m-1}^n\right] + \phi\beta g(u_m^n)}{(1+\phi+\gamma\phi h(v_m^n)u_m^{n+1})}.
\end{aligned} \tag{5.25}$$

In the next section, we will discuss and give numerical simulations to support the theoretical results.

5.4 Numerical simulations

In this section, we use scheme (5.25) to numerically approximate the solution for system (4.23). In addition, we perform 1d numerical simulations to support the results observed. The spatial domain is fixed on $\Omega = (0, 10)$. We will focus on the behaviour of the interior equilibrium $P^* = (w^*, u^*, v^*)$. Unless stated otherwise, in all the simulations we assume $f(v) = v$ and

$$g(u) = \alpha + \frac{u}{\sigma + u},$$

The hibernation function takes the form

$$q(v) = \frac{\delta + v^m}{1 + v^m}, \tag{5.26}$$

while the arousal function takes the modified version

$$p(v) = \frac{1}{1+v^m}, \tag{5.27}$$

with $m \geq 1$ and $\delta = 0.2$. We choose the baseline parameter values as follows

$$r = 1, \quad s = 1, \quad \gamma = 2, \quad \alpha = 1, \quad \sigma = 1, \quad \text{and} \quad d_v = 0.1.$$

We first simulate the selection of different patterns depending on the value of the cross-diffusion coefficient, d, and the production term β as depicted in Fig. 5.3, see Table 5.1. Snapshots of microbial population, i.e., the dormant and active, are given in a series of figures, Fig. 5.6 - 5.13. The appearance of bulk oscillations in the region P_1 is illustrated in Fig. 5.7, while the existence of oscillatory patterns in the region P_2 is summarised in Fig. 5.9. In the subcritical region P_3, stable planar solutions are observed, see Fig. 5.11. On the other hand, stable Turing patterns associated with the chemotaxis term are illustrated in Fig. 5.13 (for region P_4).

Remark 5.1. *A comment regarding the observed patterns in Fig. 5.9 and Fig. 5.13 is necessary. While stable Turing patterns associated with the instability caused by cross-diffusion have been observed in the literature (see for example, [139] and literature therein), to the best of our knowledge, this is the first time oscillating patterns associated with Hopf instability have been observed for microbial populations under environmental stress. The results here support reported population oscillations linked to* ecological suicide *[149].*

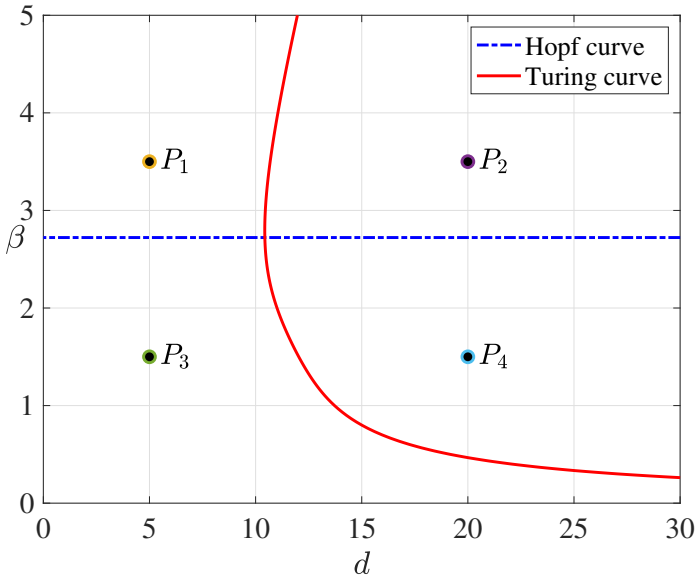

Figure 5.3: Bifurcation diagram in the $d - \beta$ space.

A coupled nonstandard finite difference and finite volume scheme that supports the qualitative behaviour of the continuous model is derived and the results provided in Fig.

5.4 and 5.5 illustrate the fast convergence properties of the proposed scheme.

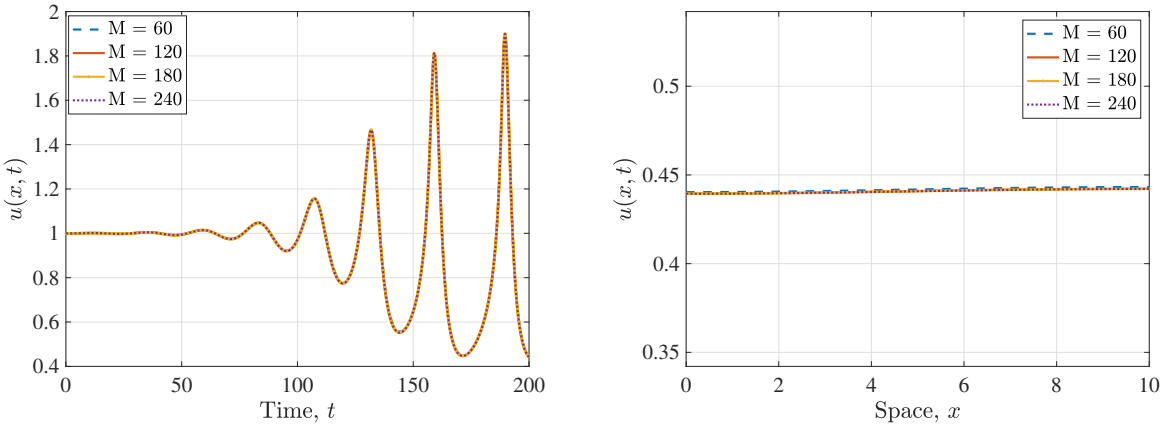

(a) (b)

Figure 5.4: Solution profile for $u(x,t)$ in the sub-critical region corresponding to point P_1 (a) in time and (b) in space.

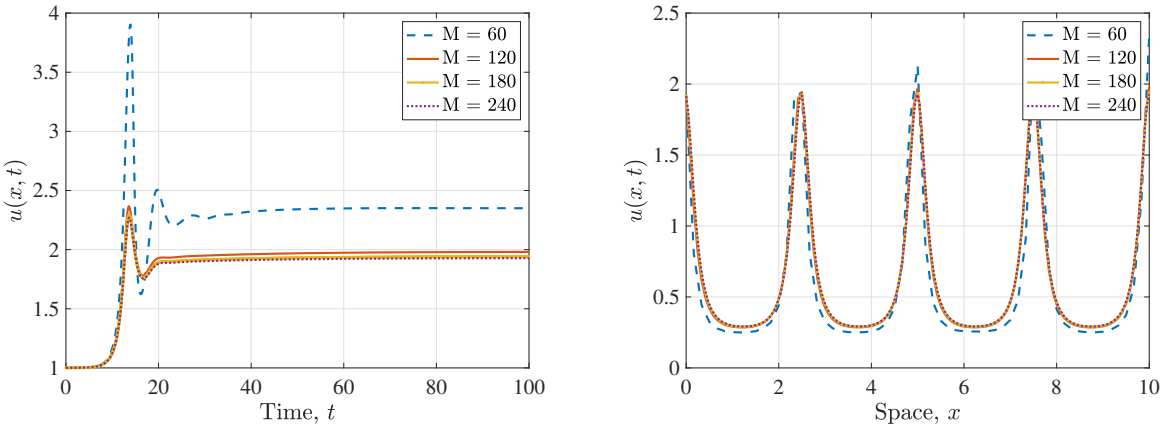

(a) (b)

Figure 5.5: Solution profile for $u(x,t)$ in the sub-critical region corresponding to point P_4 (a) in time and (b) in space.

The simulations in Figs. 5.6 – 5.13 predict one of the following stable states: spatially homogeneous steady state, bulk oscillations, oscillating patterns or stationary Turing patterns. These numerical observations are consistent with our theoretical results in Theorem 4.3.

5.5 Conclusions

In this chapter, we numerically study the phenomenon of theoretically observed patterns in 1D reaction-diffusion systems with cross-diffusion. Applying the bifurcation theory in Chapter 4 and suitable numerical methods and simulations, we investigate the Turing

Figure	r	s	β	γ	d
Fig. 4.10	1.0	1.0	2.0	2.0	-
Figs. 4.11 & 4.12	1.0	1.0	2.0	2.0	-
Fig. 5.7	1.0	1.0	3.5	2.0	5.0
Fig. 5.9	1.0	1.0	3.5	2.0	20
Fig. 5.11	1.0	1.0	1.5	2.0	5.0
Fig. 5.13	1.0	1.0	1.5	2.0	20

Table 5.1: Parameters used in the simulations.

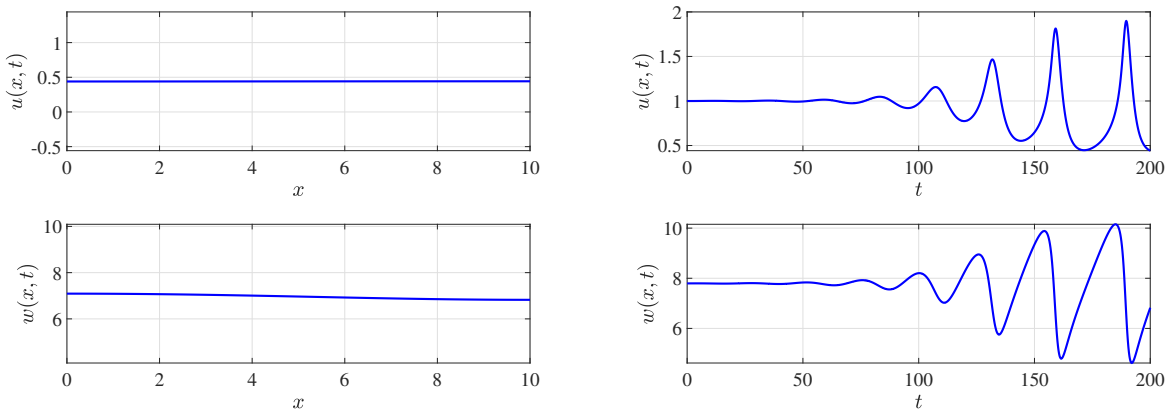

(a) (b)

Figure 5.6: Solution profiles for $u(x,t)$ and $w(x,t)$ corresponding to point P_1 of Fig. 5.3.

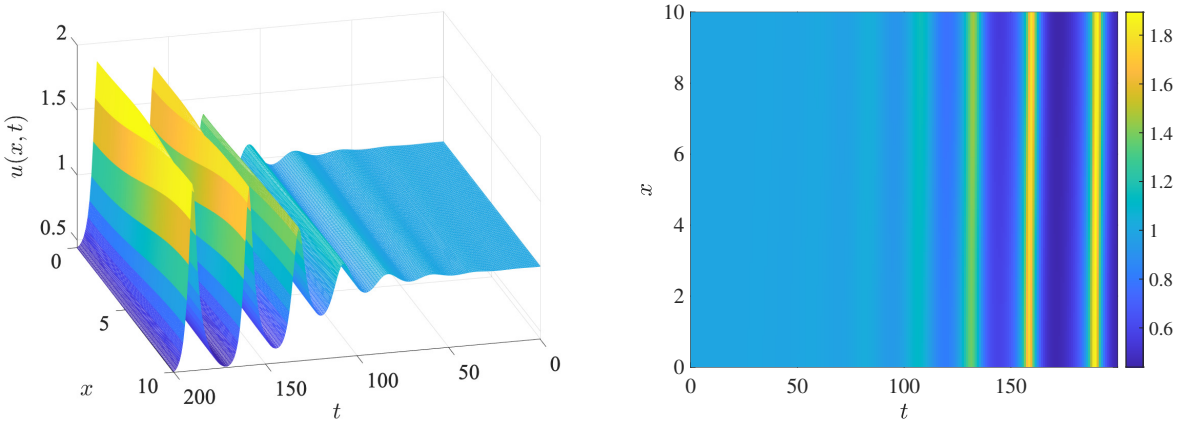

(a) (b)

Figure 5.7: Simulations in the region with $d = 5.0$ and $\beta = 3$, corresponding to point P_1 of Fig. 5.3. In this region we observe bulk oscillations.

and Hopf parameter space and the associated pattern mechanism for pattern selection. Our results support the experimental work of [149] on 'ecological suicide' of microbial populations, and in general, reveal an essential mechanism generating oscillating patterns in microbial populations under environmental stress. Particular attention is needed in the supercritical Hopf bifurcation parameter domain where no substantial theory is available.

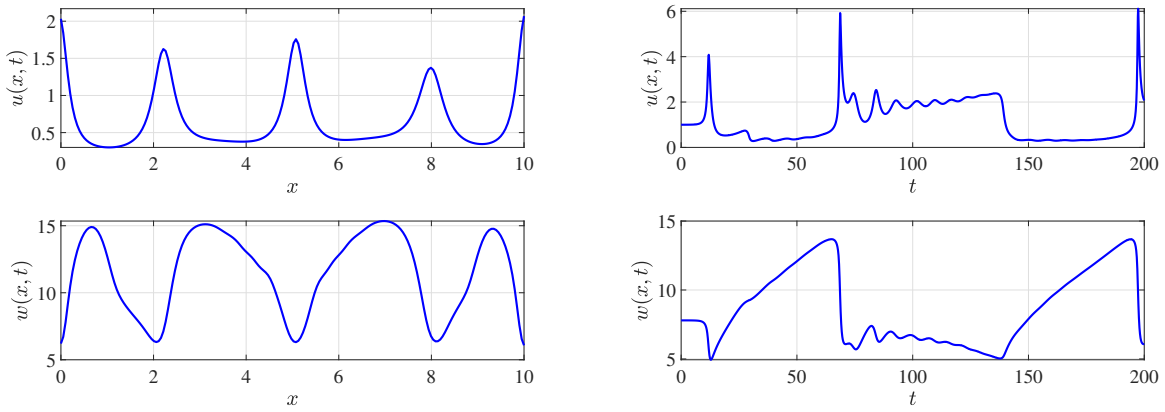

(a) (b)

Figure 5.8: Solution profiles for $u(x,t)$ and $w(x,t)$ corresponding to point P_2 of Fig. 5.3.

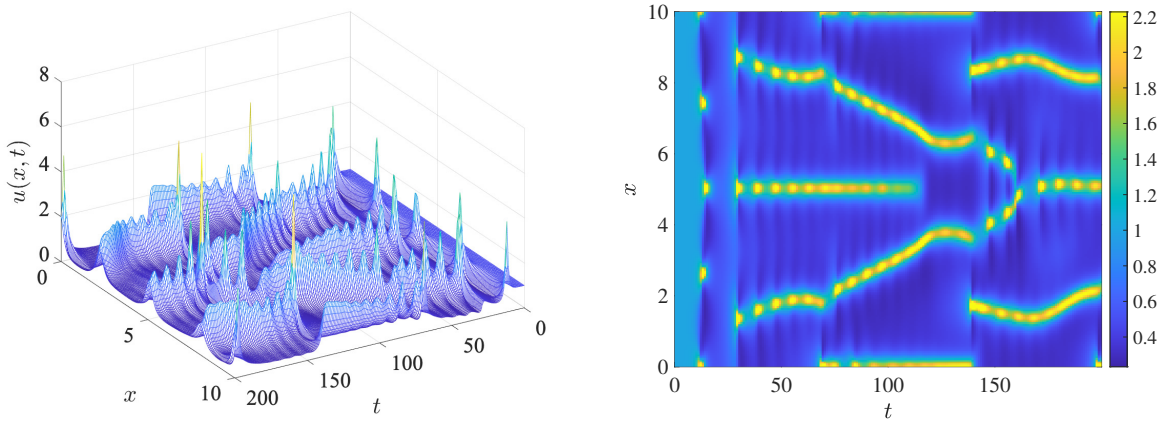

(a) (b)

Figure 5.9: Simulations in the region with $d = 15.0$ and $\beta = 3$, corresponding to point P_2 of Fig. 5.3. In this region we observe patterns.

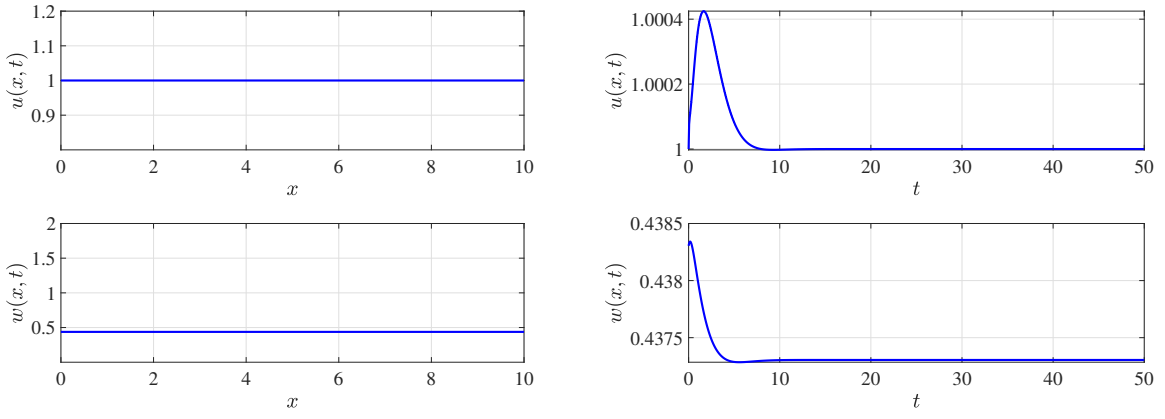

(a) (b)

Figure 5.10: Solution profiles for $u(x,t)$ and $w(x,t)$ corresponding to point P_3 of Fig. 5.3.

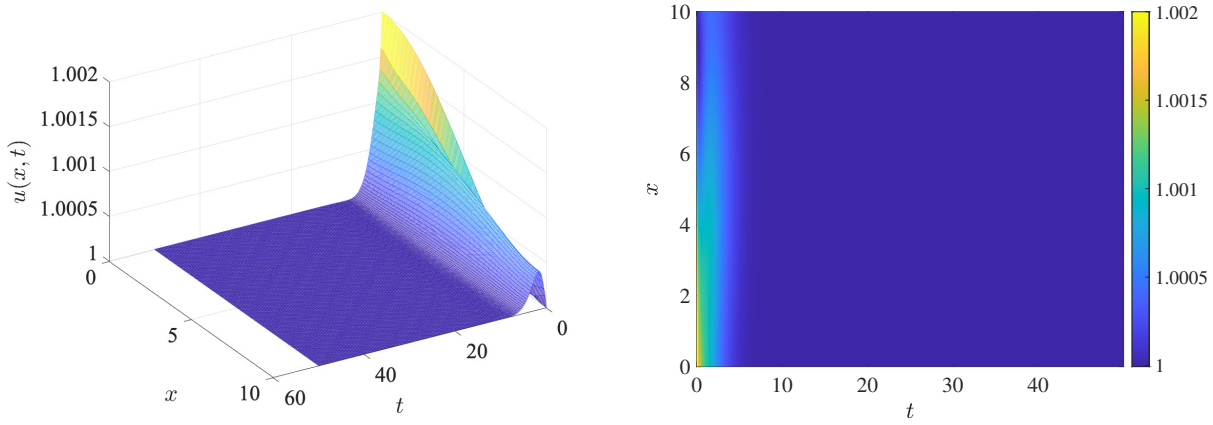

(a) (b)

Figure 5.11: Simulations in the region with $d = 5.0$ and $\beta = 1.5$, corresponding to point P_3 of Fig. 5.3. In this region we observe no patterns.

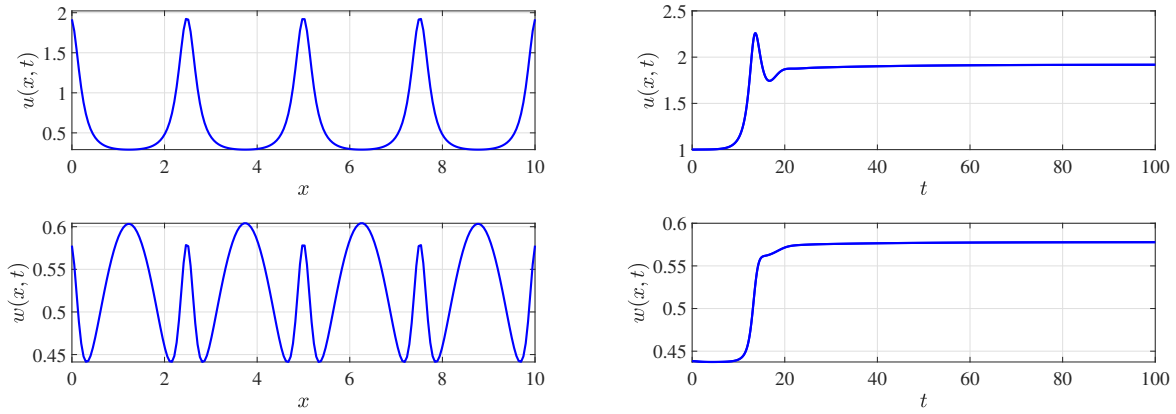

(a) (b)

Figure 5.12: Solution profiles for $u(x,t)$ and $w(x,t)$ corresponding to point P_4 of Fig. 5.3.

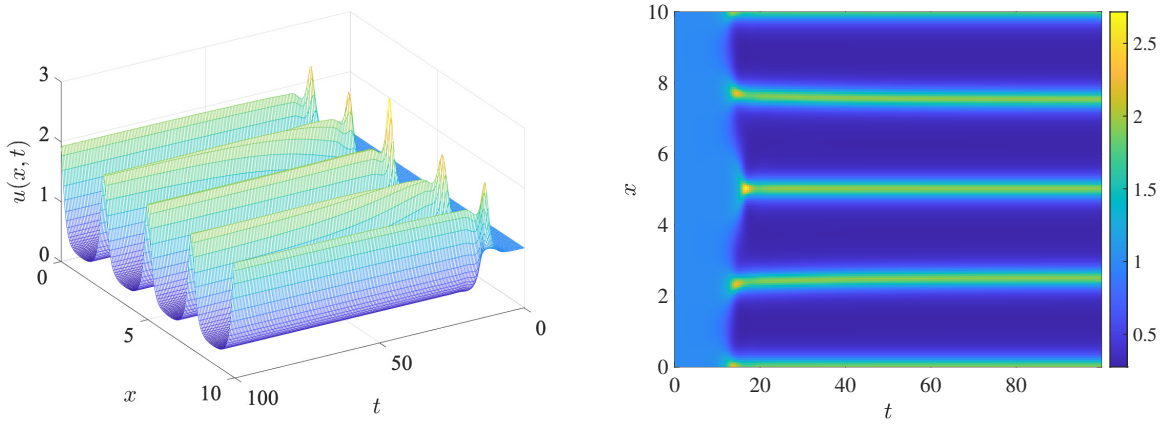

(a) (b)

Figure 5.13: Simulations in the region with $d = 5.0$ and $\beta = 1.5$, corresponding to point P_4 of Fig. 5.3. In this region we observe patterns.

Numerical simulations provide motivation for the study of the spreading speeds (traveling waves) of microbial populations.

Chapter 6

Conclusions and future work

In this thesis, we presented and investigated spatiotemporal bacterioplankton-nutrient-chemoattractant-chemorepellent interaction models that take into account the quiescent stage and chemotaxis. We studied the dynamics of the microbial population under various environmental conditions that include changes in the concentration gradient of the growth-limiting nutrient and chemoattractant as well as the presence and production of inhibiting or toxic substances. Dormancy occurs in various biological phenomena involving different species or living organisms. This work includes and focuses on the dynamics of microbes switching state naturally (due to cell-to-cell interactions) or as a result of changes in the concentration levels of the nutrient, chemoattractant, or toxins (repellent).

In the case of a bacterioplankton population under a growth-limiting nutrient, the model predicted that the population gradually dies out if the nutrient supply is below some threshold value, referred to as a population under starvation. In turn, if the nutrient levels remain above some critical value, the population is sustained in an environment. We observed that population oscillations occur when the switching of states is dependent on the active microbial density in the environment or cell-to-cell interaction other than the change in the concentration levels of the nutrient. Furthermore, we established conditions under which microbial population oscillations (boom-and-bust) may occur. However, oscillations are not observed in the bacterioplankton population dynamics when dormant cells are neglected or disregarded.

When the switch of the state depends on the concentration of a chemoattractant, we use the theory of monotone wavefronts for cooperative and partially degenerate reaction-diffusion systems [54] to show that the minimal wave speed coincides with the spreading speed when we assume constant switch rates. In the case of switch functions dependent on the chemoattractant concentration, we numerically observed that the model admits non-monotonic traveling wave profiles. Moreover, we numerically demonstrated that neglecting dormant cells overestimates the spreading speed of the bacterial colony. Numerical results also indicate the importance of the quiescent stage in the speed of spread.

Microbial populations depend on their environment to survive and proliferate. They can also modify their environment by engineering it in ways that are detrimental to their growth. We proposed and studied a reaction-diffusion model system consisting of active and quiescent microbial populations in an unfavorable environment accounting for the directed movement and switch of cells to dormancy at high concentrations. We observed the occurrence of self-sustained oscillations in the microbial population mediated by the change in concentration levels of the toxin. These results support the experimental observations in [149] showing ecological suicide as a result of environmental deterioration leading to oscillatory dynamics in microbial populations under environmental stress. We presented a theoretical and numerical investigation of the proposed model to explain and provide insight into the conditions that may lead to the extinction of the microbial population – *ecological suicide* – that has been observed in nature and experiments. A bifurcation analysis of the model and the interplay between Turing and Hopf instability were discussed. While stable Turing patterns associated with the instability caused by cross-diffusion have been observed in the literature (see, for example, [139] and literature therein), to the best of our knowledge, this is the first time oscillating patterns associated with Hopf instability have been observed for microbial populations under environmental stress. The presented theoretical and numerical results support the reported population oscillations linked to *ecological suicide* [149].

In Chapter 5 we investigated numerically, the existence of theoretically observed oscillatory dynamics in the proposed 1d reaction-diffusion systems with cross-diffusion. The designing of numerical schemes followed the sub-equation approach typical of nonstandard finite difference formulations; see [120, 29, 2], and references therein. In addition, we coupled nonstandard finite difference methods and finite volume methods to formulate schemes that are dynamically consistent with respect to the positivity of solutions and preservation of fixed points. The numerical simulations are provided to explore the spatiotemporal dynamics generated by the scheme in the different parameter regimes identified in the analysis. The interplay between Turing and Hopf instability is discussed by varying the cross-diffusion coefficient d and the production rate β. Furthermore, the proposed scheme is capable of predicting one of the following states: spatially homogeneous steady state, bulk oscillations, oscillating patterns or stationary Turing patterns. The numerical simulations are entirely consistent with our theoretical results obtained in Chapter 4.

The proposed reaction-diffusion systems are non-cooperative for general nonlinear switch functions. Most of the existing theoretical literature in this direction assumes cooperative, nondegenerate systems. Results for non-cooperative systems can be found, for example, in [180] and [86]. However, [180]'s work is not applicable to non-degenerate systems, while the work by [86] on non-cooperative degenerate time-periodic systems is also not applicable as it is impossible to construct the upper and lower cooperative

subsystems. Hence, proving the existence of traveling waves for general nonlinear switch functions remains an open problem that we will explore in the future.

Experimental observations range from bistability, successive growth, extended suicide, and stabilization. In future work, we aim to explore the variety of spatial patterns that could possibly emerge from the proposed system and the ecological consequences that follow. Moreover, we are interested in developing a theoretical framework for studying the phenomenon of pattern formation in a 2d reaction-diffusion system with cross-diffusion. That is, investigate the Turing and Hopf parameter space and the associated pattern mechanism for pattern selection. Partial differential equations are often used to model physical, chemical, and biological phenomena and their use has spread to many other fields [148]. Phenomena modeled by partial differential equations become increasingly complicated, leading to complicated partial differential equations [82]. Often, one wishes to capture different aspects of the model such as, oscillations and convective transport. Those aspects will then be reflected in a partial differential equation containing operators that makes a model very challenging to analyse, both theoretically and numerically [82]. One of the strategies used to solve complex and complicated problems is the *operator splitting* method. The general numerical method is formed using an efficient numerical scheme for each sub-equation separately and reconstructing the schemes together by operator splitting [82]. Overall, the computational advantage of splitting is that it is faster to compute the solution of the sub-problems separately, compared to when they are solved or treated together. For very high dimensional problems the operator splitting method may be the only feasible method to solve the problem.

We note that the parameter regime used in this study may be far from realistic ranges. Hence, in future there is need to support/validate the current work using realistic experimental values. However, one should note that the process of mathematical modeling is not only for verifying existing phenomena, but also used to design appropriate mathematical experiments and test different hypotheses. This work provides the foundation for mathematical experiments.

Bibliography

[1] F. Abbas, R. Sudarsan, and H. Eberl. Longtime behavior of one-dimensional biofilm models with shear dependent detachment rates. *Mathematical Biosciences & Engineering*, 9(2):215, 2012.

[2] A. A. Aderogba and M. Chapwanya. An explicit nonstandard finite difference scheme for the allen–cahn equation. *Journal of Difference Equations and Applications*, 21(10):875–886, 2015.

[3] J. Adler. Chemotaxis in bacteria. *Science*, 153(3737):708–716, 1966.

[4] W. L. Allen, I. C. Cuthill, N. E. Scott-Samuel, and R. Baddeley. Why the leopard got its spots: relating pattern development to ecology in felids. *Proceedings of the Royal Society B: Biological Sciences*, 278(1710):1373–1380, 2011.

[5] W. Alt and D. A. Lauffenburger. Transient behavior of a chemotaxis system modelling certain types of tissue inflammation. *Journal of Mathematical Biology*, 24(6):691–722, 1987.

[6] E. Angst. The fouling of ships bottoms by bacteria. *Report, Bureau Construction and Repair, United States Navy Department, Washington, DC*, 1923.

[7] R. Anguelov, T. Berge, M. Chapwanya, J. Djoko, P. Kama, J. M.-S. Lubuma, and Y. Terefe. Nonstandard finite difference method revisited and application to the ebola virus disease transmission dynamics. *Journal of Difference Equations and Applications*, 26(6):818–854, 2020.

[8] R. Anguelov, Y. Dumont, J.-S. Lubuma, and M. Shillor. Dynamically consistent nonstandard finite difference schemes for epidemiological models. *Journal of Computational and Applied Mathematics*, 255:161–182, 2014.

[9] R. Anguelov and J. J.-S. Lubuma. Nonstandard finite difference method by nonlocal approximation. *Mathematics and Computers in Simulation*, 61(3-6):465–475, 2003.

[10] R. Anguelov and J. M.-S. Lubuma. Contributions to the mathematics of the nonstandard finite difference method and applications. *Numerical Methods for Partial Differential Equations: An International Journal*, 17(5):518–543, 2001.

[11] R. Anguelov, J. M.-S. Lubuma, and M. Shillor. Dynamically consistent nonstandard finite difference schemes for continuous dynamical systems. In *Conference Publications*, volume 2009, page 34. American Institute of Mathematical Sciences, 2009.

[12] R. Anguelov, J.-S. Lubuma, and M. Shillor. Topological dynamic consistency of non-standard finite difference schemes for dynamical systems. *Journal of Difference Equations and Applications*, 17(12):1769–1791, 2011.

[13] G. Arumugam and J. Tyagi. Keller-segel chemotaxis models: A review. *Acta Applicandae Mathematicae*, 171(1):1–82, 2021.

[14] B. Ayati. Microbial dormancy in batch cultures as a function of substrate-dependent mortality. *Journal of Theoretical Biology*, 293:34–40, 2012.

[15] E. Ben-Jacob, O. Shochet, I. Cohen, A. Tenenbaum, A. Czirók, and T. Vicsek. Cooperative strategies in formation of complex bacterial patterns. *Fractals*, 3(04):849–868, 1995.

[16] H. C. Berg and D. A. Brown. Chemotaxis in escherichia coli analysed by three-dimensional tracking. *Nature*, 239(5374):500–504, 1972.

[17] L. Bilinsky and K. Hadeler. Quiescence stabilizes predator–prey relations. *Journal of Biological Dynamics*, 3(2-3):196–208, 2009.

[18] J.-P. Boon and B. Herpigny. Model for chemotactic bacterial bands. *Bulletin of Mathematical Biology*, 48(1):1–19, 1986.

[19] M. P. Brenner, L. S. Levitov, and E. O. Budrene. Physical mechanisms for chemotactic pattern formation by bacteria. *Biophysical Journal*, 74(4):1677–1693, 1998.

[20] W. J. Bruno. Patterns that grow. *arXiv preprint nlin/0402030*, 2004.

[21] E. Budrene and H. Berg. Complex patterns formed by motile cells of escherichia coli. *Nature*, 349(6310):630, 1991.

[22] E. Budrene and H. Berg. Dynamics of formation of symmetrical patterns by chemotactic bacteria. *Nature*, 376(6535):49, 1995.

[23] V. Burke, A. Sprague, and L. Barnes. Dormancy in bacteria. *The Journal of Infectious Diseases*, pages 555–560, 1925.

[24] H. Byrne, G. Cave, and D. McElwain. The effect of chemotaxis and chemokinesis on leukocyte locomotion: A new interpretation of experimental results. *Mathematical Medicine and Biology: A Journal of the IMA*, 15(3):235–256, 1998.

[25] H. M. Byrne. Biological inferences from a mathematical model for malignant invasion. *Invasion Metastasis*, 16:209–22l, 1996.

[26] V. Capasso and L. Maddalena. Convergence to equilibrium states for a reaction-diffusion system modelling the spatial spread of a class of bacterial and viral diseases. *Journal of Mathematical Biology*, 13(2):173–184, 1981.

[27] M. A. Chaplain. Mathematical modelling of angiogenesis. *Journal of Neuro-oncology*, 50(1):37–51, 2000.

[28] M. Chapwanya, R. Dozva, and G. Muchatibaya. A nonstandard finite difference technique for singular lane-emden type equations. *Engineering Computations*, 36(5):1566–1578, 2019.

[29] M. Chapwanya, J. M.-S. Lubuma, and R. E. Mickens. Positivity-preserving nonstandard finite difference schemes for cross-diffusion equations in biosciences. *Computers & Mathematics with Applications*, 68(9):1071–1082, 2014.

[30] M. Chen, M. Fan, R. Liu, X. Wang, X. Yuan, and H. Zhu. The dynamics of temperature and light on the growth of phytoplankton. *Journal of Theoretical Biology*, 385:8–19, 2015.

[31] M. Chen, M. Fan, X. Yuan, and H. Zhu. Effect of seasonal changing temperature on the growth of phytoplankton. *Mathematical Biosciences & Engineering*, 14(5&6):1091, 2017.

[32] Z. Chen, A. Gumel, and R. Mickens. Nonstandard discretizations of the generalized nagumo reaction-diffusion equation. *Numerical Methods for Partial Differential Equations: An International Journal*, 19(3):363–379, 2003.

[33] I. Chern, M. Mei, X. Yang, and Q. Zhang. Stability of non-monotone critical traveling waves for reaction–diffusion equations with time-delay. *Journal of Differential Equations*, 259(4):1503–1541, 2015.

[34] C. Chung and C.-Y. Chen. The effect of cell sedimentation on measuring chondrocyte population migration using a boyden chamber. *Journal of Theoretical Biology*, 261(4):610–625, 2009.

[35] N. Cogan and J. Keener. The role of the biofilm matrix in structural development. *Mathematical Medicine and Biology: A Journal of the IMA*, 21(2):147–166, 2004.

[36] N. Cogan and J. Keener. Channel formation in gels. *SIAM Journal on Applied Mathematics*, 65(6):1839–1854, 2005.

[37] J. Condeelis, R. H. Singer, J. E. Segall, et al. The great escape: when cancer cells hijack the genes for chemotaxis and motility. *Annual Review of Cell and Developmental Biology*, 21(1):695–718, 2005.

[38] J. Costerton, J. Ingram, and K. Cheng. Structure and function of the cell envelope of gram-negative bacteria. *Bacteriological Reviews*, 38(1):87–110, 1974.

[39] J. Costerton, R. Irvin, and K. Cheng. The bacterial glycocalyx in nature and disease. *Annual Reviews in Microbiology*, 35(1):299–324, 1981.

[40] J. Cremer, A. Melbinger, K. Wienand, T. Henriquez, H. Jung, and E. Frey. Cooperation in microbial populations: theory and experimental model systems. *Journal of Molecular Biology*, 431(23):4599–4644, 2019.

[41] E. DeLong. Microbial population genomics and ecology. *Current Opinion in Microbiology*, 5(5):520–524, 2002.

[42] B. Dibrov, M. Livshits, and M. Volkenstein. Mathematical model of immune processes. *Journal of Theoretical Biology*, 65(4):609–631, 1977.

[43] R. F. Diegelmann, M. C. Evans, et al. Wound healing: an overview of acute, fibrotic and delayed healing. *Frontiers in Bioscience*, 9(1):283–289, 2004.

[44] D. T. Dimitrov and H. V. Kojouharov. Nonstandard finite-difference methods for predator–prey models with general functional response. *Mathematics and Computers in Simulation*, 78(1):1–11, 2008.

[45] C. Dobell. *Antony van Leeuwenhoek and his" little animals."*. Russell & Russell, 1958.

[46] M. Dohi and A. Mougi. A coexistence theory in microbial communities. *Royal Society Open Science*, 5(9):180476, 2018.

[47] G. G. D'Souza. Phenotypic variation in spatially structured microbial communities: ecological origins and consequences. *Current Opinion in Biotechnology*, 62:220–227, 2020.

[48] H. J. Eberl, D. F. Parker, and M. C. Vanloosdrecht. A new deterministic spatio-temporal continuum model for biofilm development. *Computational and Mathematical Methods in Medicine*, 3(3):161–175, 2001.

[49] T. W. Engelmann. Neue methode zur untersuchung der sauerstoffausscheidung pflanzlicher und thierischer organismen. *Archiv für die gesamte Physiologie des Menschen und der Tiere*, 25(1):285–292, 1881.

[50] T. W. Engelmann. Zur biologie der schizomyceten. *Archiv für die gesamte Physiologie des Menschen und der Tiere*, 26(1):537–545, 1881.

[51] P. Entcheva-Dimitrov and A. M. Spormann. Dynamics and control of biofilms of the oligotrophic bacterium caulobacter crescentus. *Journal of Bacteriology*, 186(24):8254–8266, 2004.

[52] S. Estrela, E. Libby, J. Van Cleve, F. Débarre, M. Deforet, W. R. Harcombe, J. Peña, S. P. Brown, and M. E. Hochberg. Environmentally mediated social dilemmas. *Trends in Ecology & Evolution*, 34(1):6–18, 2019.

[53] R. Eymard, T. Gallouët, and R. Herbin. Finite volume methods. *Handbook of Numerical Analysis*, 7:713–1018, 2000.

[54] J. Fang and X. Zhao. Monotone wavefronts for partially degenerate reaction-diffusion systems. *Journal of Dynamics and Differential Equations*, 21(4):663–680, 2009.

[55] R. M. Ford and D. A. Lauffenburger. Analysis of chemotactic bacterial distributions in population migration assays using a mathematical model applicable to steep or shallow attractant gradients. *Bulletin of Mathematical Biology*, 53(5):721–749, 1991.

[56] A. Fowler. Note on a paper by Omta *et al.* on sawtooth oscillations. *SeMA Journal*, 62(1):1–13, 2013.

[57] A. Fowler. Starvation kinetics of oscillating microbial populations. In *Mathematical Proceedings of the Royal Irish Academy*, volume 114, pages 173–189. JSTOR, 2014.

[58] A. Fowler and H. Winstanley. Microbial dormancy and boom-and-bust population dynamics under starvation stress. *Theoretical Population Biology*, 120:114–120, 2018.

[59] H. Fujikawa. Diversity of the growth patterns of *Bacillus subtilis* colonies on agar plates. *FEMS Microbiology Ecology*, 13(3):159–167, 1994.

[60] H. Fujikawa and M. Matsushita. Fractal growth of *Bacillus subtilis* on agar plates. *Journal of the Physical Society of Japan*, 58(11):3875–3878, 1989.

[61] S. Ghorai and S. Poria. Pattern formation in a system involving prey–predation, competition and commensalism. *Nonlinear Dynamics*, 89(2):1309–1326, 2017.

[62] A. M. Gibson, N. Bratchell, and T. Roberts. The effect of sodium chloride and temperature on the rate and extent of growth of clostridium botulinum type a in pasteurized pork slurry. *Journal of Applied Bacteriology*, 62(6):479–490, 1987.

[63] J. E. Goldford, N. Lu, D. Bajić, S. Estrela, M. Tikhonov, A. Sanchez-Gorostiaga, D. Segrè, P. Mehta, and A. Sanchez. Emergent simplicity in microbial community assembly. *Science*, 361(6401):469–474, 2018.

[64] B. Gompertz. Xxiv. on the nature of the function expressive of the law of human mortality, and on a new mode of determining the value of life contingencies. in a letter to francis baily, esq. frs &c. *Philosophical Transactions of the Royal Society of London*, (115):513–583, 1825.

[65] J. E. González-Pastor. Cannibalism: a social behavior in sporulating *Bacillus subtilis*. *FEMS Microbiology Reviews*, 35(3):415–424, 2011.

[66] Y. Guan, N. Jiang, Y. Wu, Z. Yang, A. Bello, and W. Yang. Disentangling the role of salinity-sodicity in shaping soil microbiome along a natural saline-sodic gradient. *Science of the Total Environment*, 765:142738, 2021.

[67] M. Gyllenberg and G. Webb. Age-size structure in populations with quiescence. *Mathematical Biosciences*, 86(1):67–95, 1987.

[68] M. Gyllenberg and G. Webb. Quiescence as an explanation of gompertzian tumor growth. *Growth, Development, and Aging: GDA*, 53(1-2):25–33, 1989.

[69] M. Gyllenberg and G. Webb. A nonlinear structured population model of tumor growth with quiescence. *Journal of Mathematical Biology*, 28(6):671–694, 1990.

[70] K. Hadeler. Quiescent phases and stability. *Linear Algebra and its Applications*, 428(7):1620–1627, 2008.

[71] K. M. Hallinen, J. Karslake, and K. B. Wood. Delayed antibiotic exposure induces population collapse in enterococcal communities with drug-resistant subpopulations. *Elife*, 9:e52813, 2020.

[72] A. T. Henrici. Studies of freshwater bacteria: I. A direct microscopic technique. *Journal of Bacteriology*, 25(3):277–287, 1933.

[73] E. Hildebrand and U. Kaupp. Sperm chemotaxis: a primer. *Annals of the New York Academy of Sciences*, 1061(1):221–225, 2005.

[74] T. Hillen and K. J. Painter. A user's guide to PDE models for chemotaxis. *Journal of Mathematical Biology*, 58(1):183–217, 2009.

[75] T. Hoehler and B. Jørgensen. Microbial life under extreme energy limitation. *Nature Reviews Microbiology*, 11(2):83, 2013.

[76] T. Höfer, J. A. Sherratt, and P. K. Maini. *Dictyostelium discoideum*: cellular self-organization in an excitable biological medium. *Proceedings of the Royal Society of London. Series B: Biological Sciences*, 259(1356):249–257, 1995.

[77] N. Høiby. *Pseudomonas aeruginosa* infection in cystic fibrosis. relationship between mucoid strains of *Pseudomonas aeruginosa* and the humoral immune response. *Acta Pathologica Microbiologica Scandinavica Section B Microbiology and Immunology*, 82(4):551–558, 1974.

[78] N. Høiby. A personal history of research on microbial biofilms and biofilm infections. *Pathogens and Disease*, 70(3):205–211, 2014.

[79] N. Høiby. A short history of microbial biofilms and biofilm infections. *Apmis*, 125(4):272–275, 2017.

[80] N. Høiby and N. H. Axelsen. Identification and quantitation of precipitins against *Pseudomonas aeruginosa* in patients with cystic fibrosis by means of crossed immunoelectrophoresis with intermediate gel. *Acta Pathologica Microbiologica Scandinavica Section B Microbiology and Immunology*, 81(3):298–308, 1973.

[81] N. Hoiby, E. W. Flensborg, B. Beck, B. Friis, S. V. Jacobsen, and L. Jacobsen. *Pseudomonas aeruginosa* infection in cystic fibrosis. diagnostic and prognostic significance of *Pseudomonas aeruginosa* precipitins determined by means of crossed immunoelectrophoresis. *Scandinavian Journal of Respiratory Diseases*, 58(2):65–79, 1977.

[82] H. Holden, K. Karlsen, and K. Lie. *Splitting methods for partial differential equations with rough solutions: Analysis and MATLAB programs*, volume 11. European Mathematical Society, 2010.

[83] H. Horn and D. C. Hempel. Substrate utilization and mass transfer in an autotrophic biofilm system: experimental results and numerical simulation. *Biotechnology and Bioengineering*, 53(4):363–371, 1997.

[84] C.-H. Hsu, C.-R. Yang, T.-H. Yang, and T.-S. Yang. Existence of traveling wave solutions for diffusive predator–prey type systems. *Journal of Differential Equations*, 252(4):3040–3075, 2012.

[85] Y. Hu, P. D. Butcher, J. A. Mangan, M.-A. Rajandream, and A. R. Coates. Regulation of HMP gene transcription in *Mycobacterium tuberculosis*: effects of oxygen limitation and nitrosative and oxidative stress. *Journal of Bacteriology*, 181(11):3486–3493, 1999.

[86] M. Huang, S.-L. Wu, and X.-Q. Zhao. Propagation dynamics for time-periodic and partially degenerate reaction-diffusion systems. *SIAM Journal on Mathematical Analysis*, 54(2):1860–1897, 2022.

[87] W. Jäger, S. Krömker, and B. Tang. Quiescence and transient growth dynamics in chemostat models. *Mathematical Biosciences*, 119(2):225–239, 1994.

[88] M. D. Jendresen and P.-O. Glantz. Clinical adhesiveness of selected dental materials: an in-vivo study. *Acta Odontologica Scandinavica*, 39(1):39–45, 1981.

[89] M. D. Jendresen, P.-O. Glantz, R. E. Baier, and J. D. Eick. Microtopography and clinical adhesiveness of an acid etched tooth surface: an in-vivo study. *Acta Odontologica Scandinavica*, 39(1):47–53, 1981.

[90] S. Jones and J. Lennon. Dormancy contributes to the maintenance of microbial diversity. *Proceedings of the National Academy of Sciences*, 107(13):5881–5886, 2010.

[91] A. Kaprelyants, J. Gottschal, and D. Kell. Dormancy in non-sporulating bacteria. *Federation of European Microbiological Societies*, 104(3-4):271–285, 1993.

[92] P. Kareiva and G. Odell. Swarms of predators exhibit "preytaxis" if individual predators use area-restricted search. *The American Naturalist*, 130(2):233–270, 1987.

[93] U. B. Kaupp, N. D. Kashikar, and I. Weyand. Mechanisms of sperm chemotaxis. *Annual Review of Physiology*, 70(1):93–117, 2008.

[94] E. Keller and L. Segel. Model for chemotaxis. *Journal of Theoretical Biology*, 30(2):225–234, 1971.

[95] E. F. Keller and L. A. Segel. Initiation of slime mold aggregation viewed as an instability. *Journal of Theoretical Biology*, 26(3):399–415, 1970.

[96] E. F. Keller and L. A. Segel. Traveling bands of chemotactic bacteria: a theoretical analysis. *Journal of Theoretical Biology*, 30(2):235–248, 1971.

[97] I. Klapper. Effect of heterogeneous structure in mechanically unstressed biofilms on overall growth. *Bulletin of Mathematical Biology*, 66(4):809–824, 2004.

[98] I. Klapper. Productivity and equilibrium in simple biofilm models. *Bulletin of Mathematical Biology*, 74(12):2917–2934, 2012.

[99] I. Klapper and J. Dockery. Finger formation in biofilm layers. *SIAM Journal on Applied Mathematics*, 62(3):853–869, 2002.

[100] J. Lam, R. Chan, K. Lam, and J. Costerton. Production of mucoid microcolonies by *Pseudomonas aeruginosa* within infected lungs in cystic fibrosis. *Infection and Immunity*, 28(2):546–556, 1980.

[101] J. D. Lambert et al. *Numerical methods for ordinary differential systems*, volume 146. Wiley New York, 1991.

[102] K. Landman, G. Pettet, and D. Newgreen. Mathematical models of cell colonization of uniformly growing domains. *Bulletin of Mathematical Biology*, 65(2):235–262, 2003.

[103] I. R. Lapidus and R. Schiller. Model for the chemotactic response of a bacterial population. *Biophysical Journal*, 16(7):779–789, 1976.

[104] I. R. Lapidus and R. Schiller. A model for traveling bands of chemotactic bacteria. *Biophysical Journal*, 22(1):1–13, 1978.

[105] B. Larrivee and A. Karsan. Signaling pathways induced by vascular endothelial growth factor. *International Journal of Molecular Medicine*, 5(5):447–503, 2000.

[106] D. A. Lauffenburger and C. R. Kennedy. Localized bacterial infection in a distributed model for tissue inflammation. *Journal of Mathematical Biology*, 16(2):141–163, 1983.

[107] J. Lee, T. Hillen, and M. Lewis. Continuous traveling waves for prey-taxis. *Bulletin of Mathematical Biology*, 70(3):654–676, 2008.

[108] S. S. Lee, A. P. Jackman, and E. D. Schroeder. A two-state microbial growth kinetics model. *Water Research*, 9(5-6):491–498, 1975.

[109] A. V. Leeuwenhoek. Iv. part of a letter from mr antony van leeuwenhoek, concerning the worms in sheeps livers, gants and animalcula in the excrements of frogs. *Philosophical transactions of the Royal Society of London*, 22(261):509–518, 1700.

[110] A. V. Leeuwenhoek. Iv. part of a letter from mr antony van leeuwenhoek, frs concerning green weeds growing in water, and some animalcula found about them. *Philosophical Transactions of the Royal Society of London*, 23(283):1304–1311, 1753.

[111] S. Levin and L. Segel. Hypothesis for origin of planktonic patchiness. *Nature*, 259(5545):659–659, 1976.

[112] M. A. Lewis, B. Li, and H. F. Weinberger. Spreading speed and linear determinacy for two-species competition models. *Journal of Mathematical Biology*, 45(3):219–233, 2002.

[113] B. Li and J. H.-C. Wang. Fibroblasts and myofibroblasts in wound healing: force generation and measurement. *Journal of Tissue Viability*, 20(4):108–120, 2011.

[114] B. Li, H. Weinberger, and M. Lewis. Spreading speeds as slowest wave speeds for cooperative systems. *Mathematical Biosciences*, 196(1):82–98, 2005.

[115] D. H. Limoli, C. J. Jones, and D. J. Wozniak. Bacterial extracellular polysaccharides in biofilm formation and function. *Microbiology Spectrum*, 3(3):3–3, 2015.

[116] M. Luca, A. Chavez-Ross, L. Edelstein-Keshet, and A. Mogilner. Chemotactic signaling, microglia, and alzheimer's disease senile plaques: Is there a connection? *Bulletin of Mathematical Biology*, 65(4):693–730, 2003.

[117] T. Malik and H. Smith. A resource-based model of microbial quiescence. *Journal of Mathematical Biology*, 53(2):231–252, 2006.

[118] M. Matsushita and H. Fujikawa. Diffusion-limited growth in bacterial colony formation. *Physica A: Statistical Mechanics and its Applications*, 168(1):498–506, 1990.

[119] R. Memarbashi, F. Alipour, and A. Ghasemabadi. A nonstandard finite difference scheme for a SEI epidemic model. *Punjab University Journal of Mathematics*, 49(3), 2020.

[120] R. Mickens. *Nonstandard finite difference models of differential equations*. World Scientific, Singapore, 1994.

[121] R. Mickens. *Advances in the Applications of Nonstandard Finite Difference Schemes*. World Scientific, 2005.

[122] R. Mickens and A. Gumel. Numerical study of a non-standard finite-difference scheme for the van der pol equation [2]. *Journal of Sound and Vibration*, 250(5):955–963, 2002.

[123] R. Mickens and D. Schultz. The role of positivity in the construction of nonstandard finite difference schemes for pdes. In *Proceedings of International Conference on Scientific Computing and Mathematical Modeling, University of Wisconsin-Milwaukee*, volume 294, page 307, 2000.

[124] R. E. Mickens. Nonstandard finite difference schemes for reaction-diffusion equations. *Numerical Methods for Partial Differential Equations: An International Journal*, 15(2):201–214, 1999.

[125] R. E. Mickens. *Applications of nonstandard finite difference schemes*. World Scientific, 2000.

[126] R. E. Mickens. Discrete models of differential equations: the roles of dynamic consistency and positivity. In *Difference equations and discrete dynamical systems*, pages 51–70. World Scientific, 2005.

[127] R. E. Mickens. Dynamic consistency: a fundamental principle for constructing non-standard finite difference schemes for differential equations. *Journal of Difference Equations and Applications*, 11(7):645–653, 2005.

[128] M. Mimura, H. Sakaguchi, and M. Matsushita. Reaction–diffusion modelling of bacterial colony patterns. *Physica A: Statistical Mechanics and its Applications*, 282(1-2):283–303, 2000.

[129] J. Monod. Recherches sur la croissance des cultures bactériennes. 1942.

[130] F. Moukalled, L. Mangani, M. Darwish, F. Moukalled, L. Mangani, and M. Darwish. *The finite volume method*. Springer, 2016.

[131] J. Murray. *Mathematical biology II: Spatial models and biomedical applications*, volume 3. Springer-Verlag, Berlin Heidelberg, 2001.

[132] J. D. Murray and M. Myerscough. Pigmentation pattern formation on snakes. *Journal of Theoretical Biology*, 149(3):339–360, 1991.

[133] J. D. Murray, E. A. Stanley, and D. L. Brown. On the spatial spread of rabies among foxes. *Proceedings of the Royal Society of London. Series B. Biological sciences*, 229(1255):111–150, 1986.

[134] A. Naparstek, J. Romette, J. Kernevez, and D. Thomas. Memory in enzyme membranes. *Nature*, 249(5456):490–491, 1974.

[135] J. Nickel, I. Ruseska, J. Wright, and J. Costerton. Tobramycin resistance of *Pseudomonas aeruginosa* cells growing as a biofilm on urinary catheter material. *Antimicrobial Agents and Chemotherapy*, 27(4):619–624, 1985.

[136] L. Niehaus, I. Boland, M. Liu, K. Chen, D. Fu, C. Henckel, K. Chaung, S. E. Miranda, S. Dyckman, M. Crum, et al. Microbial coexistence through chemical-mediated interactions. *Nature Communications*, 10(1):1–12, 2019.

[137] G. Okpokwasili and C. Nweke. Microbial growth and substrate utilization kinetics. *African Journal of Biotechnology*, 5(4):305–317, 2006.

[138] D. Oliveira, A. Borges, and M. Simões. Staphylococcus aureus toxins and their molecular activity in infectious diseases. *Toxins*, 10(6):252, 2018.

[139] K. J. Painter. Mathematical models for chemotaxis and their applications in self-organisation phenomena. *Journal of Theoretical Biology*, 481:162–182, 2019.

[140] K. J. Painter, P. K. Maini, and H. G. Othmer. Complex spatial patterns in a hybrid chemotaxis reaction-diffusion model. *Journal Mathematical Biology*, 41(4):285–314, 2000.

[141] K. J. Painter, H. Othmer, and P. K. Maini. Stripe formation in juvenile pomacanthus via chemotactic response to a reaction-diffusion mechanism. *Proceedings of the National Academy of Sciences, USA*, 96:5549–5554, 1999.

[142] R. J. Palmer. Oral bacterial biofilms–history in progress. *Microbiology*, 155(Pt 7):2113, 2009.

[143] H. T. Park, J. Wu, and Y. Rao. Molecular control of neuronal migration. *Bioessays*, 24(9):821–827, 2002.

[144] L. Pasteur. Mémoire sur la fermentation acétique. In *Annales scientifiques de l'École Normale Supérieure*, volume 1, pages 113–158, 1864.

[145] C. S. Patlak. Random walk with persistence and external bias. *The Bulletin of Mathematical Biophysics*, 15(3):311–338, 1953.

[146] W. Pfeffer. Uber chemotaktische bewegungen von bacterien, flagellaten und volvocineen. *Untersuch. Bot. Inst. Tubingen*, 2:582–661, 1888.

[147] P. F. Popp and T. Mascher. Coordinated cell death in isogenic bacterial populations: sacrificing some for the benefit of many? *Journal of Molecular Biology*, 431(23):4656–4669, 2019.

[148] J. Qin. The new alternating direction implicit difference methods for solving three-dimensional parabolic equations. *Applied Mathematical Modelling*, 34(4):890–897, 2010.

[149] C. Ratzke, J. Denk, and J. Gore. Ecological suicide in microbes. *Nature Ecology & Evolution*, 2(5):867–872, 2018.

[150] C. Ratzke and J. Gore. Self-organized patchiness facilitates survival in a cooperatively growing *Bacillus subtilis* population. *Nature Microbiology*, 1(5):1–5, 2016.

[151] C. Ratzke and J. Gore. Modifying and reacting to the environmental pH can drive bacterial interactions. *PLoS Biology*, 16(3):e2004248, 2018.

[152] E. S. Rittershaus, S.-H. Baek, and C. M. Sassetti. The normalcy of dormancy: common themes in microbial quiescence. *Cell Host & Microbe*, 13(6):643–651, 2013.

[153] B. E. Rittmann and P. L. McCarty. Evaluation of steady-state-biofilm kinetics. *Biotechnology and Bioengineering*, 22(11):2359–2373, 1980.

[154] B. E. Rittmann and P. L. McCarty. Model of steady-state-biofilm kinetics. *Biotechnology and Bioengineering*, 22(11):2343–2357, 1980.

[155] D. Romero, M. F. Traxler, D. López, and R. Kolter. Antibiotics as signal molecules. *Chemical Reviews*, 111(9):5492–5505, 2011.

[156] E. T. Roussos, J. S. Condeelis, and A. Patsialou. Chemotaxis in cancer. *Nature Reviews Cancer*, 11(8):573–587, 2011.

[157] S. Ruan. Turing instability and travelling waves in diffusive plankton models with delayed nutrient recycling. *IMA Journal of Applied Mathematics*, 61(1):15–32, 1998.

[158] A. Sapkota. Autotrophs-definition, Types and 4 Examples. https://microbenotes.com/autotrophs/, 2021. Last accessed on October 14, 2021.

[159] J. Saragosti, V. Calvez, N. Bournaveas, A. Buguin, P. Silberzan, and B. Perthame. Mathematical description of bacterial traveling pulses. *PLoS Computational Biology*, 6(8):e1000890, 2010.

[160] J. A. Sherratt, E. H. Sage, and J. Murray. Chemical control of eukaryotic cell movement: A new model. *Journal of Theoretical Biology*, 162(1):23–40, 1993.

[161] R. Sigdel and C. McCluskey. Global stability for an SEI model of infectious disease with immigration. *Applied Mathematics and Computation*, 243:684–689, 2014.

[162] M. Simmons, K. Drescher, C. D. Nadell, and V. Bucci. Phage mobility is a core determinant of phage-bacteria coexistence in biofilms. *The ISME Journal*, 12(2):531–543, 2018.

[163] K. Stolpovsky, P. Martinez-Lavanchy, H. Heipieper, P. Van Cappellen, and M. Thullner. Incorporating dormancy in dynamic microbial community models. *Ecological Modelling*, 222(17):3092–3102, 2011.

[164] A. Stuart and A. Humphries. *Dynamical systems and numerical analysis*, volume 2. Cambridge University Press, 1998.

[165] H. Thieme and X. Zhao. Asymptotic speeds of spread and traveling waves for integral equations and delayed reaction–diffusion models. *Journal of Differential Equations*, 195(2):430–470, 2003.

[166] H. R. Thieme. Density-dependent regulation of spatially distributed populations and their asymptotic speed of spread. *Journal of Mathematical Biology*, 8(2):173–187, 1979.

[167] M. Tindall, P. Maini, S. Porter, and J. Armitage. Overview of mathematical approaches used to model bacterial chemotaxis II: bacterial populations. *Bulletin of Mathematical Biology*, 70(6):1570, 2008.

[168] S. Tolman, P. Meakin, and M. Matsushita. Cluster-size distribution in the incremental growth of dla clusters. *Journal of the Physical Society of Japan*, 58(8):2721–2726, 1989.

[169] H. Tronnolone, J. M. Gardner, J. F. Sundstrom, V. Jiranek, S. G. Oliver, and B. J. Binder. Quantifying the dominant growth mechanisms of dimorphic yeast using a lattice-based model. *Journal of The Royal Society Interface*, 14(134):20170314, 2017.

[170] H. Tronnolone, A. Tam, Z. Szenczi, J. Green, S. Balasuriya, E. L. Tek, J. M. Gardner, J. F. Sundstrom, V. Jiranek, S. G. Oliver, et al. Diffusion-limited growth of microbial colonies. *Scientific Reports*, 8(1):1–11, 2018.

[171] L. Tsimring, H. Levine, I. Aranson, E. Ben-Jacob, I. Cohen, O. Shochet, and W. N. Reynolds. Aggregation patterns in stressed bacteria. *Physical Review Letters*, 75(9):1859, 1995.

[172] E. Tulumello, M. C. Lombardo, and M. Sammartino. Cross-diffusion driven instability in a predator-prey system with cross-diffusion. *Acta Applicandae Mathematicae*, 132(1):621–633, 2014.

[173] E. Twizell, A. Gumel, and Q. Cao. A second-order scheme for the "brusselator" reaction–diffusion system. *Journal of Mathematical Chemistry*, 26(4):297–316, 1999.

[174] J. J. Tyson and P. K. Brazhnik. On traveling wave solutions of Fisher's equation in two spatial dimensions. *SIAM Journal on Applied Mathematics*, 60(2):371–391, 2000.

[175] R. Tyson, S. Lubkin, and J. D. Murray. A minimal mechanism for bacterial pattern formation. *Proceedings of the Royal Society of London B: Biological Sciences*, 266(1416):299–304, 1999.

[176] M. Vasse, C. Torres-Barceló, and M. E. Hochberg. Phage selection for bacterial cheats leads to population decline. *Proceedings of the Royal Society B: Biological Sciences*, 282(1818):20152207, 2015.

[177] P. F. Verhulst. Resherches mathematiques sur la loi d'accroissement de la population. *Nouveaux Memoires de l'academie Royale des Sciences*, 18:1–41, 1845.

[178] A. Volpert, V. Volpert, and V. Volpert. *Traveling wave solutions of parabolic systems*, volume 140. American Mathematical Society, 1994.

[179] J. Y. Wakano, A. Komoto, and Y. Yamaguchi. Phase transition of traveling waves in bacterial colony pattern. *Physical Review E*, 69(5):051904, 2004.

[180] H. Wang. Spreading speeds and traveling waves for non-cooperative reaction–diffusion systems. *Journal of Nonlinear Science*, 21(5):747–783, 2011.

[181] J. Wang. Dynamics of a reaction–diffusion–ODE system with quiescence. *Nonlinear Analysis: Real World Applications*, 58:103229, 2021.

[182] K. Wang and W. Wang. Propagation of HBV with spatial dependence. *Mathematical Biosciences*, 210(1):78–95, 2007.

[183] O. Wanner and W. Gujer. Competition in biofilms. *Water Science and Technology*, 17(2-3):27–44, 1985.

[184] O. Wanner and W. Gujer. A multispecies biofilm model. *Biotechnology and Bioengineering*, 28(3):314–328, 1986.

[185] L. G. Wayne and L. G. Hayes. An in vitro model for sequential study of shiftdown of *Mycobacterium tuberculosis* through two stages of nonreplicating persistence. *Infection and Immunity*, 64(6):2062–2069, 1996.

[186] H. F. Weinberger, M. A. Lewis, and B. Li. Analysis of linear determinacy for spread in cooperative models. *Journal of Mathematical Biology*, 45(3):183–218, 2002.

[187] H. F. Weinberger, M. A. Lewis, and B. Li. Anomalous spreading speeds of cooperative recursion systems. *Journal of Mathematical Biology*, 55(2):207–222, 2007.

[188] H. Winstanley, M. Chapwanya, A. Fowler, and S. O'Brien. A 2d channel-clogging biofilm model. *Journal of Mathematical Biology*, 71(3):647–668, 2015.

[189] H. Winstanley, M. Chapwanya, M. McGuinness, and A. Fowler. A polymer–solvent model of biofilm growth. *Proceedings of the Royal Society A: Mathematical, Physical and Engineering Sciences*, 467(2129):1449–1467, 2011.

[190] T. A. Witten Jr and L. M. Sander. Diffusion-limited aggregation, a kinetic critical phenomenon. *Physical Review Letters*, 47(19):1400, 1981.

[191] D. E. Woodward, R. Tyson, M. Myerscough, J. Murray, E. Budrene, and H. Berg. Spatio-temporal patterns generated by *Salmonella typhimurium*. *Biophysical Journal*, 68(5):2181–2189, 1995.

[192] S.-L. Wu and H. Wang. Front-like entire solutions for monostable reaction-diffusion systems. *Journal of Dynamics and Differential Equations*, 25(2):505–533, 2013.

[193] K. Zhang and X. Zhao. Asymptotic behaviour of a reaction diffusion model with a quiescent stage. *Proceedings of the Royal Society A: Mathematical, Physical and Engineering Sciences*, 463(2080):1029–1043, 2007.

[194] T. Zhang, W. Wang, and K. Wang. Minimal wave speed of a bacterial colony model. *Applied Mathematical Modelling*, 40(23-24):10419–10436, 2016.

[195] X.-Q. Zhao and W. Wang. Fisher waves in an epidemic model. *Discrete & Continuous Dynamical Systems-B*, 4(4):1117, 2004.

[196] C. E. Zobell and E. C. Allen. The significance of marine bacteria in the fouling of submerged surfaces. *Journal of Bacteriology*, 29(3):239–251, 1935.